tment
ortation
Highway
afety
ration

DOT HS 807 000
Final Report

June 1986

Component Head Test Accident Reconstruction Feasibility Analysis

Technical Report Documentation Page

1. Report No.	2. Government Accession No.	3. Recipient's Catalog No.
DOT HS 807 000		

4. Title and Subtitle

Component Head Test Accident Reconstruction Feasibility Analysis

5. Report Date: June 1986

6. Performing Organization Code: NRD-22

7. Author(s)

R.A. Saul, M. Farson, D.A. Guenther

8. Performing Organization Report No.: SRL-73

9. Performing Organization Name and Address

National Highway Traffic Safety Admin.
Vehicle Research and Test Center
P.O. Box 37
East Liberty, Ohio 43319

10. Work Unit No. (TRAIS)

11. Contract or Grant No.

12. Sponsoring Agency Name and Address

National Highway Traffic Safety Admin.
400 7th Street, S.W.
Washington, D.C. 20590

13. Type of Report and Period Covered

Final
10/83 -- 12/84

14. Sponsoring Agency Code

15. Supplementary Notes

Final Report for SRL-73

16. Abstract

Motor vehicle accidents cause about 44% of all head injuries in the U.S., and are the most common source of severe head injuries. This project was conducted to determine the feasibility of reconstructing vehicle accident head injuries with a component head impactor.

A Hybrid III dummy headform was modified allowing it to be propelled in free flight. The headform was instrumented with a nine-accelerometer array to permit the measurement of rotational accelerations. Tests were conducted into various vehicle interior components to evaluate repeatability and response sensitivity. Three accident cases were reconstructed by reproducing the vehicle damage pattern caused by the occupant head impact.

The results indicated that it is feasible to reconstruct accident head injuries with a component head impactor. Further reconstructions are recommended to better understand the dynamic events associated with brain injury and to improve head injury criteria.

17. Key Words	18. Distribution Statement
Accident Investigation Accident Reconstruction Head Injury Brain Injury Hybrid III	Available to U.S. public through the National Technical Information Service, Springfield, VA 22161

19. Security Classif. (of this report)	20. Security Classif. (of this page)	21. No. of Pages	22. Price
Unclassified	Unclassified		

Form DOT F 1700.7 (8-72) Reproduction of completed page authorized

TABLE OF CONTENTS

LIST OF FIGURES

LIST OF FIGURES
(Continued)

LIST OF FIGURES
(Continued)

LIST OF TABLES

ACKNOWLEDGMENTS

The discussion and conclusions in this report represent the opinions of the author and not necessarily those of the NHTSA. The United States Government does not endorse products or manufacturers. Trade or manufacturer's names appear herein solely because they are essential to the object of the report. This document is disseminated under the sponsorship of the Department of Transportation in the interest of information exchange. The United States Government assumes no liability for the contents or use thereof.

The authors would like to express appreciation to Gerda England and Mike Groves for their fine data processing and test performance. The authors are also grateful to Susan Weiser in the preparation of this report.

DEPARTMENT OF TRANSPORTATION
NATIONAL HIGHWAY TRAFFIC SAFETY ADMINISTRATION

TECHNICAL SUMMARY

CONTRACTOR	CONTRACT NUMBER
National Highway Traffic Safety Administration Vehicle Research and Test Center	SRL-73
REPORT TITLE	REPORT DATE
Component Head Test Accident Reconstructon Feasibility	June 1986
REPORT AUTHOR(S)	
R.A. Saul, M. Farson, D.A. Guenther	

Each year between 400,000 and 500,000 Americans suffer head injuries severe enough to cause death or admission to a hospital. Of those who survive, many will never return to a normal life. Motor vehicle accidents cause about 44% of all head injuries in the U.S., and are the most common source of severe head injuries. This study was initiated to determine the feasibility of reconstructing vehicle accident head injuries with a component headform.

A free-motion headform was designed to allow the simulation of glancing impacts. A Hybrid III headform was modified allowing it to be propelled in free flight at up to 40 mph velocities. The headform was also instrumented with a nine-accelerometer array to permit the calculation of rotational accelerations.

Prior to evaluating the ability of the free-motion headform device to reproduce accident head impact damage patterns, preliminary tests were conducted to evaluate the headform repeatability and sensitivities. The conclusions from those tests were that:

- Repeatable head impact velocities were achieved with the current test apparatus.

- The headform response was sensitive to relatively small velocity changes.

- The headform response effectively discriminated between vehicle interior components of different stiffnesses.

- Based upon neck pendulum tests, the nine-accelerometer rotational acceleration array mounting and software was found to produce reasonably good angular position and velocity versus time results, implying reasonable rotational acceleration measurement.

(Continue on additional pages)

- Varying impact location on the head was critical to the HIC and rotational acceleration response, with the glancing impacts having a higher rotational acceleration and a lower HIC.

- The free-motion headform response for windshield impacts compared very well to a full Hybrid III dummy crash test head response.

Accident reconstructions were the most important phase of the feasibility study. The primary goal in the accident reconstruction phase was to determine the relation between the measured headform response and the injuries observed in the accidents. The approach in the accident reconstructions was to reproduce the accident damage pattern in the laboratory with the headform. Accident cases were selected from a study being conducted in conjunction with the Washington Hospital Trauma Center and the National Center for Statistics and Analysis. In that study, severe head and neck injury cases which were the result of motor vehicle accidents were studied in detail. Upon receipt of such cases, the hospital contacted a special NCSA accident investigation team for an in-depth analysis to determine the dynamic events associated with the head-neck injury. These accident cases were reviewed and evaluated for reconstructability based on the observed damage pattern due to head contact, and the level of injury. From the thirty-four available cases, three were selected for reconstruction. The three selected cases had head injury levels of AIS 2, 3, and 5 due, respectively, to striking the windshield, windshield/hood, and the right front passenger door. The free-motion headform reconstruction tests led to the following conclusions:

- The accident damage patterns were satisfactorily reproduced for the three reconstructions.

- Despite different head injury mechanisms, HIC values for the reconstructions increased with increasing head injury levels.

- One of the three accident reconstructions was of a diffuse head injury (Aries concussion). The highest peak rotational acceleration was also experienced for this case, the result of initial, short duration spikes.

- The damaged accident vehicle components, which were available for two of the three reconstructions, were very useful (if not essential) to reproducing the damage pattern.

- The peak rotational accelerations were generally the result of short duration (3-5 msec) pulses.

- Two of the three reconstructions required impact velocities which were less than the vehicle delta-V. This appeared to be reasonable based upon crash test results with unrestrained occupants.

- For the third reconstruction, a velocity which was higher than the delta-V was required to obtain sufficient impact energy to reconstruct the damage pattern with the headform. This result was not unexpected, since the accident investigation gave indications that the occupant may have rotated slightly, impacted the windshield with the top of his head, and therefore had a greater effective mass (and energy) due to compressive neck loads.

The following areas of further investigation and development are recommended on the basis of the results of this feasibility study:

- The rotational head injury criterion needs further refinement to determine the significance of short time duration pulses. Diffuse injuries normally associated with rotational effects require time durations greater than those associated with the peaks found in the reconstructions. This may indicate that the rotational acceleration criterion can neglect the higher frequency pulses. Subdural hematoma head injuries are thought to be related to acceleration onset rate (i.e., higher frequencies), but little research has been done to develop a criterion for them.

- Computer simulation of the accident cases should be incorporated into the reconstruction process to improve the understanding of probable occupant kinematics, contact velocities, and impact energy levels.

- Development of a unified method of identifying and documenting occupant damage patterns is recommended. A unified approach would allow not only better damage pattern reconstruction, but also a method for more widespread data collection from accident investigation teams.

- Finally, improvement to the component headform which would allow it to simulate a wider variety of accident occupant head impacts would be desirable. The current design is limited to frontal impacts. Design modifications could be made to simulate other impact orientations or to attain a variable mass headform.

Despite these areas in which the accident reconstruction methodology can be improved, the results of this head component reconstruction feasibility study indicated that information obtained directly from the accident environment can be valuable in the refinement and development of human injury criteria, and that the approach should continue to be pursued. The free-motion headform component test device also appears to provide a realistic and economic approach for obtaining head injury predictions for vehicle interior component impacts with potential applications to vehicle component design and safety standard development.

1.0 INTRODUCTION

According to the National Institutes of Health, almost one million people in the United States suffer from the effect of head injuries (1).* Each year between 400,000 and 500,000 Americans suffer head injuries severe enough to cause death or admission to a hospital. Of those who survive, many will never return to a normal life. Motor vehicle accidents cause about 44% of all head injuries in the U.S., and are the most common source of severe head injuries.

No two brain injuries are alike. The effect of the brain damage varies according to the location and severity of the injury, as well as individual tolerance differences. The injuries suffered by motor vehicle drivers and passengers are largely determined by the extent to which the vehicle interior structures have been designed to absorb energy from head impacts. In 1981, test hardware was developed at the Vehicle Research and Test Center for component testing of vehicle interiors. The equipment has been used to measure force-deflection properties of vehicle interior components and to determine relationships between component stiffness and potential for head injury (2). That test hardware was restrictive in the types of impacts and kinematics it could simulate, and was not amenable for reproducing most head impacts which occur in motor vehicle accidents. Specifically, impacts could be made only in a direction normal to the impacting surface, no simulation of head rotation was possible, and impact orientations of a normally seated occupant could not typically be simulated. Searle (3) reported on the development of a free-flight headform to be used in a more realistic evaluation of vehicle interior components.

---

*Numbers in parenthesis represent references at the end of this paper.

This consisted of a smooth, rigid aluminum sphere of 6.5 inch (16.5 cm) diameter and having a mass of 15 lb (6.8 kg). The main advantage of this method was its ability to impact surfaces without the requirement of being normal to the impacting surface. This allowed components to be tested in a more realistic manner. The procedure proved to be repeatable and demonstrated the ability to discriminate among different vehicle components. However, problems were encountered in velocity measurement, and it had inadequate biofidelity for accident reconstructions.

Independent of these component hardware developments, the Motor Vehicle Manufacturers Association sponsored The University of Michigan Transportation Research Institute to conduct detailed accident investigation and occupant computer model simulations in order to develop a method for obtaining enhanced biomedical data from accident cases (4). The National Highway Traffic Safety Administration (NHTSA) also conducted a joint project with the Washington Hospital Trauma Center. In that study, severe head and neck injury cases which were the result of motor vehicle accidents were investigated in detail. Upon receipt of such cases, the hospital contacted a NHTSA accident investigation team for an in-depth analysis to determine the dynamic events associated with the head-neck injury.

This study was initiated to determine the feasibility of reconstructing Washington Hospital Trauma Center head injuries with a component head impactor. If found to be feasible, it is hoped that such a methodology would lead to further head injury reconstructions in order to better understand the dynamics which lead to brain injury. The insights gained could lead to better head injury criteria and safer vehicle interior design. The approach taken in the study was to design and fabricate a free-motion headform, to conduct some preliminary tests, and then to reconstruct a few selected accident cases from the Washington Hospital study.

2.0 HEADFORM DESIGN

It was desired to develop a head component design which represented as closely as possible an actual head during an impact. Previous designs have been used to gather force-deflection information or to rate components relative to each other, thus simulating the head dynamics as accurately as possible was not a primary concern in those studies. In an effort to simulate glancing blows it was determined essential to use some kind of free-flying device. To retain as much biofidelity as possible, a Hybrid III headform was modified to accomodate this requirement. An additional requirement which resulted from a survey of accident cases was that the headform should be capable of up to 40 mph impact velocities.

The free-motion headform impactor (FMHF) design consisted of a Hybrid III headform mounted on a compressible fluid impact accelerator (Figure 2.1). The standard aluminum cap on the back of the Hybrid III head was replaced by a 1/4" thick steel plate (Figure 2.2), allowing the headform to be held against the impactor ram face by a permanent magnet (Figure 2.3). The position of the head with respect to the ram face was determined by two locating pins attached to the impactor and extending into the back plate of the head. A leather pad was attached to the ram face and the back plate of the head was covered with duct tape to protect the headform accelerometers upon firing the impactor. The headform was ballasted to make it represent an "effective" mass of actual heads during impact (2). The resulting mass properties of the headform were as follow:

TABLE 2.1

Mass Properties of the Headform

Mass (without skin)= 8.25 lb.
Mass (with skin)= 10.65 lb.
Ix= .121 in-lb-s**2
Iy= .211 in-lb-s**2
Iz= .159 in-lb-s**2

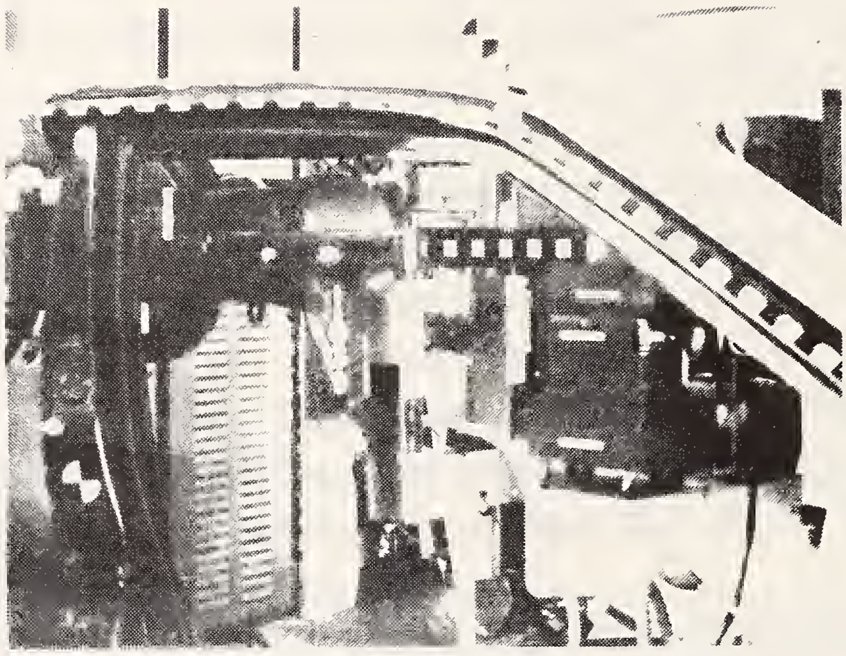

FIGURE 2.1 -- Free Motion Headform Mounted on Compressible Fluid Impactor.

FIGURE 2.2 -- Modified Hybrid III Headform.

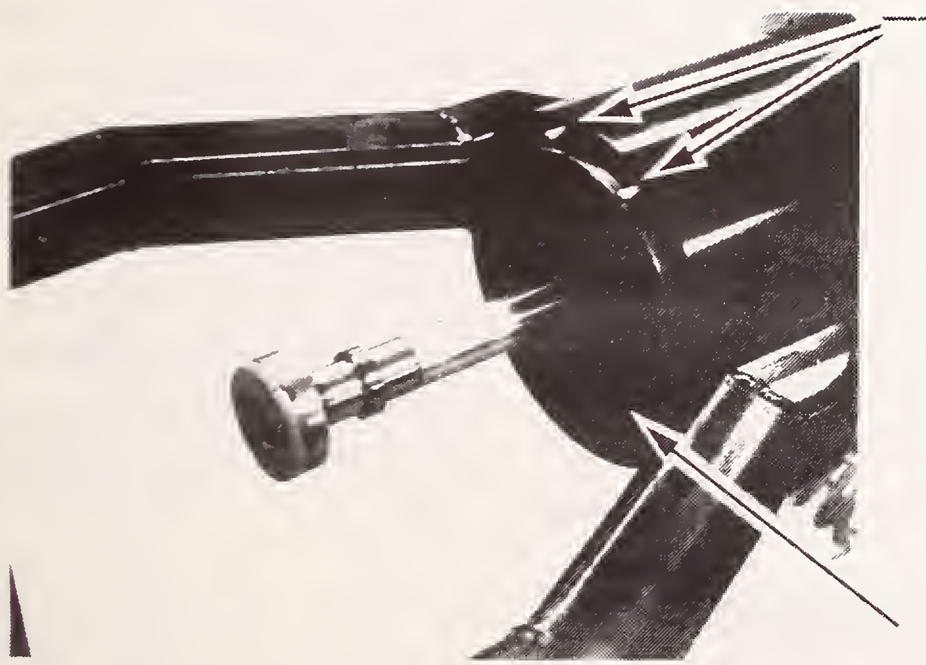

FIGURE 2.3 -- Fluid Impactor Ram Face.

where I is the polar moment of inertia of the headform with skin covering, and the subscripts refer to the coordinate axes as shown in Figure 2.4. Due to symmetry the y axis is a principal axis. Since the x and z axes are not principal there is also a cross-product of inertia I_{xz}. This quantity was not evaluated. Published values for an average I_y of .206 in-lb-s**2 (5) for cadavers indicate the modified Hybrid III headform has good biofidelity in this respect. The natural frequency of the headform (as measured from the free vibrations resulting from a 0.3 msec impulse) was nearly 4000 Hz, insuring that the headform behaved as a rigid body in the frequency range of interest.

When the impactor was fired, the ram separated the headform from the permanent magnet. During acceleration, the headform was held against the ram by its inertial force. Upon deceleration of the ram, the headform separated, was in free flight, and then impacted the vehicle component of interest. Movement of the skin covering relative to the headform occurred during the acceleration and the initial free-flight. The initial spacing between the headform and the vehicle component was sufficient to allow this relative motion to decay before impact. There was typically very little rotational motion of the FMHF during free-flight. High speed film analysis indicated no rotation, while the 9-accelerometer array data indicated the resultant rotational velocity to be 5-10 rad/s at time of impact.

3.0 DATA COLLECTION AND VALIDATION

3.1 General

Instrumentation for the tests consisted of a 3-2-2-2 rotational accelerometer array (Figure 2.4) in the headform, and an event mark indicating time of contact with the vehicle component. The rotational acceleration array was fabricated by Denton Inc. and utilized Endevco 7264 accelerometers. The event mark was triggered by a pair of aluminum foil strips attached to both the

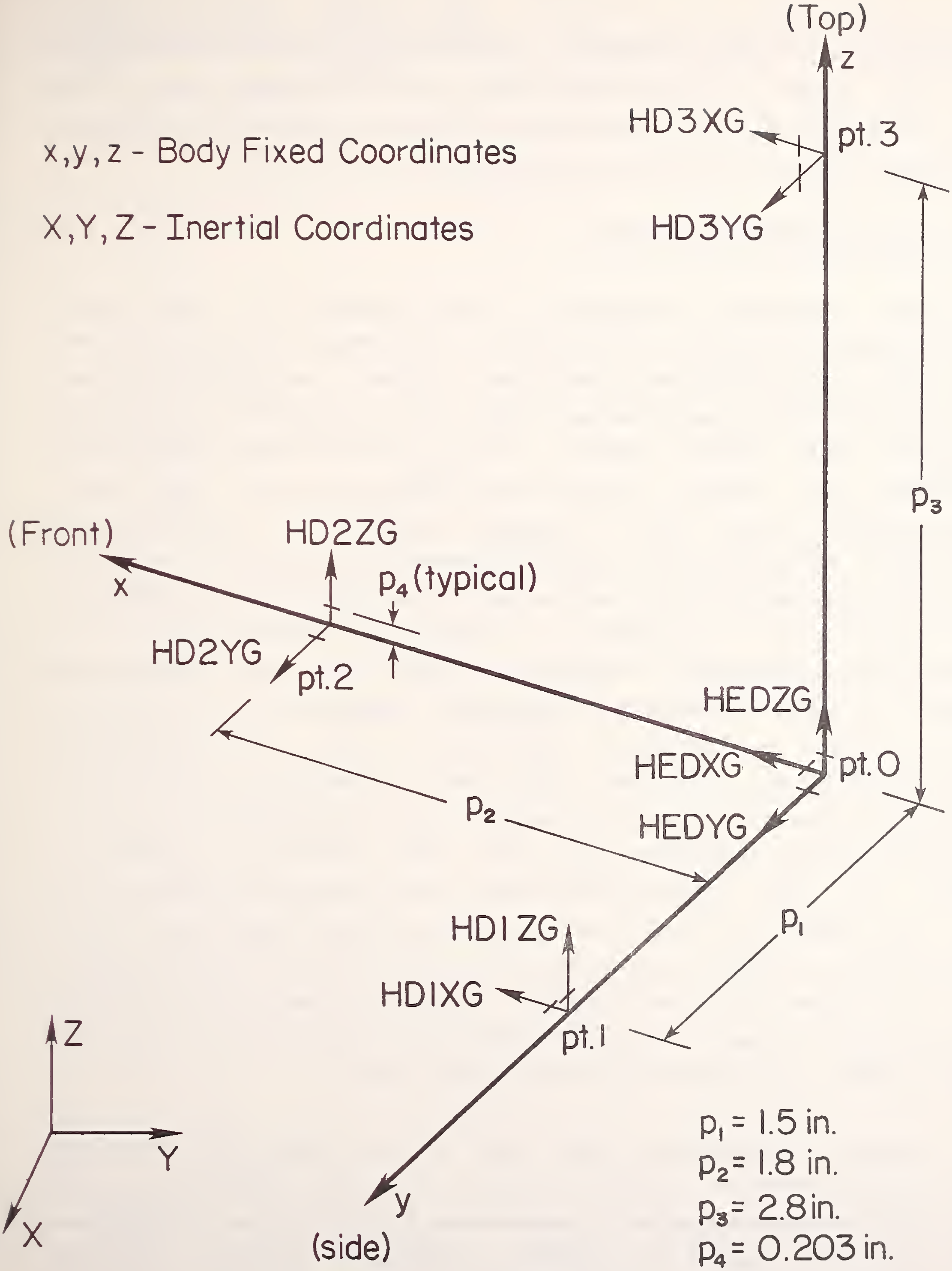

FIGURE 2.4 -- Coordinate Axis and Accelerometer Locations.

headform and target surfaces. All data were analog filtered at SAE J211 Class 1000 and digitized at 8000 Hz sample rate. The data were then digitally processed through a Butterworth lowpass phaseless filter algorithm to SAE channel class 1000.

3.2 Nine Accelerometer Array

Some concerns regarding the accuracy of the nine-accelerometer rotational acceleration measurement capability have been cited in unpublished literature. Since a calibration procedure for the nine-accelerometer array was non-existent, head/neck extension and flexion tests, as well as head drop tests were conducted to verify that the installation of the nine-accelerometer array and a program written to calculate the rotational accelerations produced reasonable results. Mounting of the accelerometers with any offset with respect to the desired axes would have introduced a "cross axis sensitivity" in the accelerometer readings, in addition to the cross axis sensitivity present in accelerometers themselves (typically 2% for Endevco 7264) given a perfect mounting. Since the head/neck extension/flexion and head drop tests produced two dimensional motions of the head (in x-z planes), all accelerometers in the y directions were expected to give zero readings. As shown in Figure 3.1, for the head drop test the maximum acceleration in the x-z plane at the c.g. was 304g (vector sum) while the y acceleraton at that time was 6g, or 2% of the full acceleration. This is close to the reported cross-axis sensitivity of the accelerometer itself, indicating that the mounting of the y-axis accelerometer introduced no significant error.

Similar comparisons were made for the other two locations with accelerometers mounted in the y direction (Figures 3.2 and 3.3). The y-axis at point 3 registered 3 1/2% of the x acceleration at that point and at point 2 registered virtually 0 during the initial impact. The assumption of planar motion is only valid during the initial impact so the readings beyond 3 msec

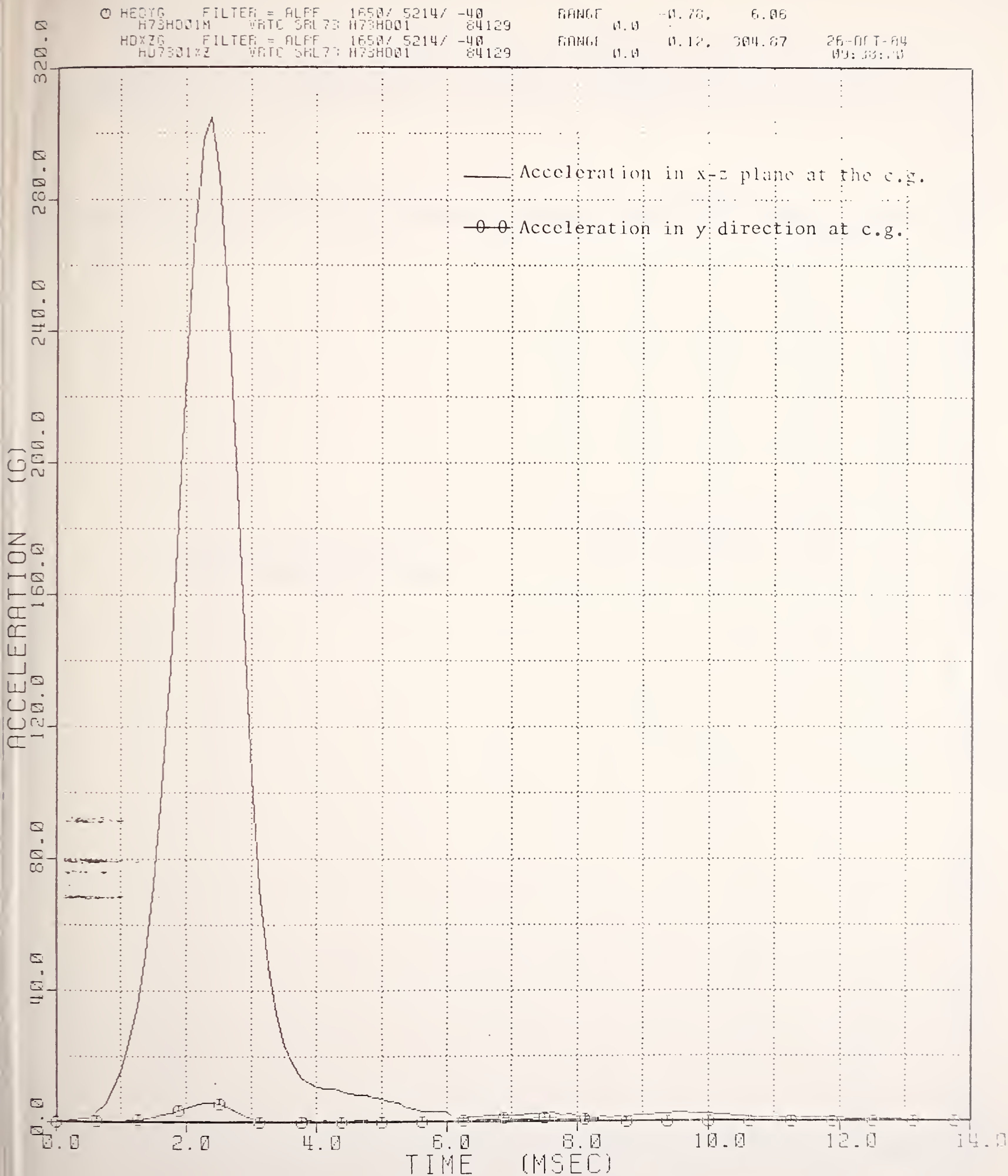

FIGURE 3.1 -- Head Drop Test Results For Cross-Axis Sensitivity (C.G. Location).

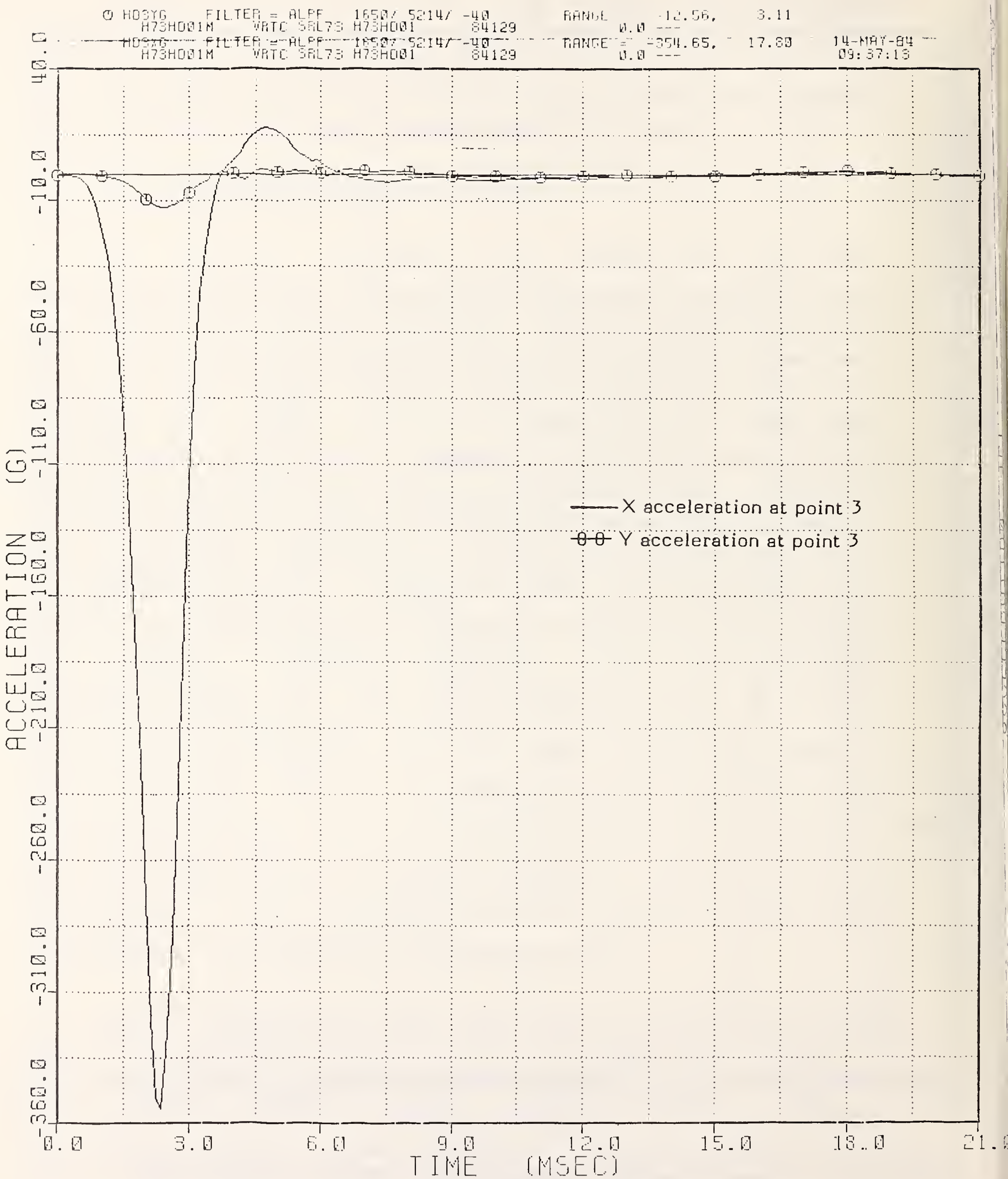

FIGURE 3.2 -- Head Drop Test Results For Cross-Axis Sensitivity (Point 3 Location).

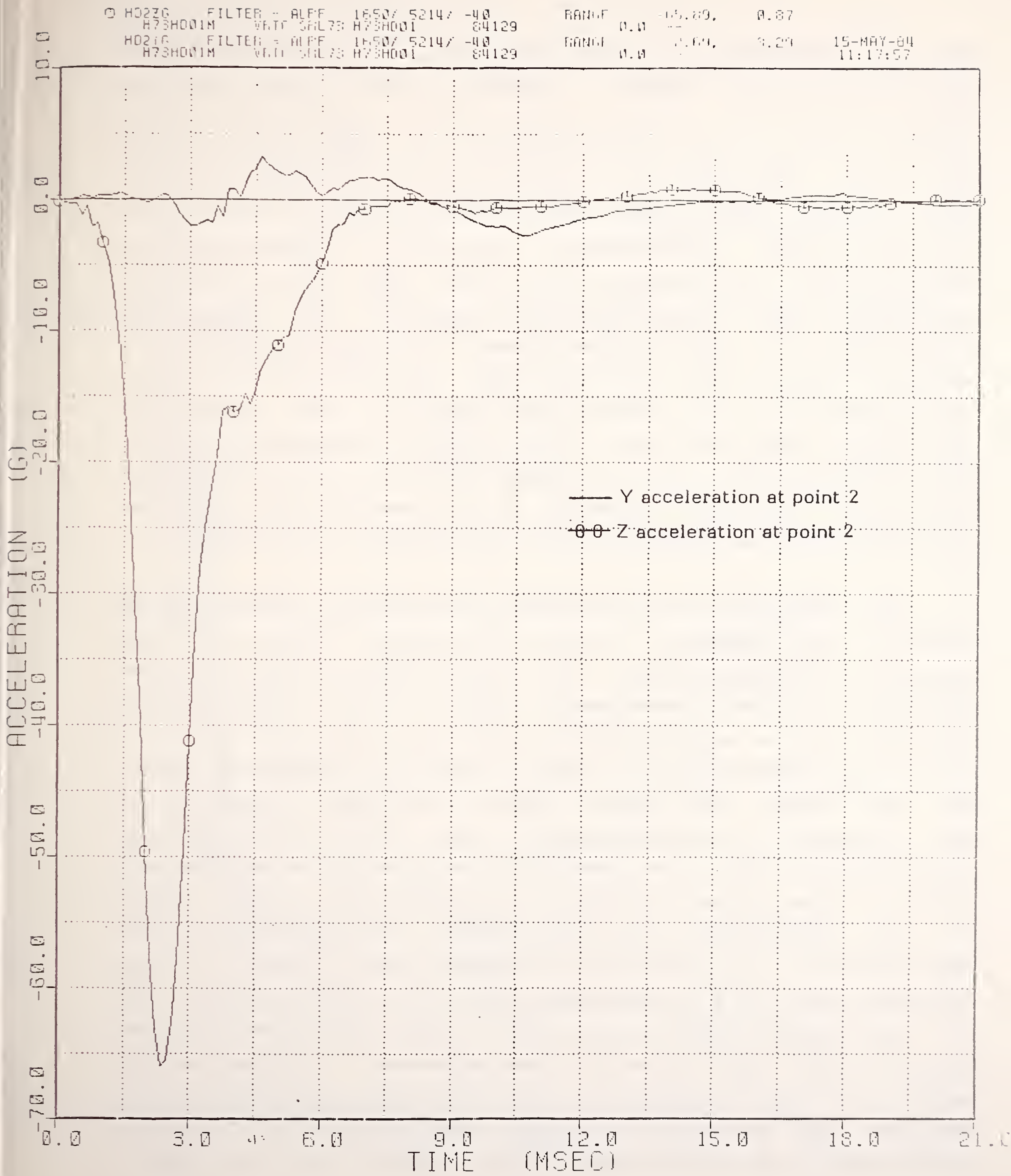

FIGURE 3.3 -- Head Drop Test Results For Cross-Axis Sensitivity (Point 2 Location).

were not considered to be a valid test of the cross-axis sensitivity and were ignored. Figures 3.4 and 3.5 show that the flexion test gave slightly worse lateral acceleration results (typically 5% of full acceleration in x-z plane) than the head drop test. This may be accounted for by the longer duration impacts which allow some motion in the y-direction due to the rotational angle instrumentation mounting. Although strictly speaking only 3 accelerometers were tested, the results indicated reasonably good installation in terms of the cross axis sensitivity. It was concluded, based on the head drop and neck pendulum tests, that the cross-axis sensitivity of the accelerometers due to mounting was negligible, and the observed cross-axis sensitivity was of the same magnitude as the accelerometer itself. The combined mounting and accelerometer cross-axis sensitivity appeared to be less than 5%, which was considered to be satisfactory for the purposes of this project.

The accuracy of the rotational calculations was checked by comparing the angle vs. time and angular velocity vs. time responses obtained through the 9 accelerometer method to those obtained by direct measurement using the two rotary potentiometers of the neck calibration procedure. Figures 3.6 -- 3.9 show these comparisons for both the flexion and extension tests. For both cases, the general shape of the angular velocity from the integrated nine-accelerometer data and the differentiated potentiometer data agree reasonable well, while the maximum and minimum values differ slightly. For the extension test, (Figure 3.7) the difference for both maximum and minimum values was approximately 3 r/s, while for the flexion test, (Figure 3.6) the difference was 2 r/s at the maximum and 8 r/s at the minimum. It is also apparent that for the first 30 msec the two methods give results which are in very close agreement. In comparing the angle vs. time (Figures 3.8 and 3.9), good agreement is also obtained for the first 35-40 msec. The divergence of the nine-accelerometer and potentiometer methods beyond 40 msec for both

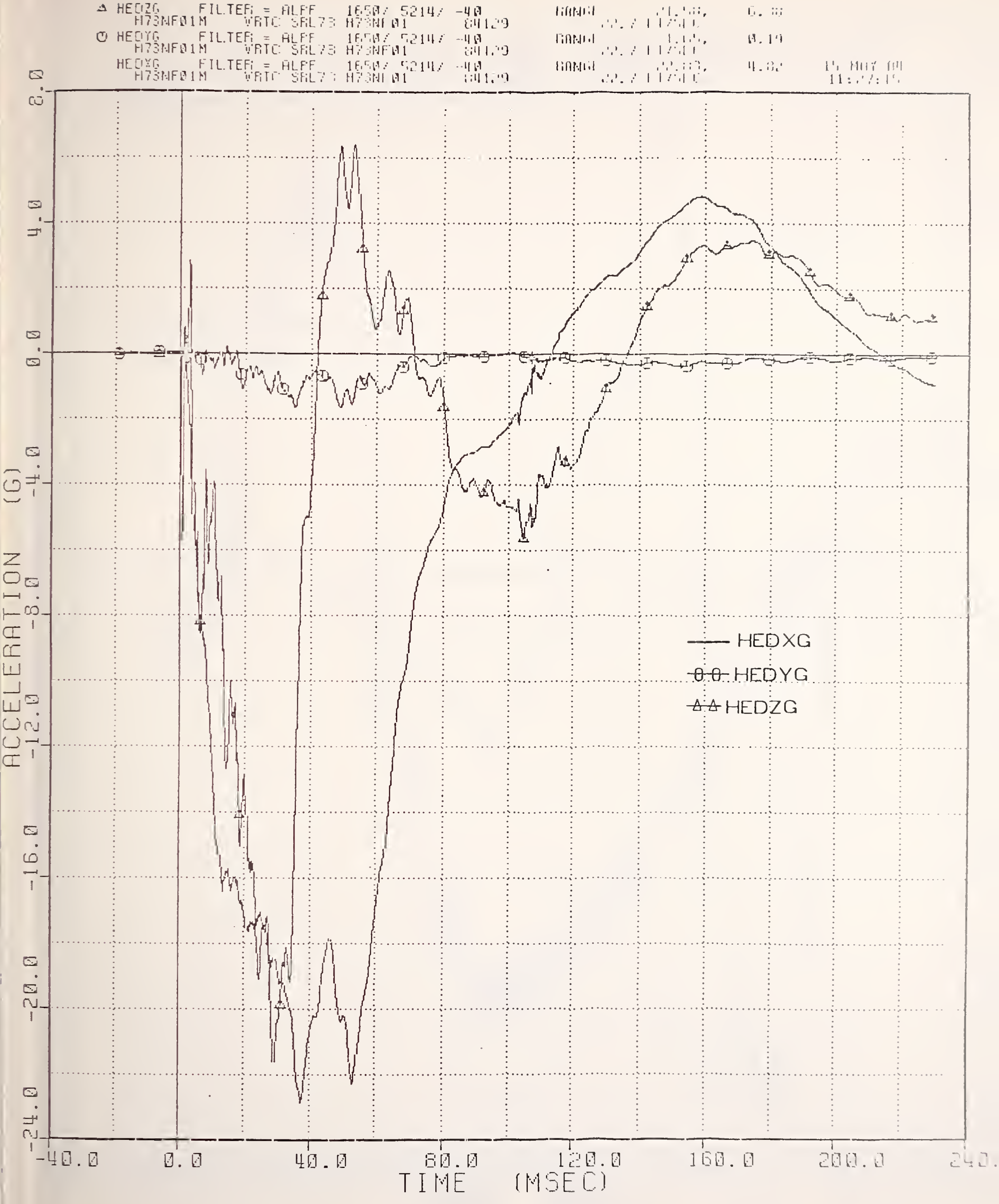

FIGURE 3.4 -- Neck Flexion Cross-Axis Sensitivity at Head C.G.

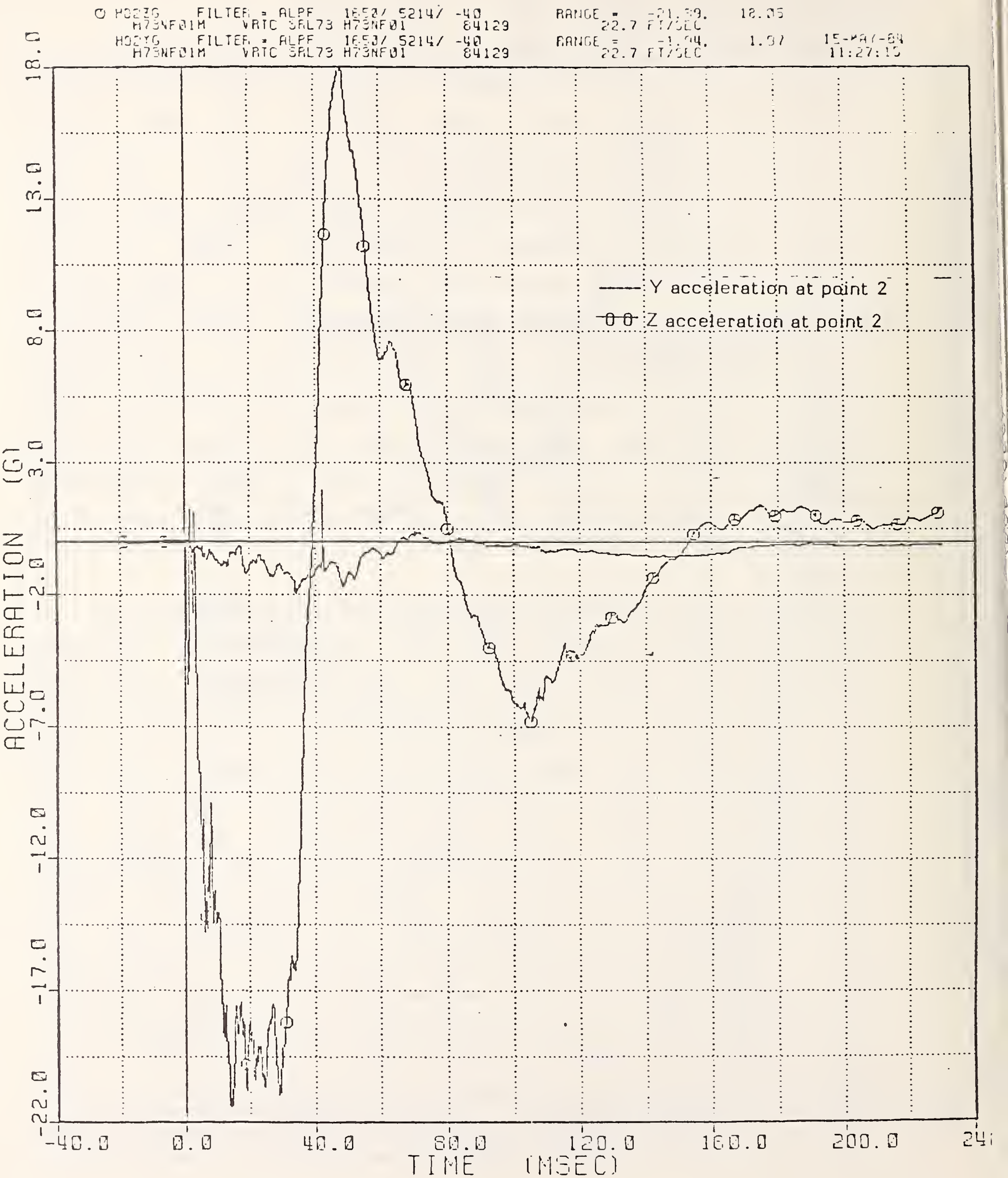

FIGURE 3.5 -- Neck Flexion Cross-Axis Sensitivity at Head Point #2.

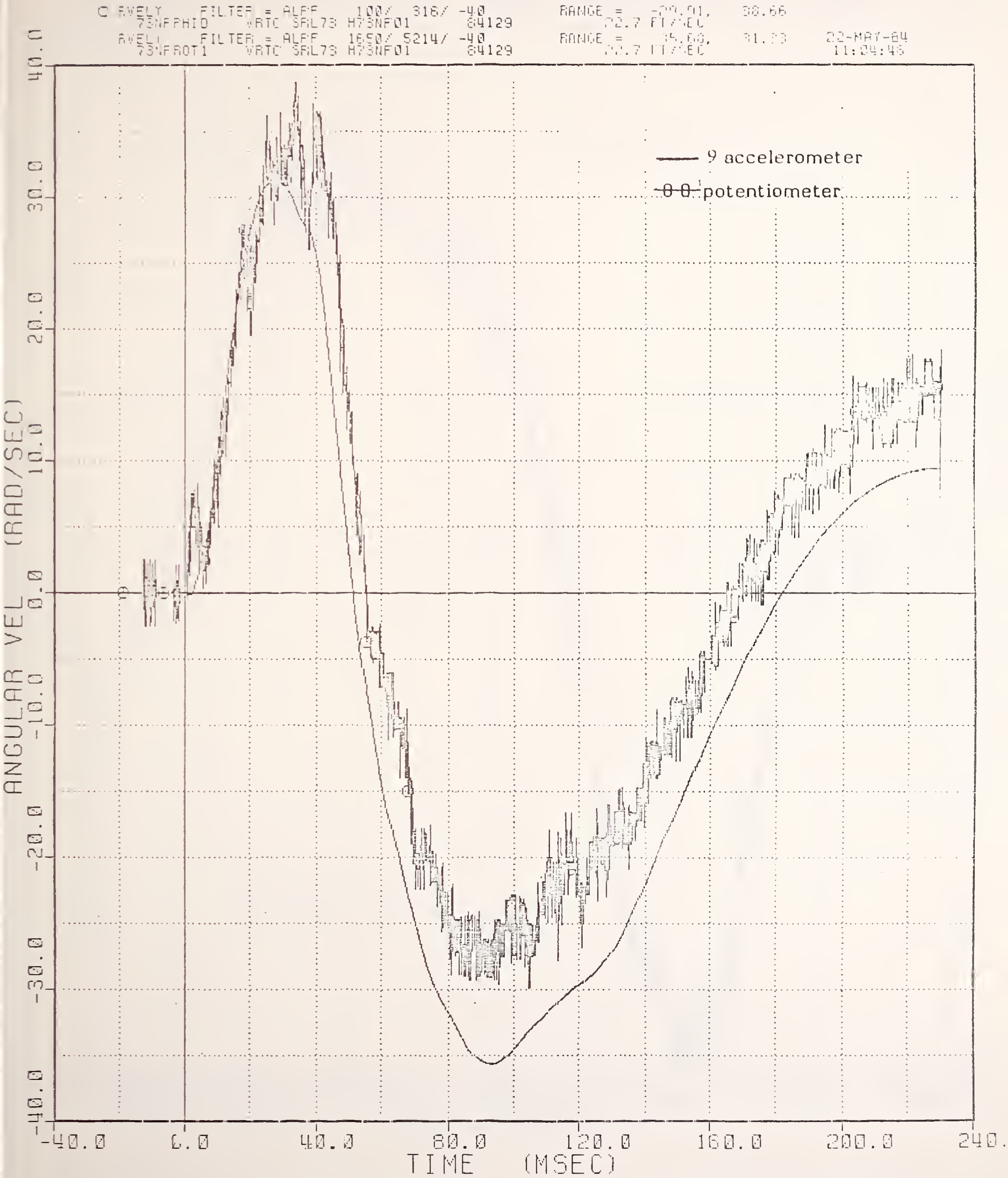

FIGURE 3.6 -- Comparison of Angular Velocity Versus Time From 9-Accelerometer and Potentiometer Data For Neck Flexion Pendulum Test.

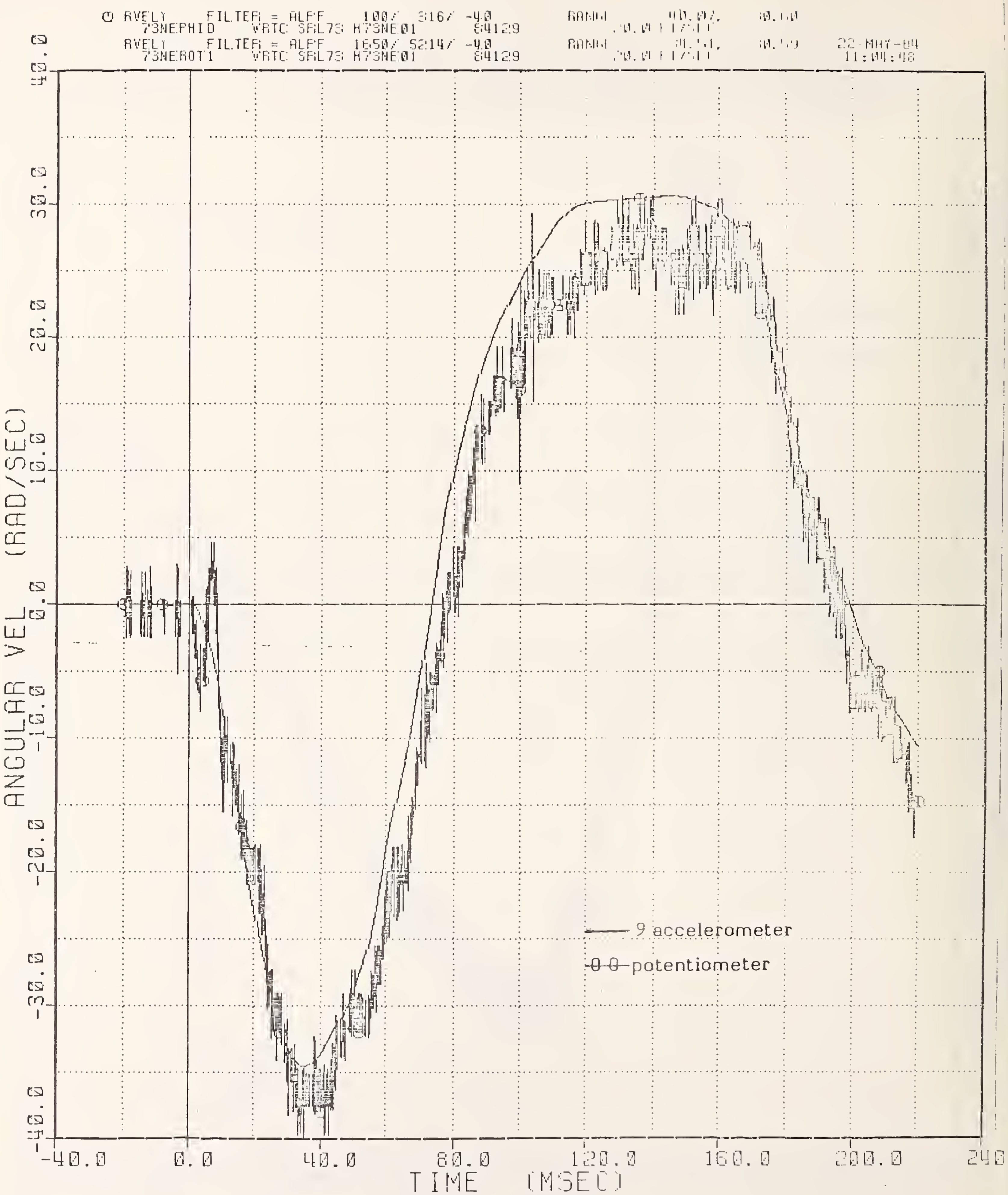

FIGURE 3.7 -- Comparison of Angular Velocity Versus Time From 9-Accelerometer and Potentiometer Data For Neck Extension Pendulum Test.

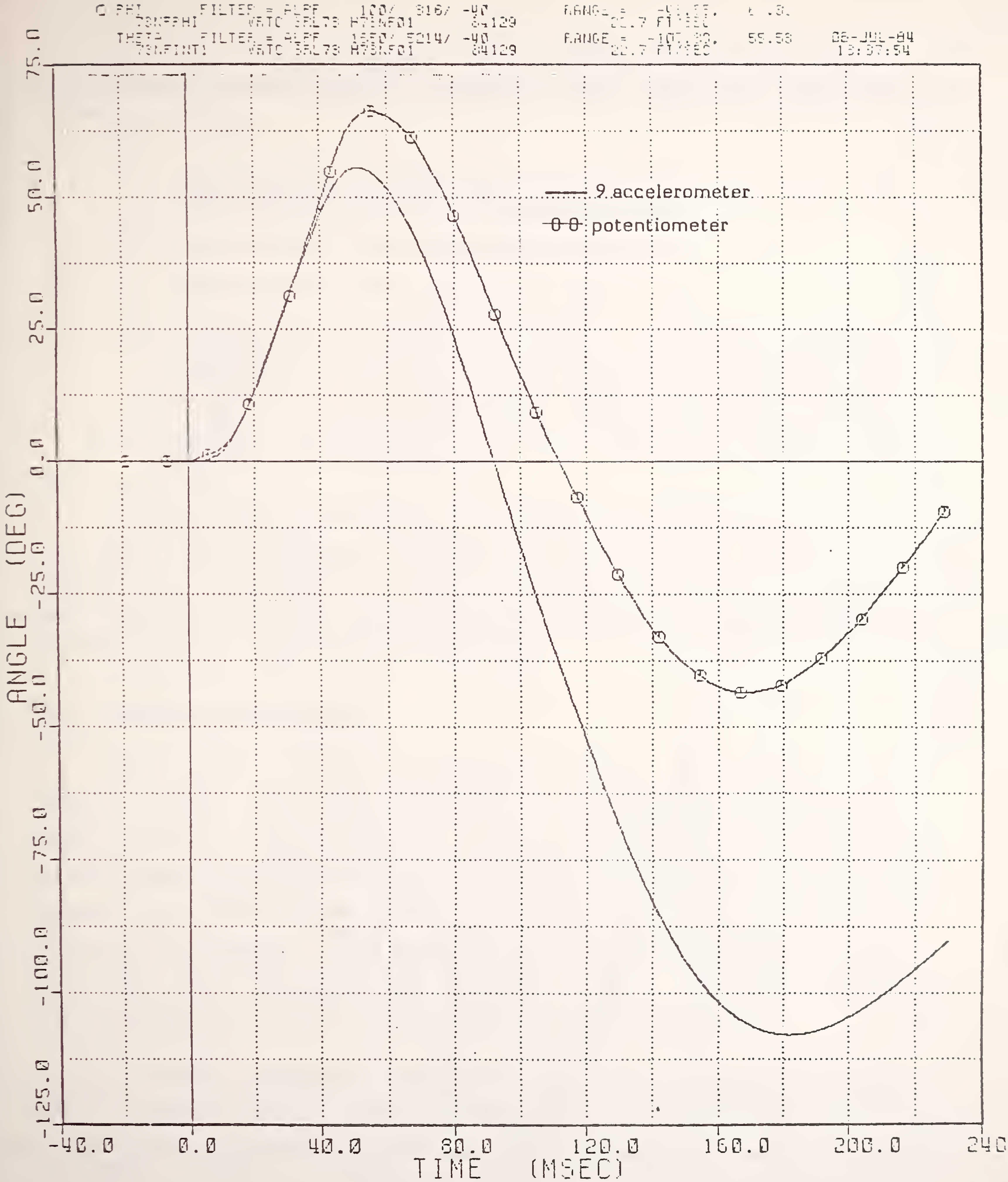

FIGURE 3.8 -- Comparison of Angle Versus Time From
9-Accelerometer and Potentiometer Data
For Neck Flexion Pendulum Test.

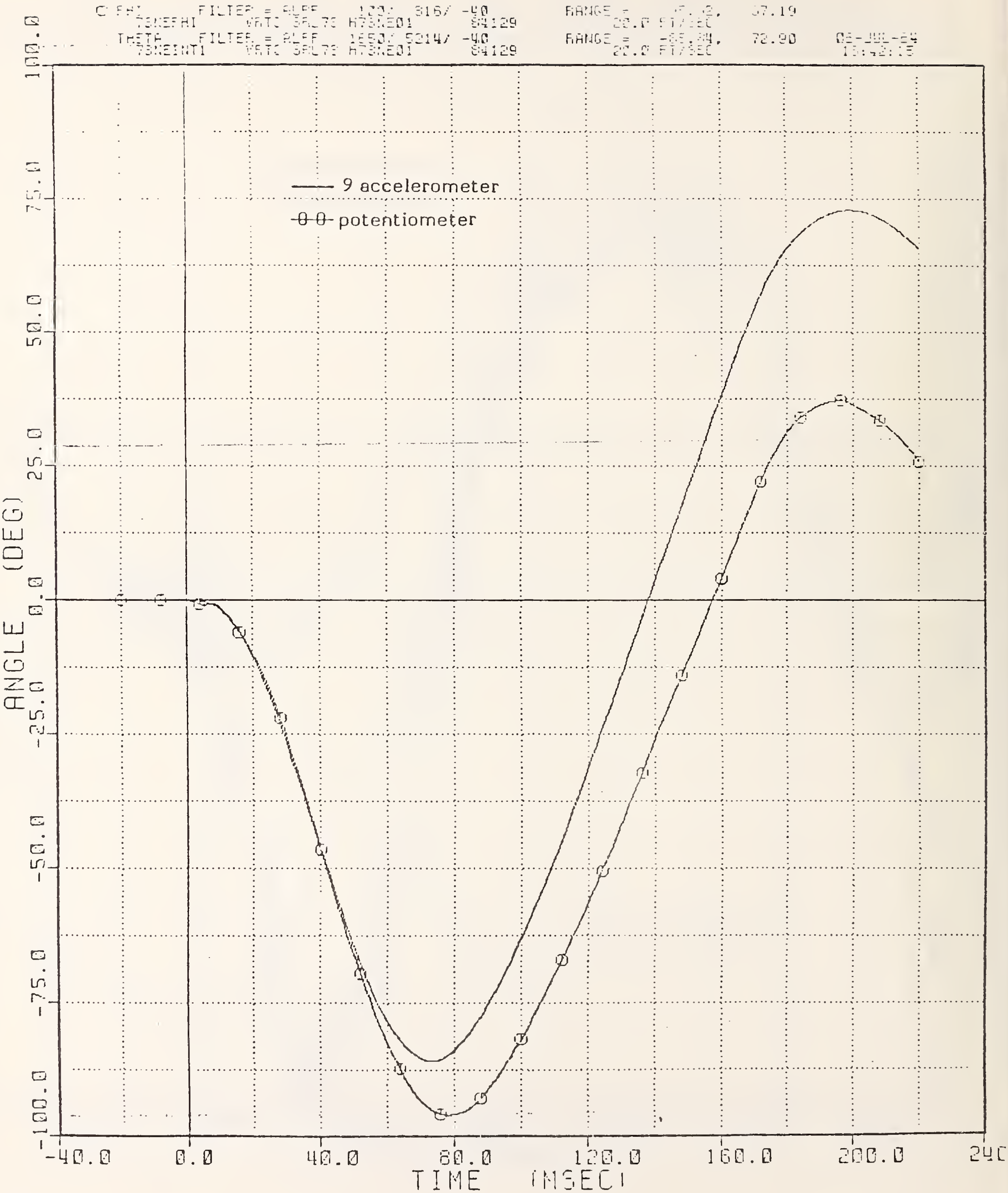

FIGURE 3.9 -- Comparison of Angle Versus Time From
9-Accelerometer and Potentiometer Data
For Neck Extension Pendulum Test.

the flexion and extension velocity and position could have several sources:

- Accelerometer cross-axis sensitivity and bias (and resulting accumulated integration errors).
- Potentiometer measurement inaccuracies.
- Potentiometer differentiation processing.
- Utilization of a body-fixed rather than Euler coordinate system. (In Figures 3.10 and 3.11, the rotational velocities in the X and Z directions indicate that beyond 40 msec the headform does not move in a planar motion. For such a case, integration of body fixed angular velocities does not yield an angle. See Appendix A for details.)

Since the head activity of interest occurs during the first 30 msec, the agreement between the two angular velocity and position calculations for the neck pendulum tests were considered satisfactory for the purpose of determining the feasibility of reconstructing accident head injuries.

3.3 Velocity Measurement

The first velocity measurement system used for the free motion head form consisted of two Microswitch MLS4B-1000 photoelectric controls spaced a known distance apart. The front of the head form then served as a breaker to trip these two light beams as it was in free flight, thus giving the average velocity over that distance. This method did not give repeatable results and was also very sensitive to camera lights. The main problem was apparently the type of photoelectric controls used.

A second velocity measurement system, a single polarized light beam, was used in conjunction with a one inch flag attached

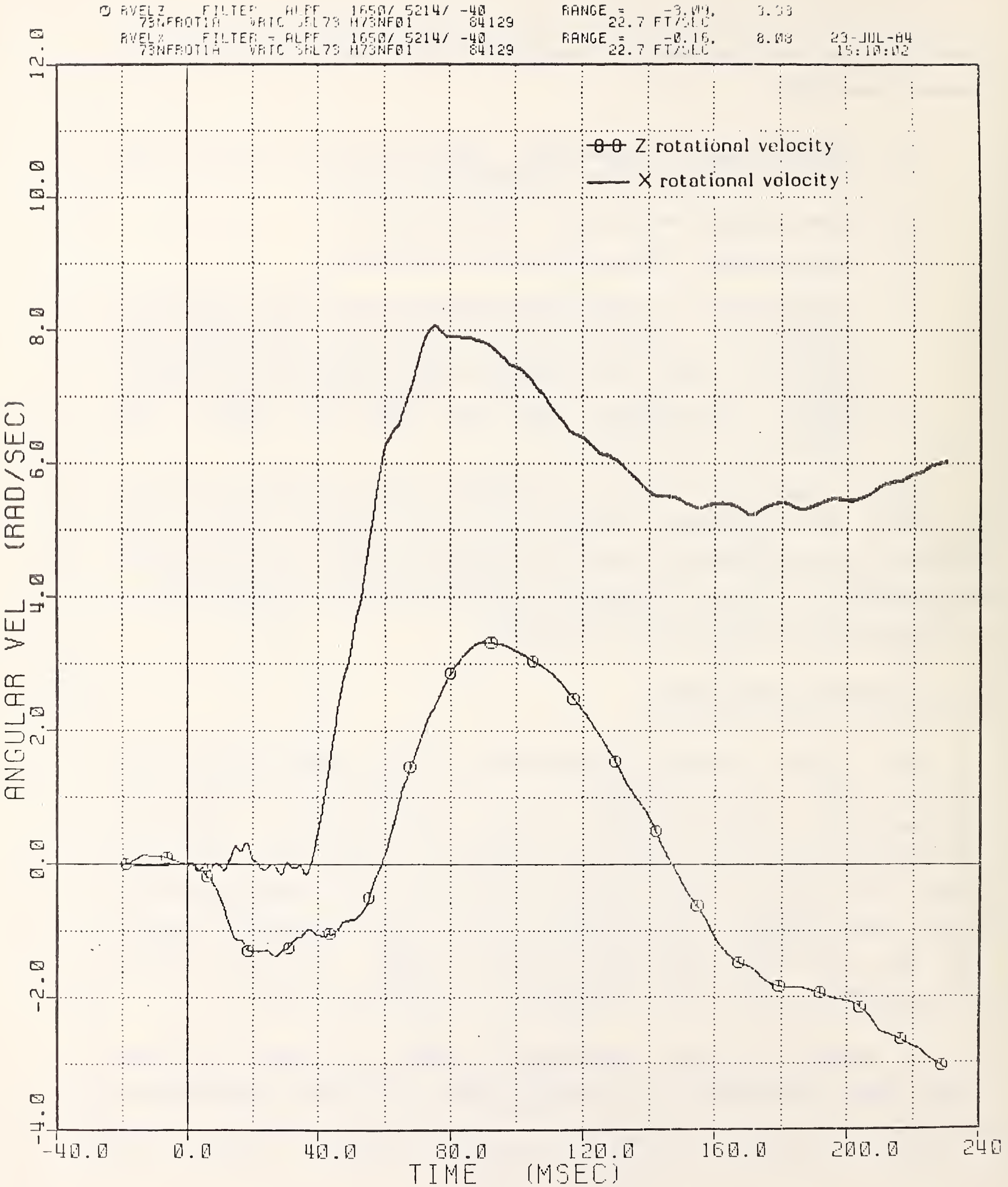

FIGURE 3.10 -- Effect of Non-Planar Motion for the Neck Flexion Pendulum Test

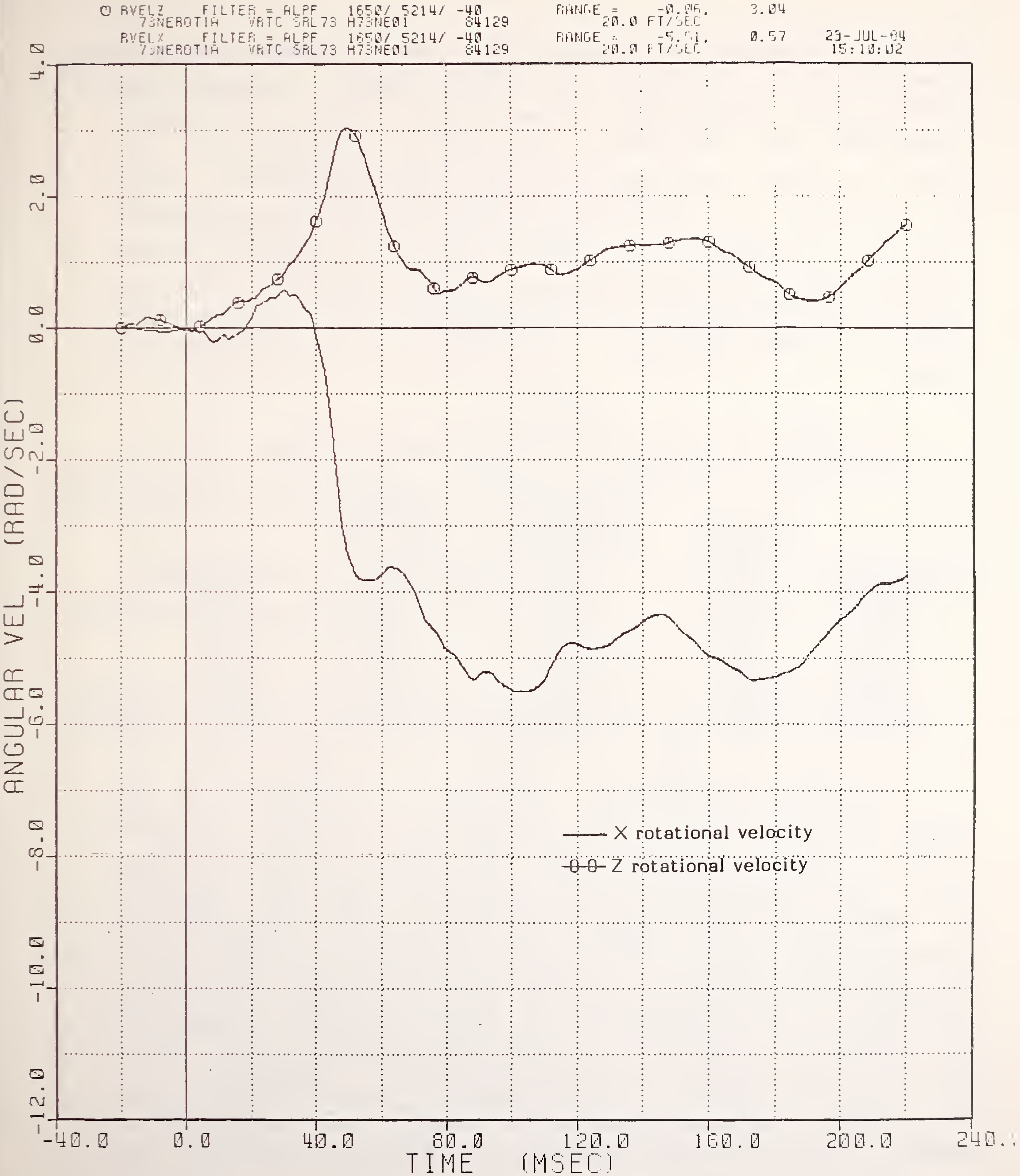

FIGURE 3.11 -- Effect of Non-Planar Motion for the Neck Extension Pendulum Test

to the bottom of the head. This system proved to be both repeatable and insensitive to camera lights. However, the results were consistently higher than the velocity obtained by integrating the headform C.G. acceleration (see Table 3.1). In order to better understand the light trap measurements, a flag was attached to a head/neck calibration pendulum and the light trap was situated so that the velocity could be measured as the pendulum was swung through the vertical position. Since the velocity of the pendulum could be calculated from conservation of energy, a known velocity was generated to test the light trap system.

TABLE 3.1

Velocity Measurement Summary Using 1" Flag

Test Number	Impactor Pressure (psi)	Maximum Velocity From Integration (mph)	Velocity From Light Trap (mph)	% Difference
S73015	1900	8.15	9.98	22.5
S73016	1900	8.15	9.94	22.0
S73023	1900	7.95	9.61	20.9
S73024	1900	7.85	9.56	21.8
S73019	3398	15.83	19.06	20.4
S73020	3394	15.62	18.80	20.4
S73017	5218	24.20	29.34	17.5
S73018	5218	24.34	29.36	20.6

It was initially found that the velocity measured by the light trap system was, in fact, higher than the actual velocity. Further testing indicated that this could be corrected by two means: 1.) allowing the flag to break the light beam closer to the receiver of the light trap system, or 2.) increasing the width of the flag. This finding was thought to be due to the diffraction of light around the edges of the flag causing the receiver to see a gradual drop in light intensity as opposed to step inputs. Figure 3.12 illustrates the light intensity vs. time at the collector being affected by the diffraction. The curved lines represent the actual intensity that the collector senses. The net effect will be a measured time less than the actual time, which yields a measured velocity higher than the actual velocity.

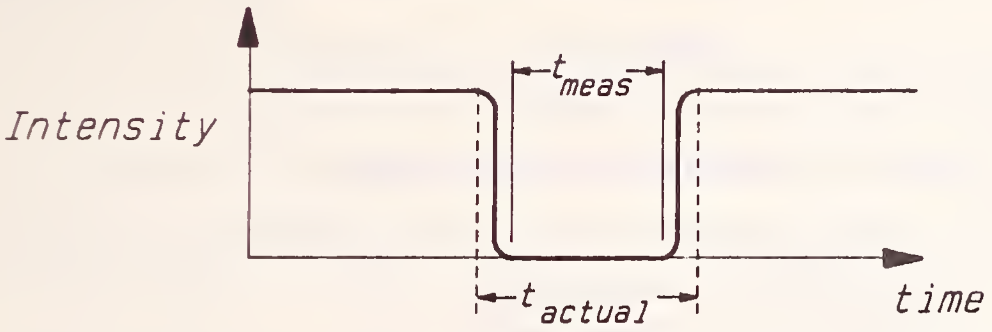

FIGURE 3.12 - Light Intensity at the Receiver

To help correct this measurement problem, a 2 1/4" flag was attached to the pendulum. Table 3.2 illustrates the pendulum test results obtained after this modification.

TABLE 3.2

Comparison of Measured Light Trap Velocity (2 1/4" flag) to the Theoretical Velocity of a Pendulum

Angle of Pendulum	Theoretical Speed (mph)	Measured Speed (mph)	Error (mph)	Percentage Error
30	5.23	5.33	0.10	1.9
45	7.73	7.93	0.20	2.6
68	11.29	11.57	0.28	2.5
90	14.29	14.69	0.40	2.8
120	17.50	17.83	0.33	1.9

Although the measured velocities were still somewhat higher than the actual velocity, the results were a significant improvement over the performance using a one inch flag (Table 3.1), and were considered to be very satisfactory. A number of test shots were then made on the impactor for another comparison of measured velocities using the light trap and 2 1/4" flag to the acceleration of the headform. The results (Table 3.3) indicated that the light trap velocity was close to the integrated values, with an average difference of only 1.8%. The effect of rotation during free flight was a potential source of error for both measurement systems. For the integrated acceleration, the effect would be to always cause a lower velocity than normal, while for the light trap it could produce a high or low value, depending on the type of rotation.

TABLE 3.3
Light Trap Velocity With 2 1/4" Flag Versus Integrated Acceleration

Test Number	Gun Pressure (psi)	Velocity at Impact From C.G. Accel. (mph)	Velocity From Light Trap (mph)	Difference (mph)	Percentage Difference
S73026	2400	12.02	11.38	0.64	5.3
S73027	2400	11.90	11.99	-0.09	-0.7
S73028	3596	19.14	18.82	0.32	1.7
S73029	3596	19.00	18.65	0.35	1.8
S73030	5794	30.14	29.74	0.40	1.3
S73031	5794	30.15	29.81	0.34	1.1
S73032	5800	30.70	31.04	0.66	2.1
S73033	5800	31.15	31.57	-0.42	-1.3
S73034	5978	30.17	31.72	-0.55	-1.8
S73035	3504	19.12	19.30	-0.18	-0.9

In summary, since both light trap and integration acceleration measurement methodologies produced very similar values, both measurements were assumed to be very close to the true velocity. Since the integrated velocity had proven to be more consistent and allowed the determination of velocity at impact, this value was used as the reported impact velocity for all tests.

4.0 PRELIMINARY TESTING

Prior to evaluating the ability of the free-motion headform device to reproduce accident head impact damage patterns, a series of preliminary tests were conducted to evaluate the following:

- Headform response repeatability,
- Velocity sensitivity of the head form response,

- Sensitivity to head impact location and initial orientation,
- Sensitivity due to striking different vehicle components, and
- The effect neglecting the neck has on head response.

The preliminary tests were conducted with vehicles which had been previously tested for other purposes. The vehicle preparation for the tests of this program involved removal of the seats, cutting the vehicle in half and removing the rear half, orienting the front half for impact by the headform, and securing the vehicle in place.

4.1 Repeatability

The repeatability of the FMHF measurements was evaluated by impacting a point on the same car several times, or in some cases, the same point on different cars. A definite determination of the repeatability was complicated at higher impact velocities by the fact that the effective stiffness of a component changed by a noticeable amount after each impact. In an effort to minimize this effect, three series of tests were done at 10 and 20 mph (Table 4.1). These tests indicated good repeatability, although there was still a trend of increased headform response for subsequent tests, and slight dents were observed after each test. Four comparisons were then made by impacting the same point on three different cars of the same model (Table 4.2). In the Rabbit test series the comparisons were good. The Citation tests were good when comparing the left and right sides of Citation 2, but the impact to Citation 1 right upper A-pillar was considerably softer. Citation 1 had previously been used in a severe side impact test to the left side causing considerable deformation. The reduced structural integrity of the compartment is most likely the cause of this difference. The other three comparisons, however, indicated good repeatability.

TABLE 4.1

FMHF Repeatability of Single Vehicle Impacts

Test Number	Car/Impact Point	Speed (mph)	HIC	Peak Resultant Head Acceleration (G)	Peak Resultant Rotational Acceleration (rad/s^2)	Peak Resultant Rotational Velocity (rad/s)
S73052	Rabbit 1/FRR	9.06	24	26.6	3260	39.4
S73053	"	8.75	27	29.8	3770	32.2
S73054	"	9.1	31	34.3	4030	34.3
S73055	Rabbit 1/RMAP	9.49	92	57.4	6240	33.3
S73056	"	9.4	88	59.8	6110	41.9
S73058	Rabbit 1/RMAP	20.56	741	141.4	15120	67.5
S73059	"	20.0	765	147.8	16570	64.2

FRR -- Front Roof Rail
RMAP -- Right Middle A-pillar
LUAP -- Left Upper A-pillar
RUAP -- Right Upper A-pillar
SRR -- Side Roof Rail

TABLE 4.2

FMHF Repeatability on Different Vehicle Impacts

Test Number	Car/Impact Point	Speed (mph)	HIC	Peak Resultant Head Acceleration C.G. (g)	Peak Resultant Rotational Acceleration (rad/s^2)
S73080	Citation #2/LUAP	20.2	1276	228.6	20460
S73081	Citation #2/RUAP	20.4	1191	194.6	15520
S73035	Citation #1/RUAP	19.1	767	167.2	18010
S73047	Rabbit #1/SRR	9.94	119	66.6	6410
S73092	Rabbit #2/SRR	9.35	116	65.8	7450
S73058	Rabbit #1/RMAP	20.6	741	141.4	15120
S73090	Rabbit #2/RMAP	19.7	768	150.1	14670

FRR -- Front Roof Rail
RMAP -- Right Middle A-pillar
LUAP -- Left Upper A-pillar
RUAP -- Right Upper A-pillar
SRR -- Side Roof Rail

4.2 Velocity Sensitivity

Velocity sensitivity was determined by using the right middle A-pillar of a Rabbit and impacting the same point several times. The results (Table 4.3 and Figures 4.1 -- 4.4) indicated a reasonable sensitivity to velocity which was felt necessary to correlate with accident data. The responses indicated a power relation between velocity and HIC, and linear relations between velocity and C.G. acceleration, rotational acceleration and rotational velocity (at least for velocities below 20 mph). The linearity of maximum C.G. and angular accelerations is illustrated further in Figure 4.5.

TABLE 4.3

FMHF Velocity Sensitivity

Number	Impact Velocity (mph)	HIC	Peak Resultant C.G. Acceleration (g)	Peak Resultant Rotational Acceleration (rad/s**^{2})	Peak Resultant Rotational Velocity (rad/s)
S73055	9.5	92	57.4	6240	33.3
S73056	9.4	88	59.8	6110	41.9
S73057	10.8	150	69.8	7790	43.0
S73058	20.6	741	141.4	15120	67.5
S73059	20.0	765	147.8	16570	64.2
S73061	31.5	2108	210.5	19300	95.8

4.3 Pitch Sensitivity

A series of tests to determine the effect of impact orientation and impact point on the head response was performed on the Citation right-middle A-pillar. This was accomplished by increasing the angle between the impact direction and the surface of the A-pillar (Figure 4.6). Changing the pitch changed not only the initial inclination of the head with respect to the impact surface, but also the impact point on the head. Consequently, both effects are combined in the results of Table 4.4, which shows the tests grouped according to first impacts (Test Nos. 69,71,73) and second impacts (Test Nos. 70,72,74) at a given point. The first and second impact groupings were made in

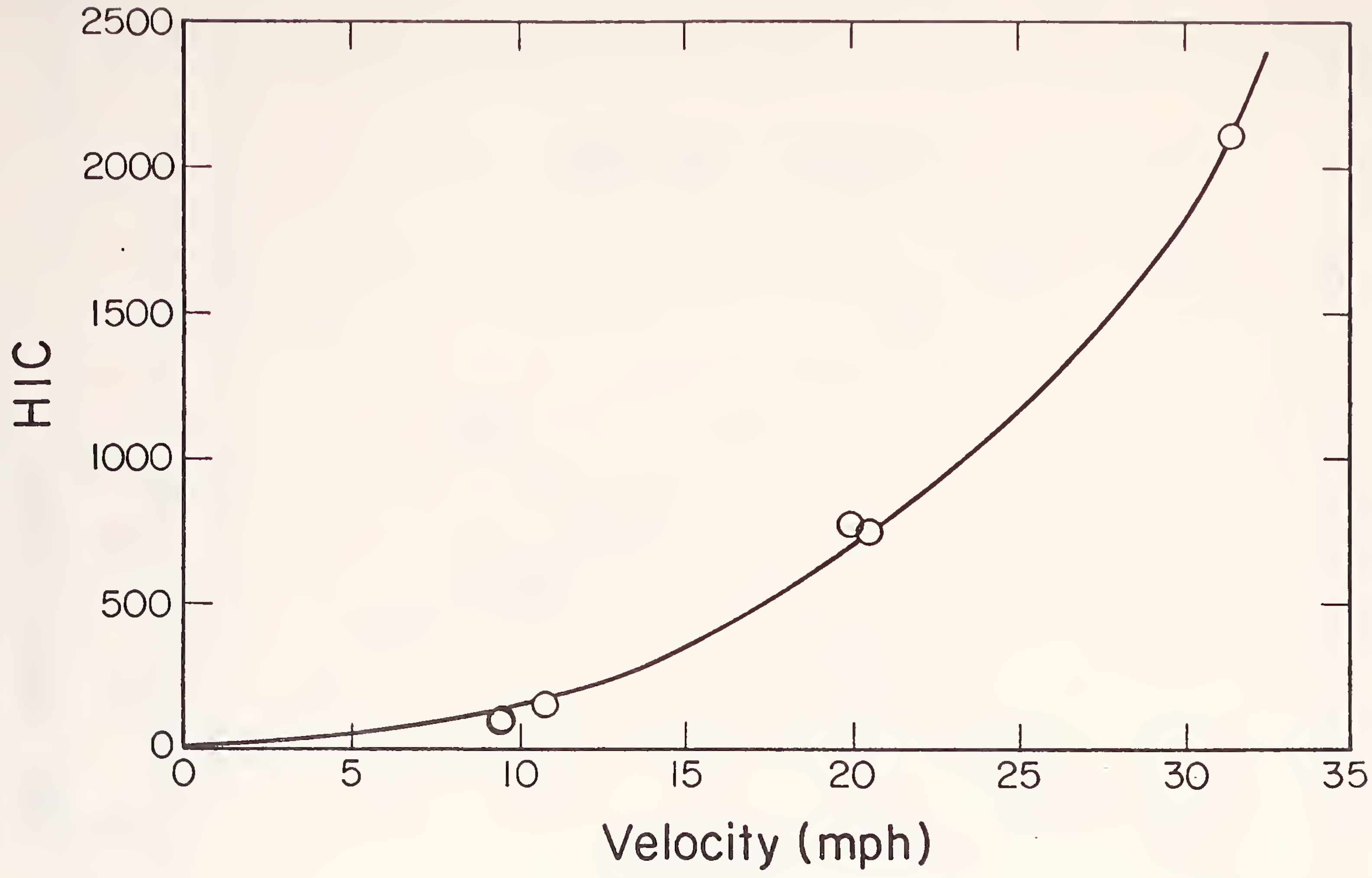

FIGURE 4.1 -- FMHF HIC Sensitivity Impact Velocity.

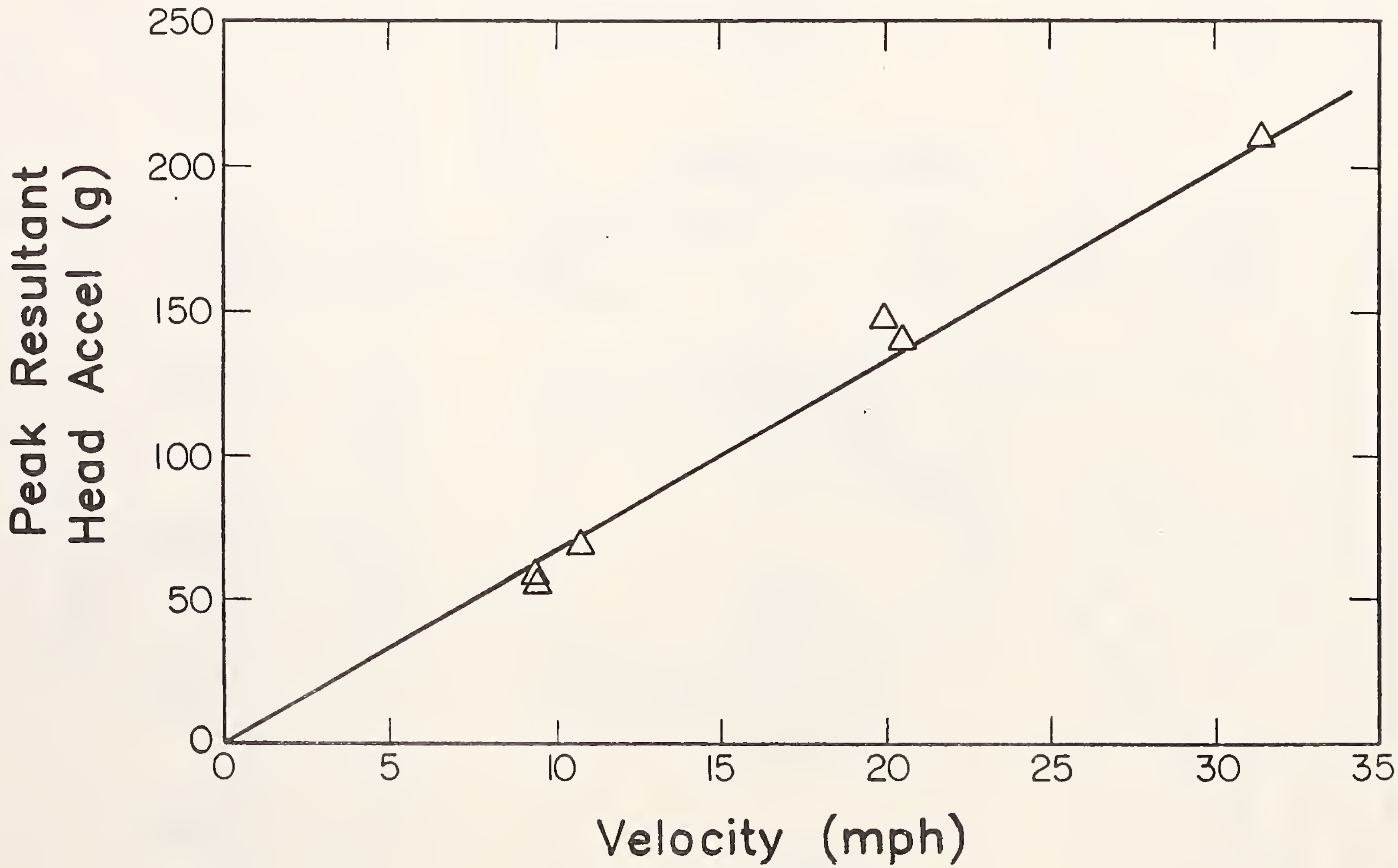

FIGURE 4.2 -- FMHF Peak C.G. Resultant Head Acceleration
Sensitivity to Impact Velocity.

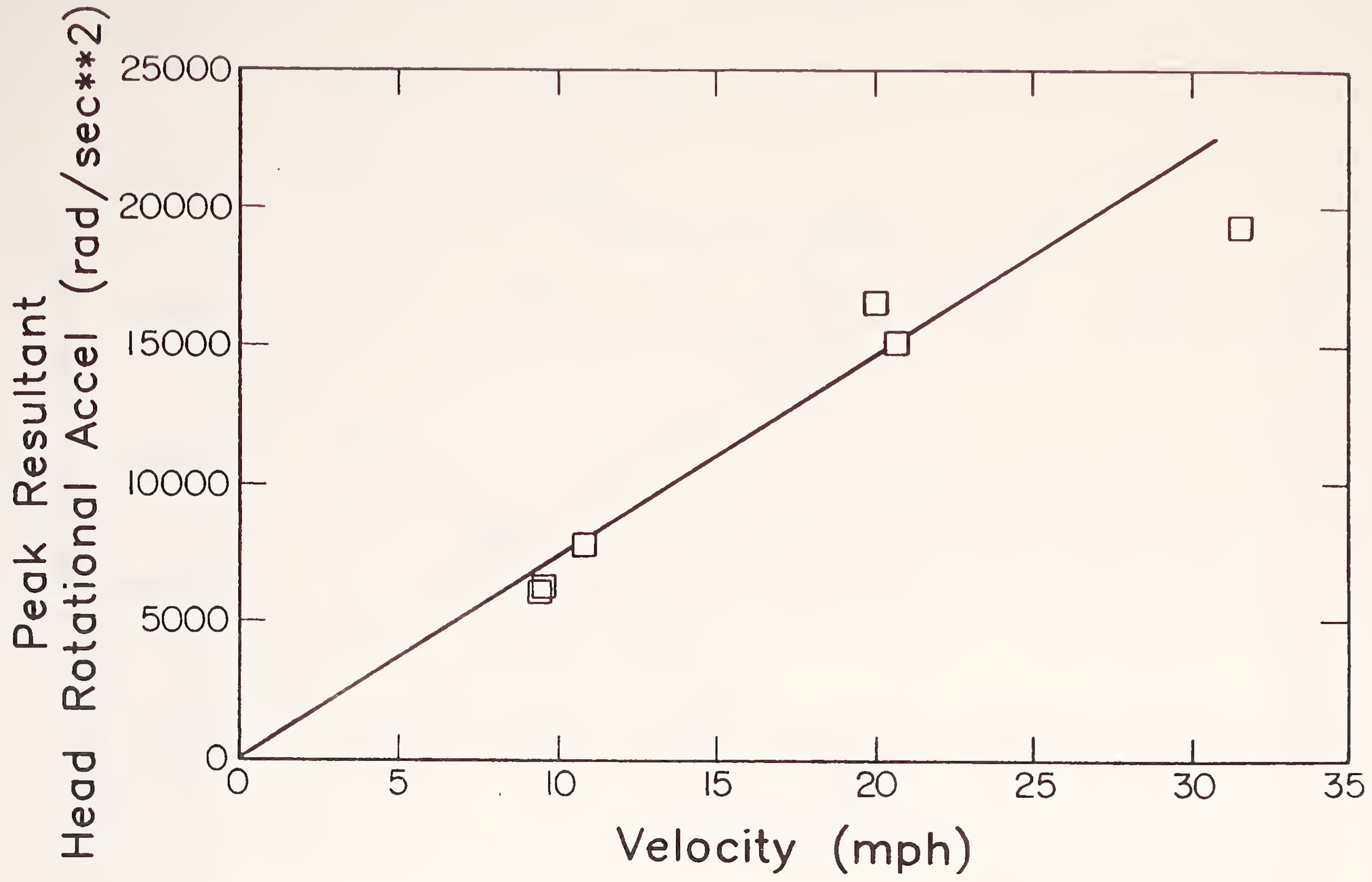

FIGURE 4.3 -- FMHF Peak Resultant Rotational Acceleration Sensitivity to Impact Velocity.

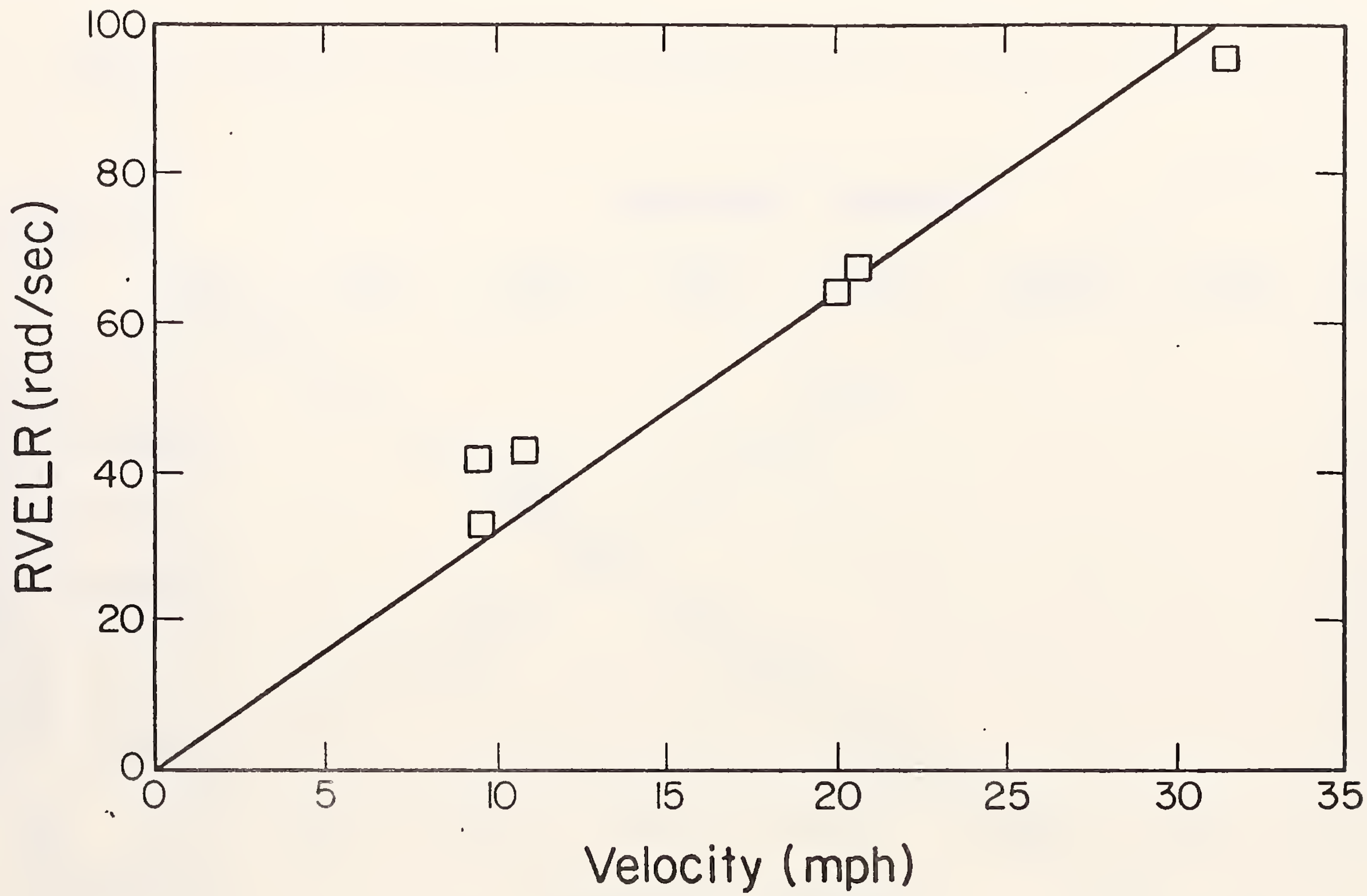

FIGURE 4.4 -- FMHF Peak Resultant Rotational Velocity Sensitivity to Impact Velocity.

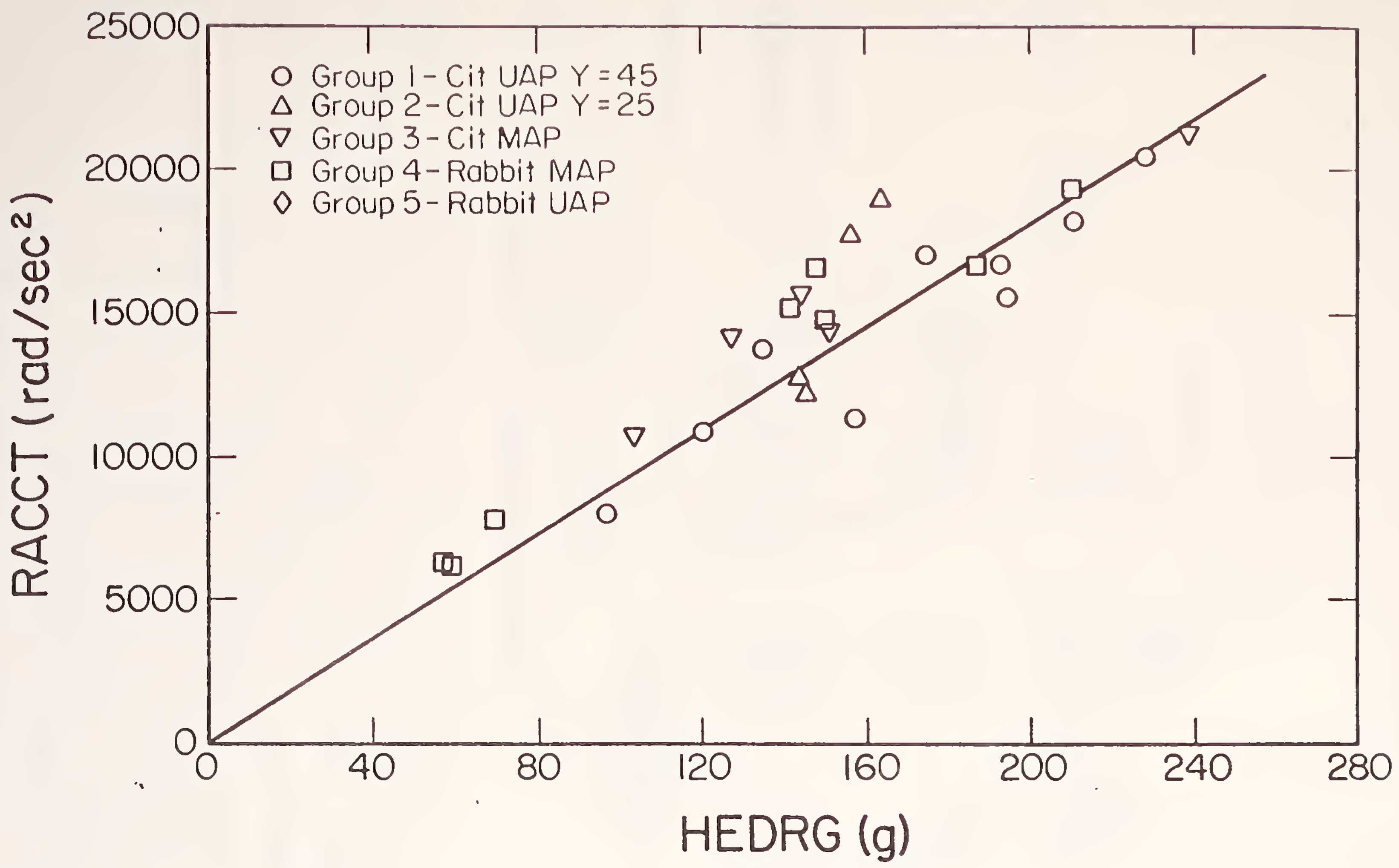

FIGURE 4.5 -- FMHF Peak Linear Acceleration Versus Angular Acceleration for Various Components.

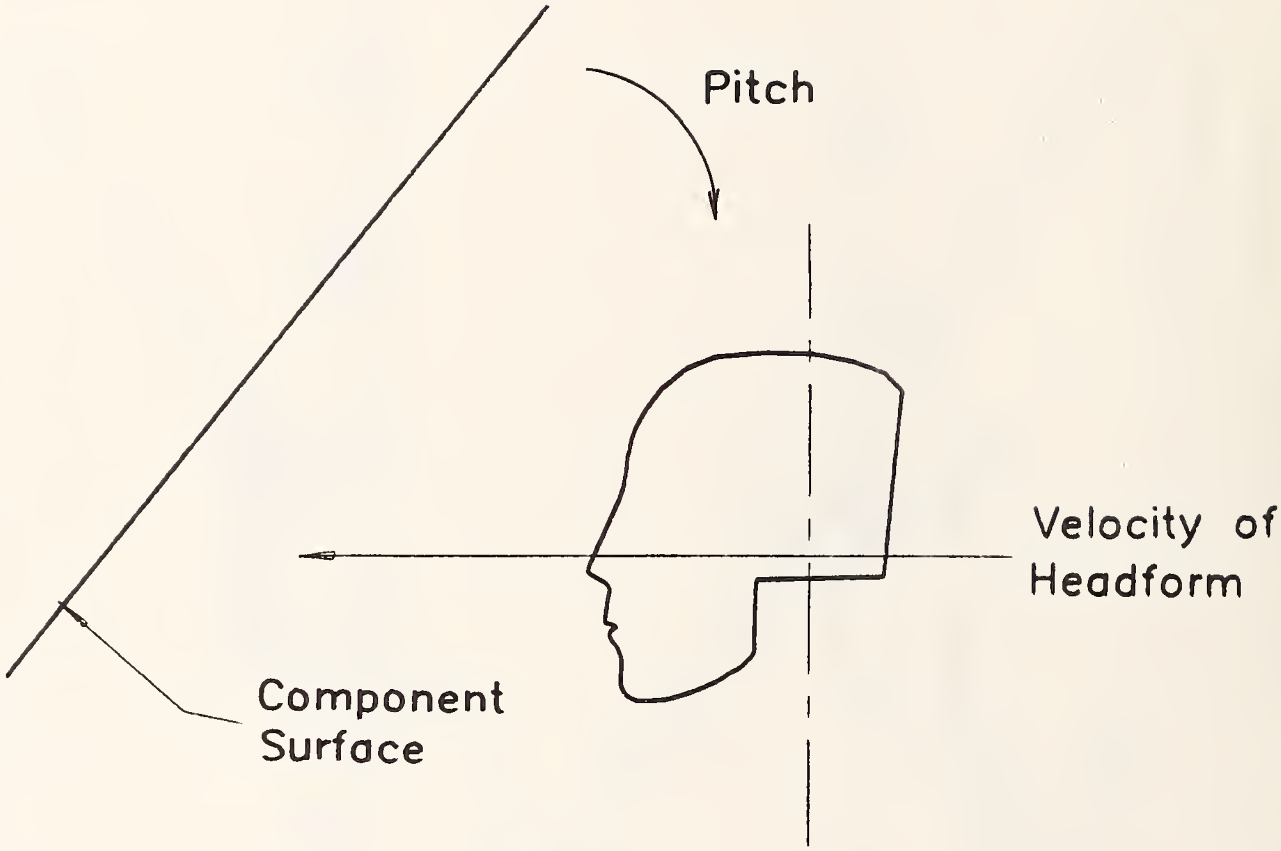

FIGURE 4.6 -- Pitch Illustration.

an attempt to distinguish the multiple impact effect discussed previously. The results indicated that decreasing the pitch (more glancing) caused lower HIC values and little sensitivity to rotational acceleration for a pitch less than 50 degrees.

TABLE 4.4

Pitch Sensitivity

Test No	Pitch* (deg)	Velocity (mph)	HIC	Peak Result. Accel. (g)	Peak Result. Rot. Accel. (rad/s^2)	HIC Normalized to 15 mph	Comments
69	62	15.3	543	124.0	7980	525	First
71	49[1]	13.4	423	108.3	10300	519	Impact
73	35	13.7	296	104.0	10720	374	
70	62	13.7	583	131.0	9020	661	Second
72	49[1]	14.8	660	147.3	13300	672	Impact
74	35	16.2	512	133.5	12240	440	

*Pitch defined in Figure 4.6.

[1]Angle for a normally seated passenger.

4.4 Vehicle Component Stiffness Sensitivity

Finally, several tests were conducted to determine the damage patterns which would be produced by various typical vehicle component impacts. This series was conducted on a Chevrolet Citation. Although the tests were done at various speeds, it was apparent (Table 4.5) that an appreciable difference in components was detected by the free-motion headform. For example, at 20 mph the HIC for the dash was 253, as compared with 900 and 1276 for the left upper A-pillar. Also, the 40 mph windshield test had a HIC far lower than the 20 mph upper A-pillar. These results were judged to be reasonable and indicated that the test method can be used to distinguish differences between components as described by Searle (3).

TABLE 4.5

Sensitivity Due to Vehicle Component Impacts

Test No	Component	Velocity (mph)	HIC	Peak Result. Rot. Accel.	Peak Result. Accel.
68	Windshield	41.2	618	8250	124
69	RMAP, Pitch 62	15.3	543	7980	124
75	Dash	21.0	253	4080	63
76	Steering wheel hub	16.2	525	7420	104
77	Steering wheel rim	16.3	166	6680	71
78	Left windshield header	14.4	161	10710	70
79	LUAP	19.9	900	16700	193
80	LUAP - 1" above #79	20.2	1276	20400	229
84	Door window ledge	30.4	1174	12900	302
85	Door window ledge (without panel)	30.5	1195	12360	270

RMAP -- Right Middle A-pillar

LUAP -- Left Upper A-pillar

4.5 Neck Influence on Head Impact Response

An obvious question which arose when designing the head as a free-motion headform was the effect the absence of the neck would have on the head response. To examine this, two tests were compared:

1) A 30 mph Ford Mustang barrier test (7) with two unrestrained 50th percentile Hybrid III dummies, one of which (the passenger) was instrumented with a 9-accelerometer array similar to the FMHF.

2) A FMHF component test at 30 mph into a Chevrolet Citation windshield.

The FMHF test used a Citation which was prepared as previously described. Figures 4.7 -- 4.12 show the head responses for the crash test Mustang passenger with those of the FMHF. Several observations were made:

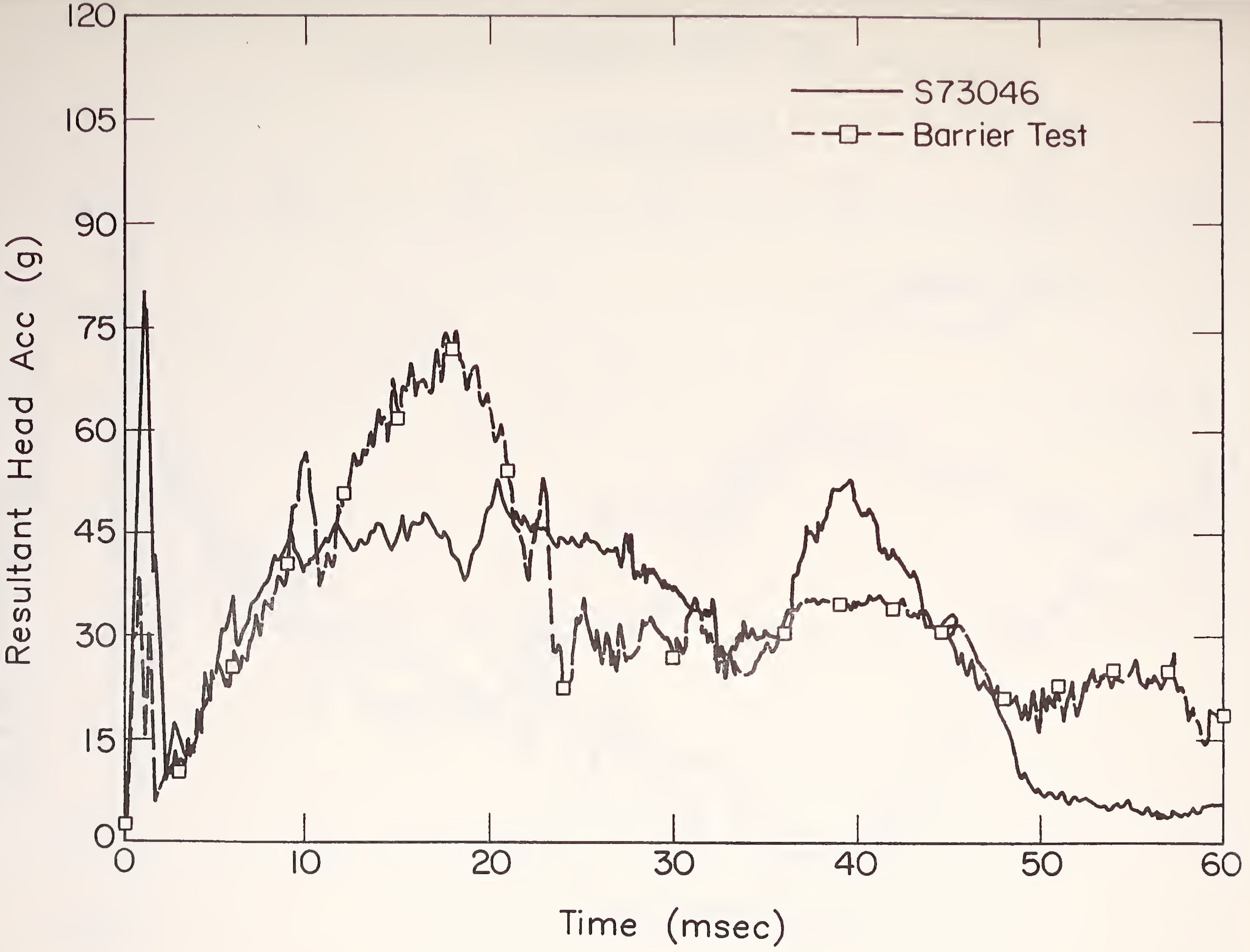

FIGURE 4.7 -- FMHF and Barrier Test-Resultant Head Acceleration Comparison.

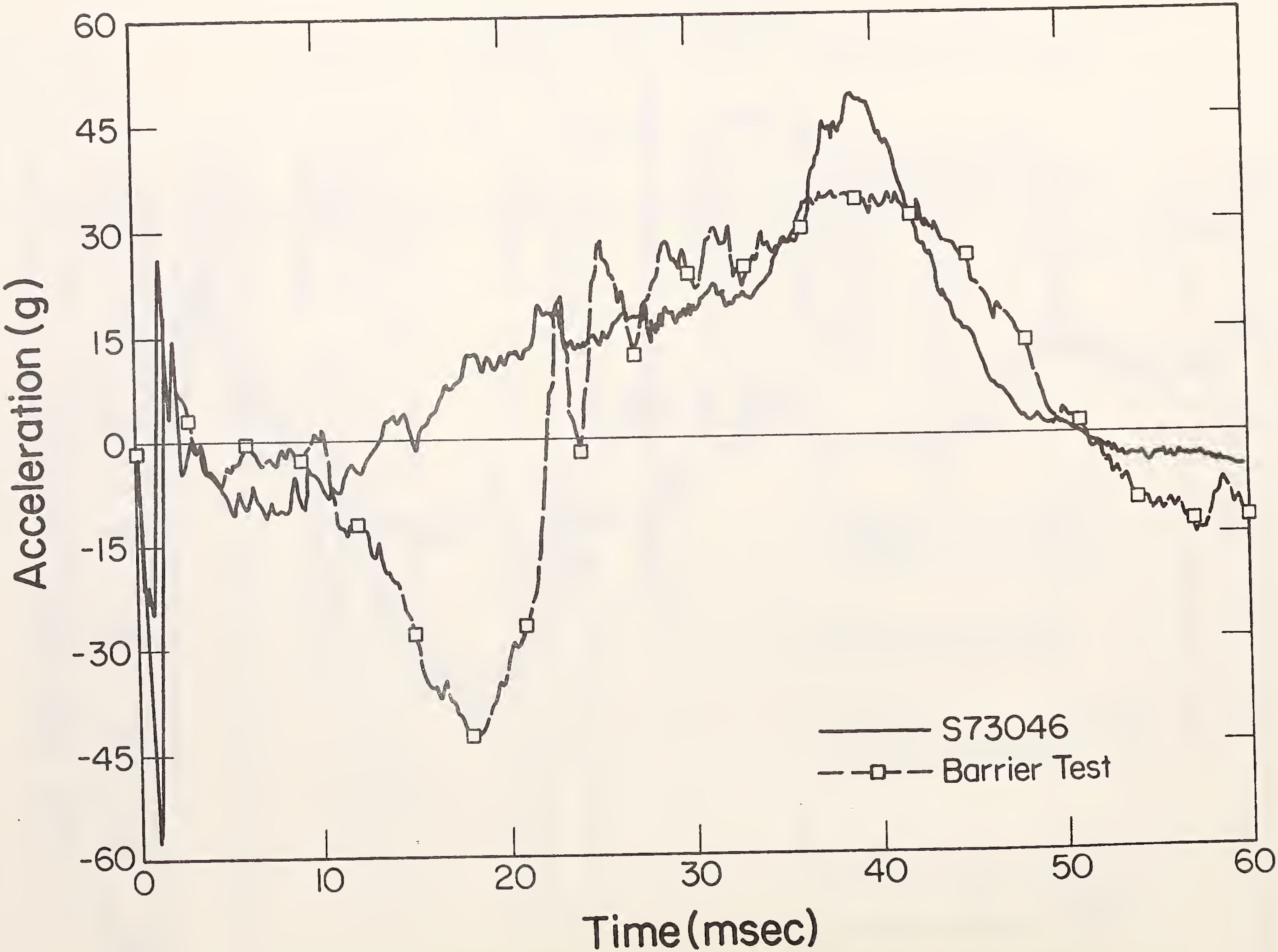

FIGURE 4.8 -- FMHF and Barrier Test-Z Axis C.G. Acceleration Comparison.

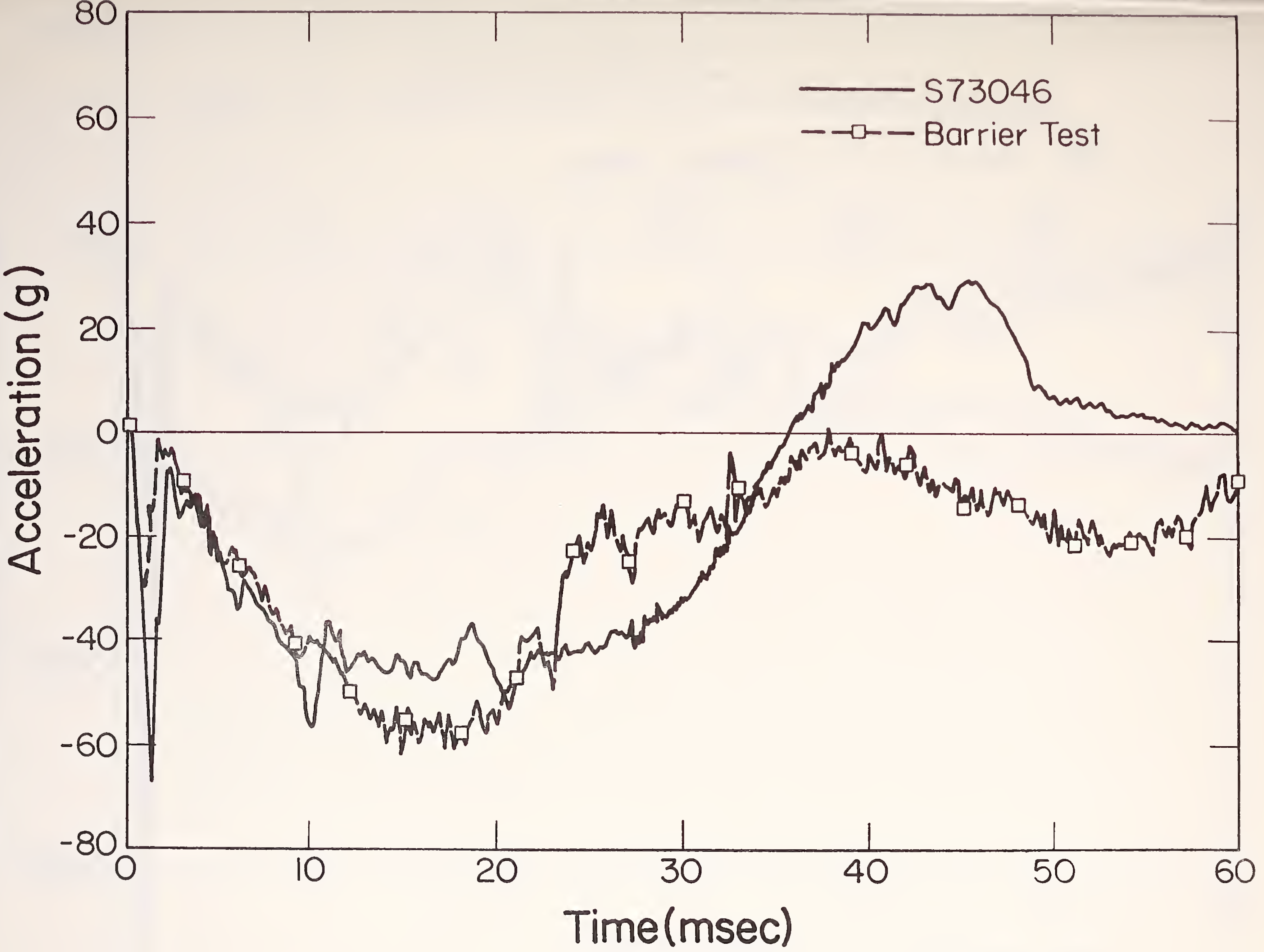

FIGURE 4.9 -- FMHF and Barrier Test-X Axis C.G. Acceleration Comparison.

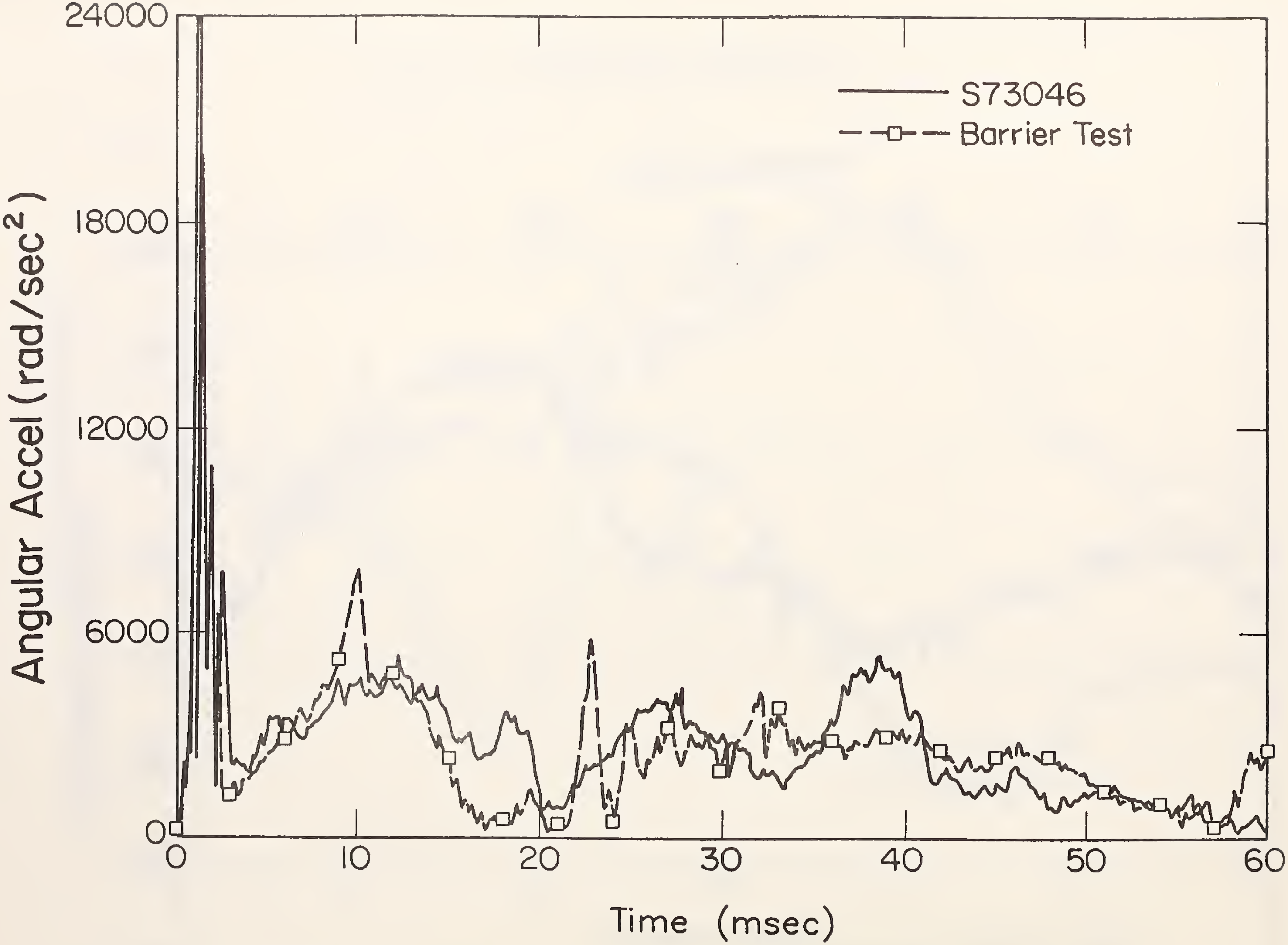

FIGURE 4.10 -- FMHF and Barrier Test-Resultant Rotational Acceleration Comparison.

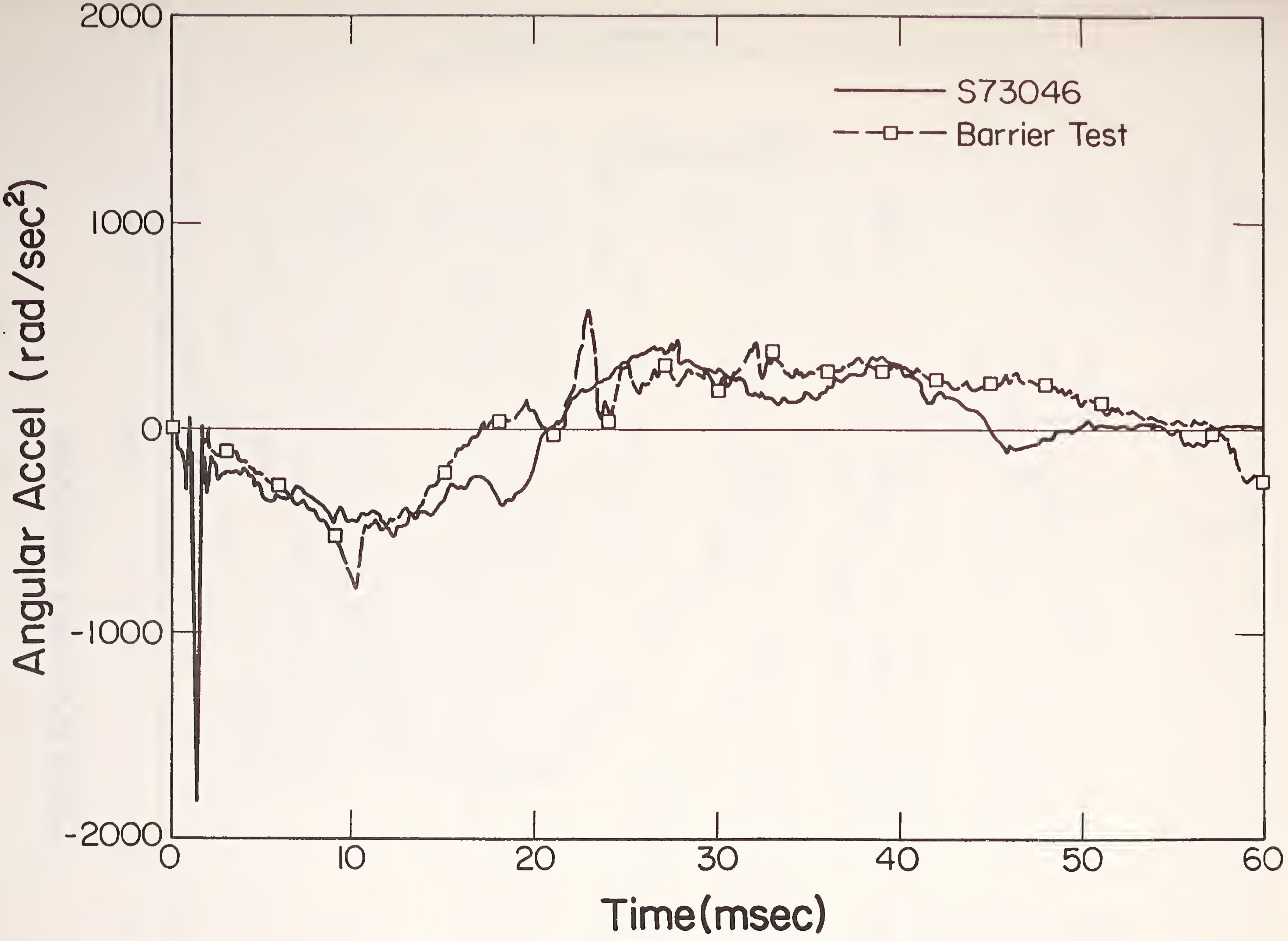

FIGURE 4.11 -- FMHF and Barrier Test-Y Axis Rotational Acceleration Comparison.

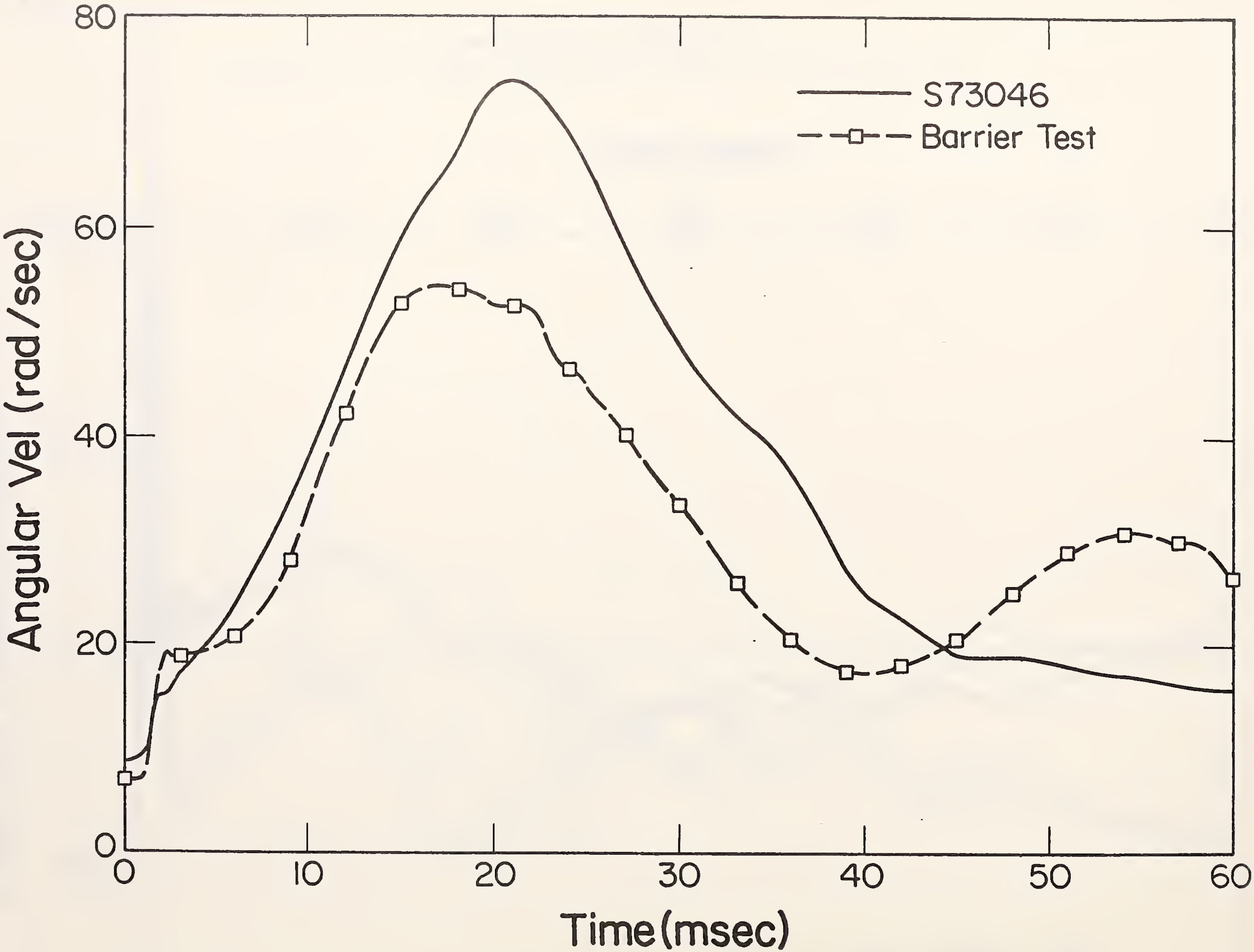

FIGURE 4.12 -- FMHF and Barrier Test-Resultant Rotational Velocity Comparison.

1) The resultant head c.g. accelerations (Figure 4.7) compare very well for the first 12 msec, and reasonably well for 48 msec.

2) The major difference in the resultant c.g. signal (from 12 to 22 msec) can be traced to the z-axis component (Figure 4.8), while the smaller deviations (from 22 to 45 msec) are a result of differences in x-axis (Figure 4.9).

3) The resultant rotational acceleration for the two tests compare very well throughout the impact (Figure 4.10) and are due primarily to the y components (Figure 4.11).

4) The form of the rotational velocity responses compare very well throughout the impact but the magnitudes begin diverging at 15 msec (Figure 4.12).

5) HIC values were very similar at 434 and 414 for the FMHF and barrier test, respectively.

6) The damage patterns for the two cases were comparable, with the barrier test having a somewhat deeper windshield bulge and the FMHF test having a somewhat more oblong bulge.

The initial peaks for both the crash and FMHF tests (Figures 4.7 -- 4.11) were due to the initial stiffness of the glass. For the first several msec after the glass was cracked, there was still considerable stiffness associated with the glass. However, it was quickly fragmented and "blown" out. The plastic laminate then became the primary element resisting the headform and the resulting force was very low. As the headform continued through the windshield, the plastic imposed a more gradual force increase.

A qualitative kinematic response comparison between the FMHF and the passenger head is illustrated in Figures 4.13a -- d. (Note that the driver head response is not a valid comparison since it contacted the steering wheel first.) As with the accelerometer data, the positions of the passenger head and the FMHF vary only slightly for the two tests. For each test, time equal to zero was taken to be the frame before initial crack propagation was observed. The passenger head was initially tipped forward slightly more than the FMHF. At 10 msec neither headform had undergone much rotation, however, the FMHF had slid down the windshield several inches. At 20 msec, the rotation of the full dummy headform as well as its motion down the windshield was noticeable but not as much as the FMHF. These comparisons continued to diverge at 30 msec, at which time the FMHF has moved approximately 3-4 inches further down the windshield and rotated roughly 30 more degrees than the full dummy headform.

The cause of the response differences appears to be associated with the neck loading as shown in Figures 4.14 -- 4.16. During the first 10 msec the crash test passenger neck forces in the X and Z directions were relatively low, actually passing through zero at 10 msec. During this time interval the head response comparisons were quite good. There followed a rapid rise in the neck forces which peaked around 20 msec. These correspond directly to the divergence in the head z and x axis accelerations (Figures 4.8 and 4.9). It is interesting to note that the neck forces apparently have only a minimal effect on the headform rotational acceleration (Figures 4.10 and 4.11), but that the rotational velocities diverged after about 16 msec (Figure 4.12).

In general, this correlation was judged to be very good and indicated that reconstructions with the component headform would be able to simulate actual head impacts. Whether such correlation can be expected on other vehicle components is unknown. Since other component impacts are typically of much shorter

FIGURE 4.13a -- FMHF and Barrier Test-Position Comparison,
0 msec.

FIGURE 4.13b -- FMHF and Barrier Test-Position Comparison, 10 msec.

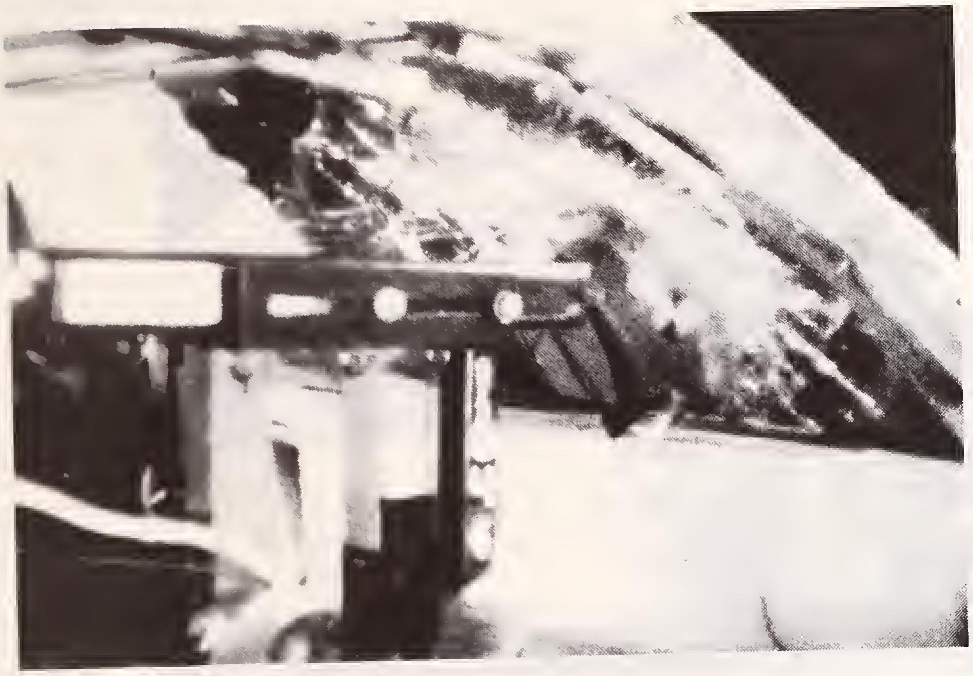

FIGURE 4.13c -- FMHF and Barrier Test-Position Comparison, 20 msec.

FIGURE 4.13d -- FMHF and Barrier Test-Position Comparison, 30 msec.

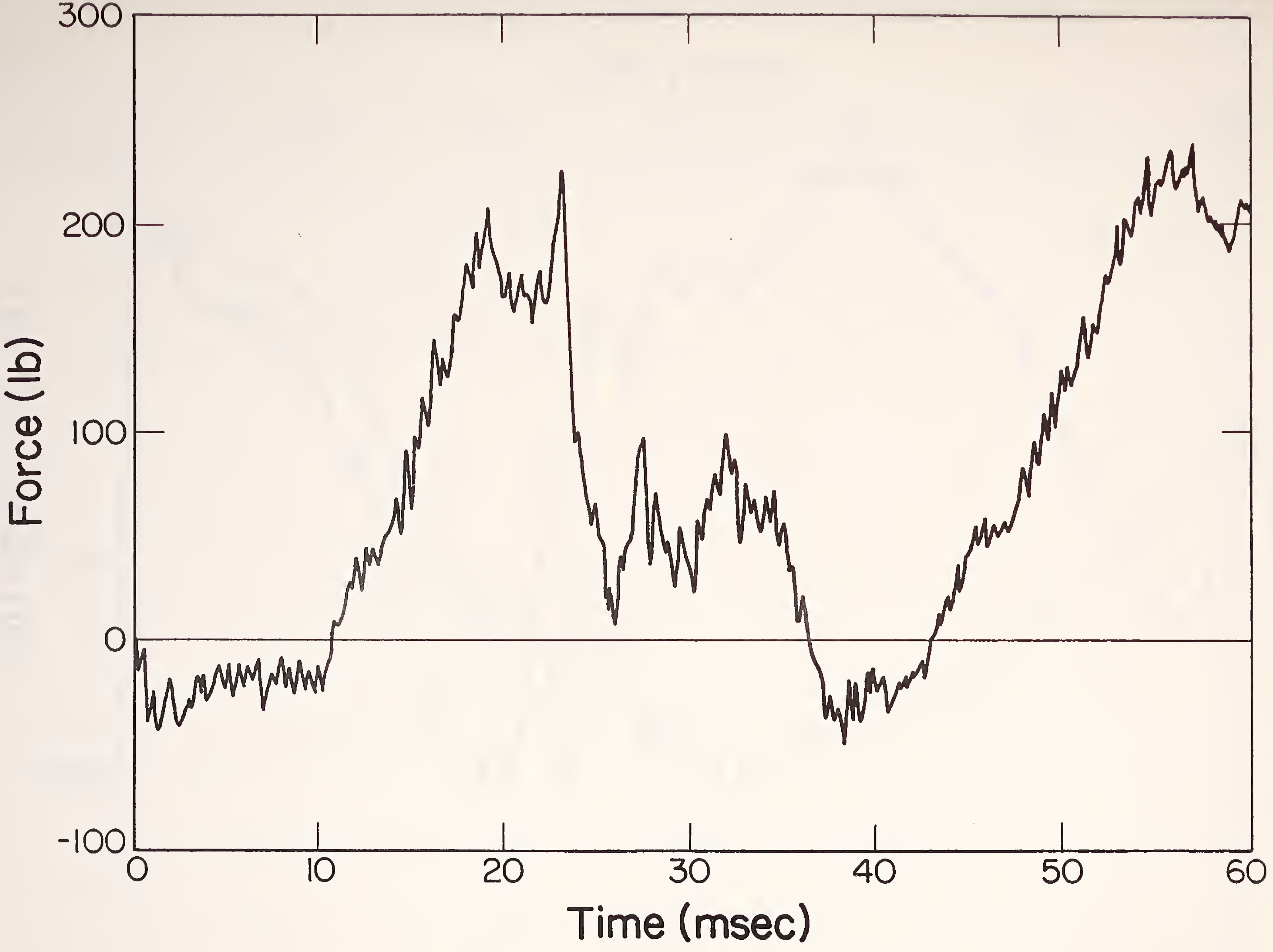

FIGURE 4.14 -- Hybrid III Crash Test Dummy Neck X-Axis Force.

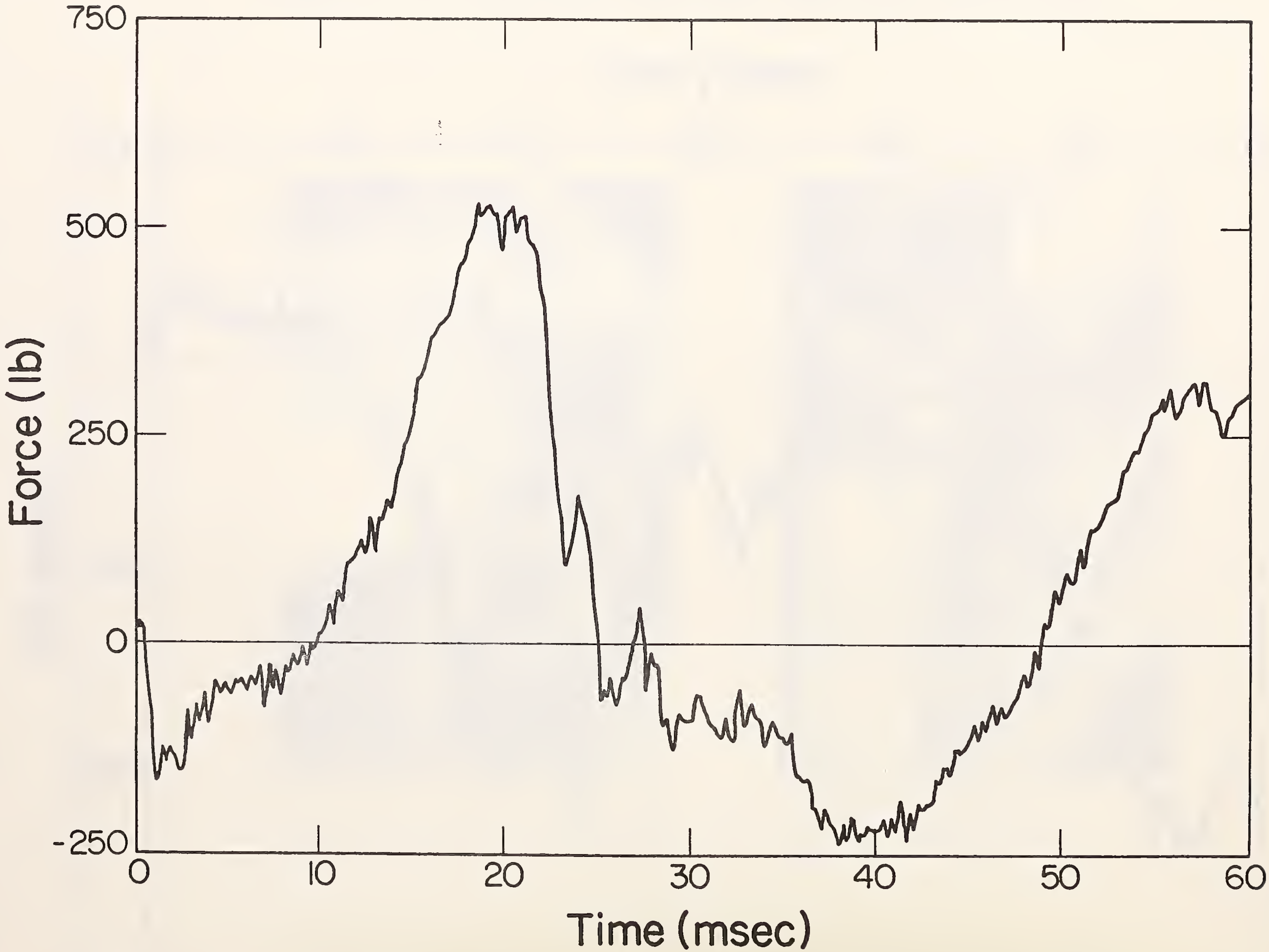

FIGURE 4.15 -- Hybrid III Crash Test Dummy Neck Z-Axis Force.

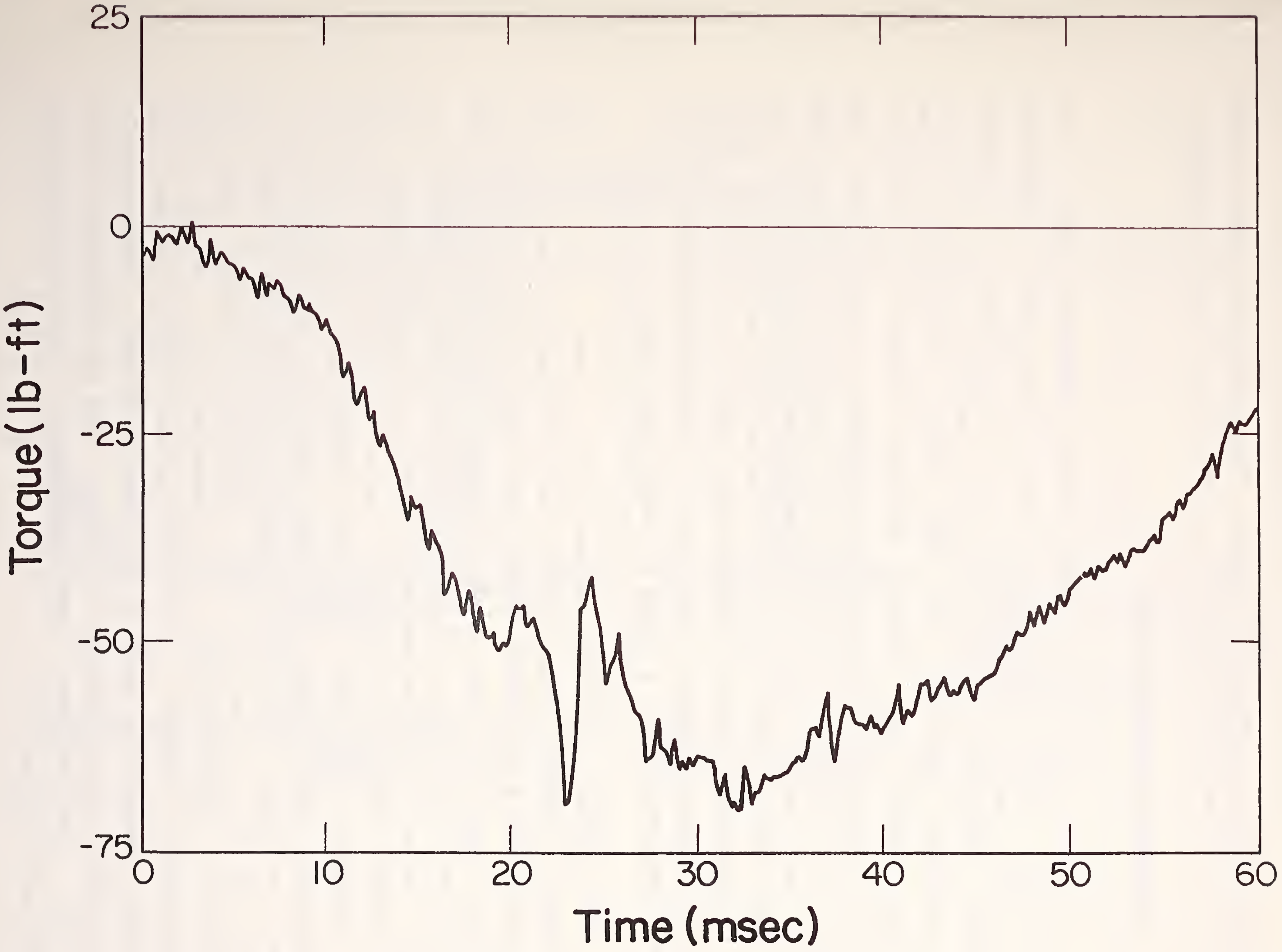

FIGURE 4.16 -- Hybrid III Crash Test Dummy Neck Y-Axis Moment.

duration than windshield impacts, the correlation might be expected to be better since the neck involvement would be reduced.

5.0 ACCIDENT RECONSTRUCTIONS

Accident reconstruction was the most important phase of the feasibility study. The primary goal in the accident reconstuction phase was to determine the relation between the measured headform response and the injuries observed in the accidents. This section describes the steps taken to reconstruct three accident cases. The results were not intended to determine a definite relation between headform response and head injury, but merely to indicate if reconstruction of interior occupant head impacts was feasible, and if the results were consistent with the observed injury. The approach in selecting the accident cases for reconstruction was to review those cases from the Washington Hospital Trauma Center which were investigated and to select three, preferably with a range of head injury severity levels.

The special accident investigation teams following the Washington Hospital case studies had performed 34 head and neck accident studies for NHTSA. These were evaluated for reconstructability based on the observed damage pattern due to head contact, and the level of injury. Of those cases, 10 reported no damage pattern, 9 contained head damage patterns which could not be isolated from other effects, 4 were discarded due to primary head contact with more than one component, 5 resulted in no significant head injury, and 3 were discarded for other miscellaneous reasons. The three cases selected resulted in head AIS levels of 2, 3, and 5. The components impacted were the windshield, windshield/hood, and passenger door. The pertinent investigation results and the reconstruction process are described below for each of the three accidents. The accident descriptions are paraphrased directly from the accident reports (8,9,10). The accident case information from the reports is summarized in Table 5.1.

TABLE 5.1
Accident Reconstruction Case Information

Subject Vehicle	1982 Dodge Aries	1983 Chevrolet S-10 Pickup	1974 Plymouth Duster
Impacted object	Concrete Post	Chevrolet Chevelle	Cadillac Coupe deVille
Pre-crash velocity (mph)	15	---	18.5
Delta-V (mph)	14	44	25.2 (lateral)
Principal Direction of Force	11-12 O'clock	12 O'clock	3 O'clock
Subject Occupant			
- Sex	M	M	M
- Age	52	32	74
- Weight	170 lb	170 lb	150 lb
- Height	72 in	67 in	71 in
- Seating Position	Driver	Driver	Driver
- Restraint	None	None	lap & shoulder belt
- Head AIS	2	3	5
- Head Injury Description	Concussion with loss of consciousness less than one hour limited amnesia; chin and left frontal scalp lacerations.	Posterior frontal lobe contusion; cerebral edema.	Bilateral parietal-temperal frontal cerebral contusions & hematoma, corpus callosum hematoma, clinical basical skull fracture with bilateral hemotypanum. Intraventricular bleed 3rd and lateral ventricals bilaterally including occipital horns.
- Other major injuries	Right rib fractures; spleen, liver, and hepatoduodendal ligament lacerations.	Fracture of right ribs 3-8; liver laceration; sigmoid colon hematoma, fracture of left femur and tibia.	Myocardial, small bowel mesenteric, pancreatic, cecal, and ileum contusions.

5.1 Dodge Aries Case

This case was selected for reconstructin since it represented a less severe injury from the Washington Hospital Study for which the damage pattern was available.

5.1.1 Aries Accident Description

The case vehicle, approaching the main gate of a facility, drifted out of its lane. The left wheels climbed a curb and the vehicle collided head-on with a concrete post protecting the gate's guard station. The subject, driver of the Aries, was probably in a normal seated position precrash. At impact, he was thrown forward, to the left and slighty upward. His forehead and chin contacted the windshield causing the lacerations and concussion (Figure 5.1). The right side of his abdomen contacted the steering wheel, collapsing the column one half inch and causing his rib fractures and abdominal injuries.

5.1.2 Aries Accident Reconstruction

A damaged 1982 Aries was obtained for the reconstructions. Two tests were conducted on each windshield (driver and passenger side impacts) prior to replacement with a new windshield.

In reconstructing this accident, the impact velocity was the only parameter treated as an unknown. The impact orientation was horizontal and directed from the position of a normally seated occupant to the impact point on the windshield. It should be noted that the initial impact point represented by the center of the crack pattern in Figure 5.1a, is at the top of the bulge shown in Figure 5.1b. A summary of the reconstruction attempts is given in Table 5.2. The first test was at 14.8 mph, approximately the delta-v of the crash, and produced no damage. After performing a series of tests, the damage pattern was judged

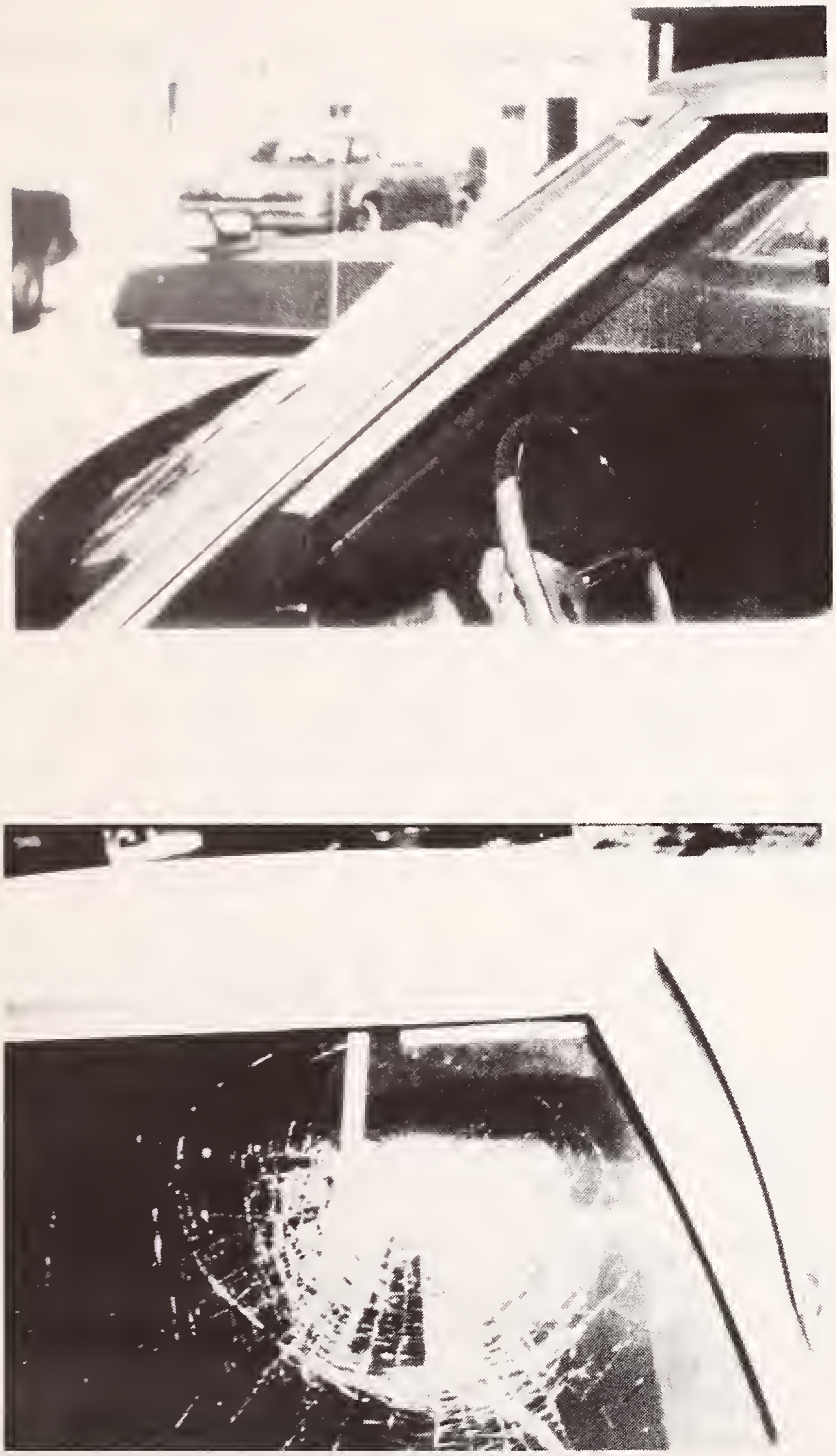

FIGURE 5.1 -- Aries Accident Damage Pattern.

TABLE 5.2

Dodge Aries Reconstruction Attempts

Test Number	Velocity (mph)	HIC	Peak Resultant Rotational Acceleration (rad/s^2)	Peak Resultant Rotational Velocity (rad/s)	Comment
S73093	14.8	236	10290	51.5	No cracks in windshield
S73094	20.1	394	13410	64.8	No cracks in windshield
S73095	30.8	405	59270	89.3	Too severe
S73096	25.9	536	60710	81.9	Too severe
S73097	22.9	291	55410	93.0	Good

to be satisfactory at an impact speed of 22.9 mph (Figure 5.2). As observed in Figure 5.2 the FMHF produced a somewhat more oblong damage pattern than the actual accident due to rotating and sliding down the windshield. The patterns were compared on the basis of maximum depth. Since the only documentation of the accident damage pattern was Figure 5.1, it was difficult to determine exactly how closely the reconstruction actually compared. However, since the damage in test S73096 was noticeably more severe than S73097 (1 inch deeper than the 1/2 inch bulge of S73097) and test S73094 produced no crack at all, it was felt that S73097 was reasonably close to the optimum impact velocity. In view of the good correlation seen in the previous section between the full Hybrid III dummy and the FMHF, this accident reconstruction was considered to be a good representation of the accident. The unusually high value for resultant rotational acceleration occurred during the first 3 msec of the impact and was due to the initial spikes commonly associated with windshield impacts. The acceleration responses for reconstruction test S93097 are contained in Apendix B.

5.2 Chevrolet S-10 Case

This was a severe head-on collision in which the driver contacted both the windshield and the hood as it was folded up against the windshield (Figure 5.3). Although the occupant head did impact two components, this case was selected due to the good documentation of the damage pattern (the damaged hood was available).

5.2.1 S-10 Accident Description:

The S-10 pickup was traveling westbound in the 2nd eastbound lane of a divided roadway, and a Chevelle was traveling eastbound in the same lane. The vehicles impacted in a head-on configuration, with the entire frontal plane of the S-10 experiencing direct contact. Responding to the 12 o'clock impact force, the

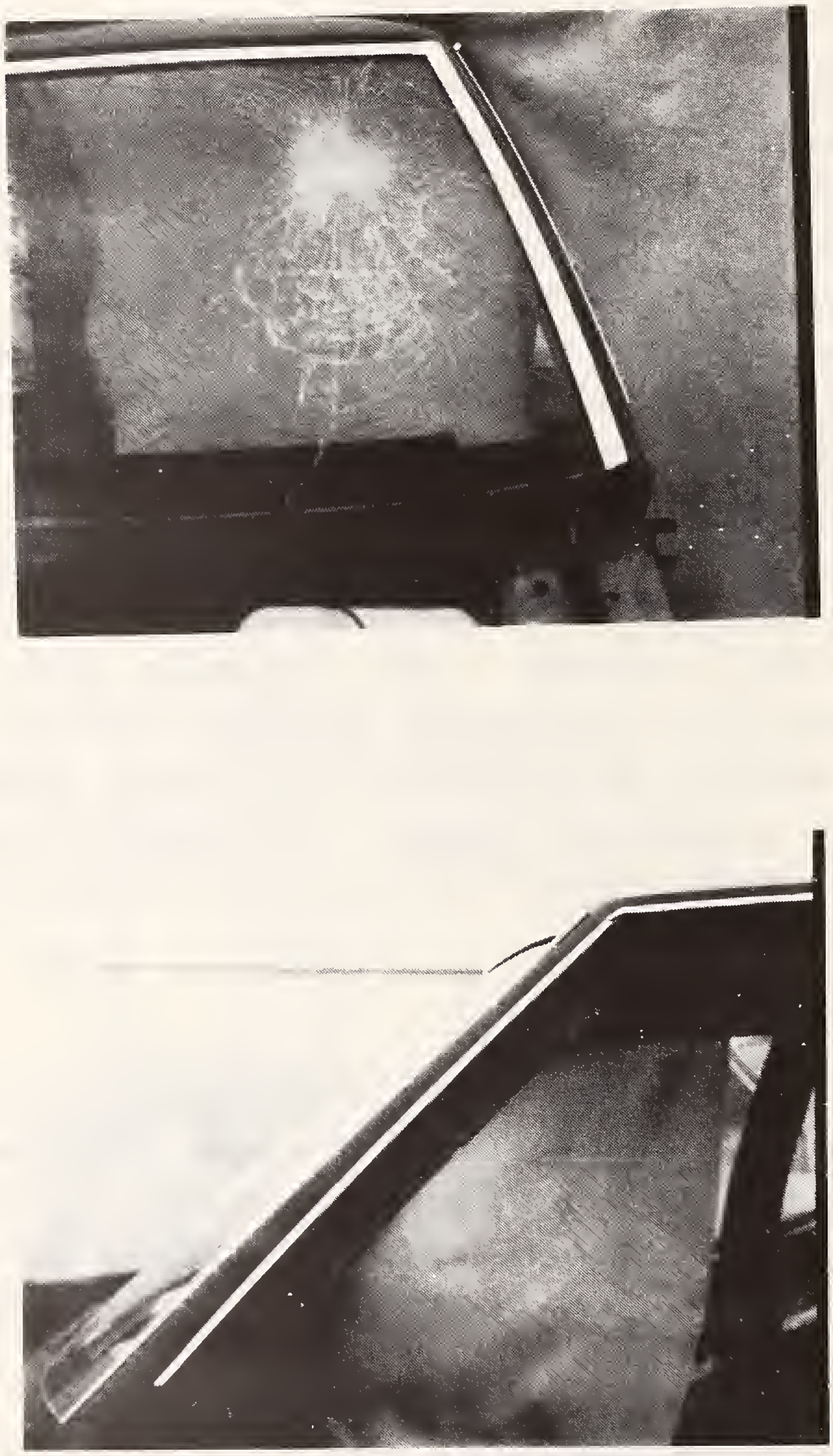

FIGURE 5.2 -- Aries Reconstruction Damage Pattern.

FIGURE 5.3 -- S-10 Accident Damage.

case occupant moved directly forward. It is likely that the case occupant's head rotated slightly downward due to deceleration of the torso as the steering column stroked. His head and face contacted the windshield, which presumably (judging from crash tests) was in a flexible state as a result of being cracked by the vehicle crush. Based upon the accident damage (Figure 5.3), the accident investigation team concluded that the hood was positioned against the windshield at the time of occupant loading and was subsequently impacted by the occupant's head.

5.2.2 S-10 Accident Reconstruction

The cab of a wrecked S-10 pick-up was obtained for the reconstructions. As in the Aries reconstructions, two tests were conducted on the windshield and hood prior to replacement.

In reconstructing this accident there were initially three unknown parameters: 1.) the impact velocity, 2.) the placement of the hood relative to the windshield, and 3.) the method of restraining the front of the hood. As can be seen in Figure 5.3, the head impact point on the hood was very near a sharp bend. The left A-pillar had been crushed back severely, producing some damage to the windshield. It was felt the fold in the hood would affect the stiffness at the impact point, so all hoods were bent prior to conducting the reconstruction attempt. To simulate the vehicle engagement of the accident, the front edge of the hood was rigidly secured (Figure 5.4). The cab was placed on rubber mats and 500 lbs of ballast were placed inside to eliminate cab movement. The windshield was also cracked before each test to better simulate the accident windshield damage which was likely.

A summary of reconstruction attempts is given in Table 5.3. Crash and sled test results with unrestrained dummies indicate that the head impact velocity with the windshield is approximately 75-90% of the vehicle delta-v. The reconstruction impact velocity was nominally set, therefore, at 37 mph (85% of

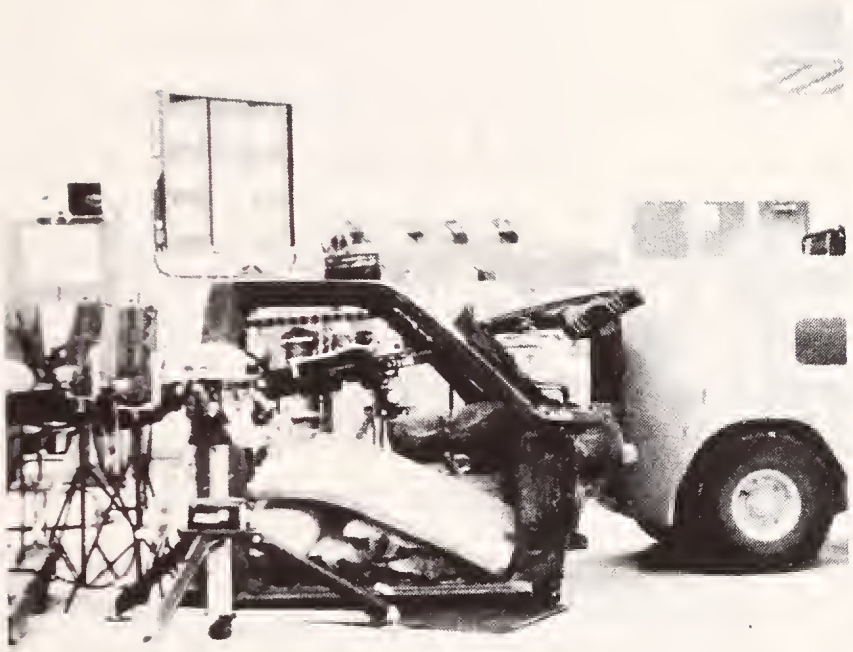

FIGURE 5.4 -- S-10 Reconstruction Apparatus.

TABLE 5.3

Chevy S-10 Reconstructions

Test Number	Velocity (mph)	Gun Pitch (deg)	Distance of Hood From Windshield (inch)	HIC	Peak Resultant Rotational Acceleration (rad/s^2)	Comment
S73099	37.9	32	3-1/2	1720	19600	Broad shallow dent in hood
S73100	--	--	--	--	--	Gun malfunction
S73101	38.6	15	3-1/2	1911	55730	Broad shallow dent in hood
S73102	35.8	15	1	3308	86130	Hit somewhat high, on the fold of the hood rather than beneath it
S73103	36.5	10	1	1787	53380	Judged to be good, see Figures 5.5, 5.6
S73104	36.3	10	1	1795	24460	Judged to be good, see Figures 5.5, 5.6

the accident delta-v). Initially, the spacing between the hood and windshield was set at 3 1/2 inches. It appeared that with this spacing, any combination of other parameters would cause the headform to rotate during windshield impact and contact the hood with its full face rather than the forehead. The first two reconstruction tests, S73099 and S7101, resulted in a hood dent which was broad and shallow rather than the local deformation observed in the accident. By placing the hood as close to the windshield as possible (about 1 inch) the hood was impacted by the forehead and a closer resemblance to the accident deformation was obtained. Slight adjustment of the headform orientation was required to duplicate the damage location. The speed required to obtain a satisfactory dent reproduction was found to be 36.5 mph. Tests S73103 and S73104 were both done at this nominal speed, one on each side of the same hood, to check repeatability. Figure 5.5 shows the contours of the two reconstructions and the original dent. These were measured from right to left across the deepest section of the dent using a construction contour measurement device. Test 103 had a compact dent such as the original, but was not as deep (Figure 5.3, 5.5 and 5.6), while test S73104 had a broader shape than the original but was of the correct depth. It was difficult to determine which better represented the accident. The responses of both were very similar. Consequently, the average values of these tests were used as the reconstruction results. The acceleration responses for these two reconstruction tests are contained in Appendix C. The windshield damage for these tests did not appear to be as severe as in the accident case, but the accident windshield was not well documented and the importance of reproducing the glass deformation was not considered to be critical to the results.

In summary, this accident reconstruction required that several assumptions be made regarding the impact velocity, hood placement and restraint, and initial hood deformation. Considering these factors, the damage pattern appeared to have been duplicated quite well.

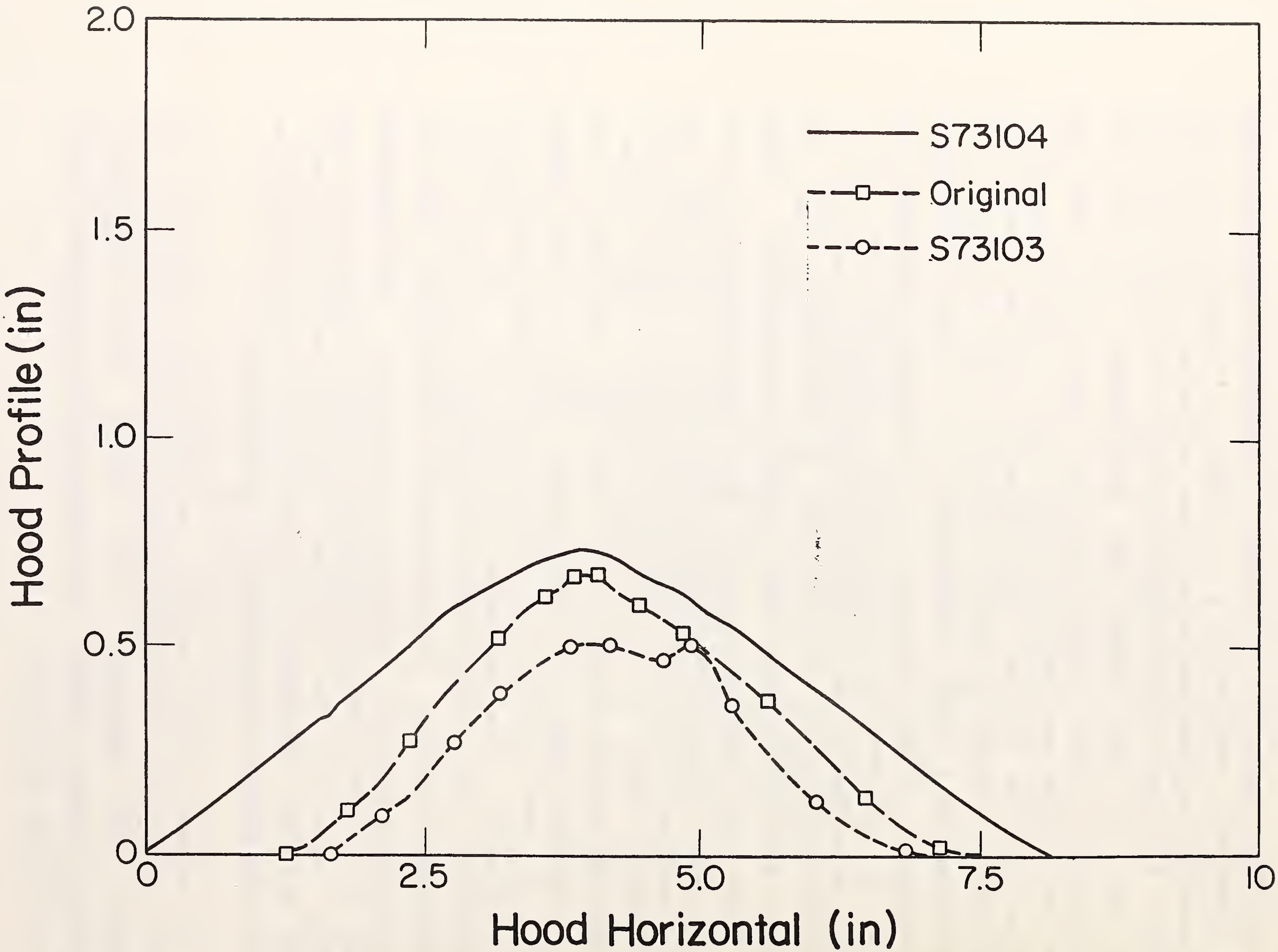

FIGURE 5.5 -- S-10 Reconstruction Contours.

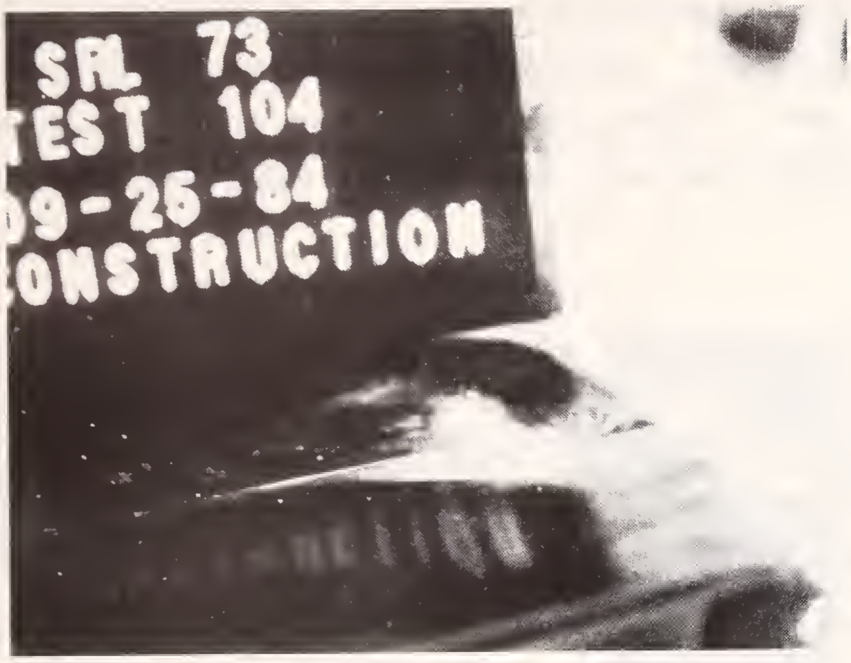

a) Test S73104

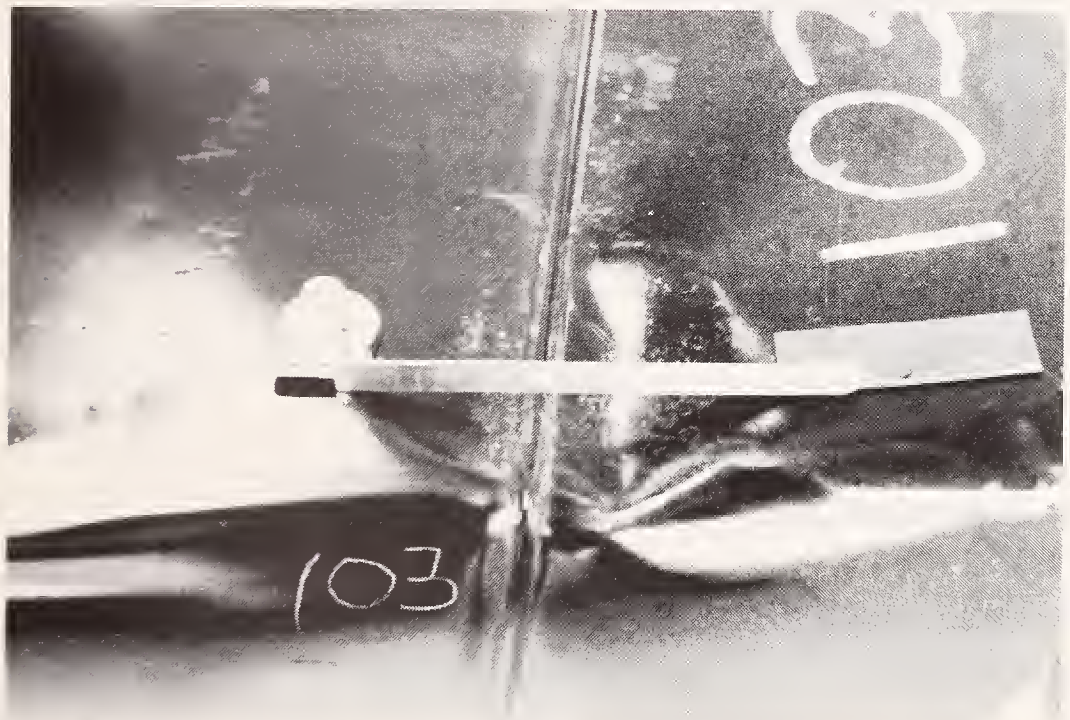

b) Test S73103

FIGURE 5.6 -- S-10 Reconstruction Damage Patterns.

5.3 Plymouth Duster Case

This case was selected due to a relatively high injury level (head AIS=5) and the fact that the head contacted a different component, the door. The door which the occupant hit was available, but the damage pattern due to the head contact was not very extensive.

5.3.1 Accident Description

The subject vehicle, a 1974 Plymouth Duster, was traveling through an intersection at an estimated pre-impact speed of 20 mph. A 1969 Cadillac, which was traveling at a calculated speed of 51.7 mph, skidded and then impacted the Duster broadside on the right side (Figure 5.7). The Duster was contacted near its center of gravity and rotated slightly. In response to the three o'clock direction of force, the three-point belted case occupant (driver) was displaced to his right causing him to slide laterally across the seat cushion. His three-point belt system most likely restrained his pelvic motion allowing rotation of his torso. The right side of his head contacted the right door window sill (Figure 5.8). The accident investigation indicated that an intrusion of 14.5 inches occurred on the Duster right door.

5.3.2 Accident Reconstruction

The observed damage pattern on the door due to the head impact consisted of: 1.) a slight crack on the plastic cover (Figure 5.8); 2.) a backward bend of a metal tab intended to support the plastic (Figures 5.8 and 5.9); and 3.) a slight dent in the metal window sill (Figure 5.10). The window sill dent illustrated in Figure 5.10 was the horizontal dent. There was also a verical dent of approximately the same magnitude. The

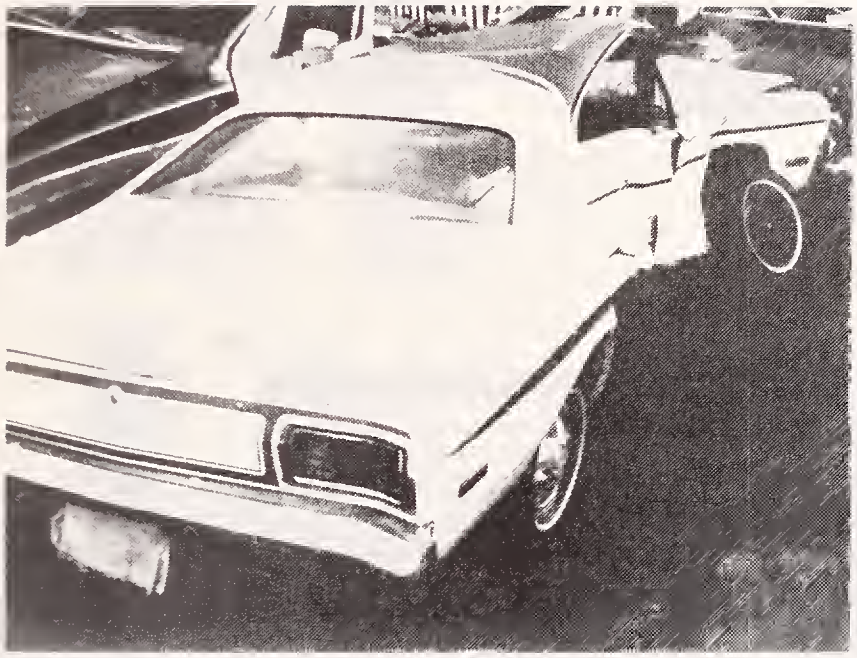

FIGURE 5.7 -- Duster Accident Damage Pattern.

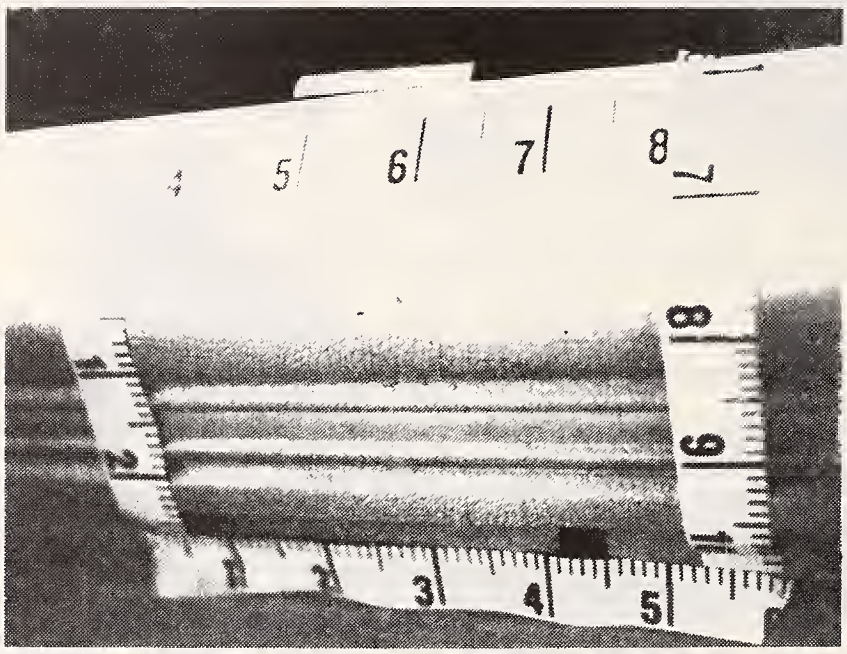

FIGURE 5.8 -- Head Contact Area on Right Front Door.

FIGURE 5.9 -- Window Sill Plastic Covering and Support Tab Accident Damage.

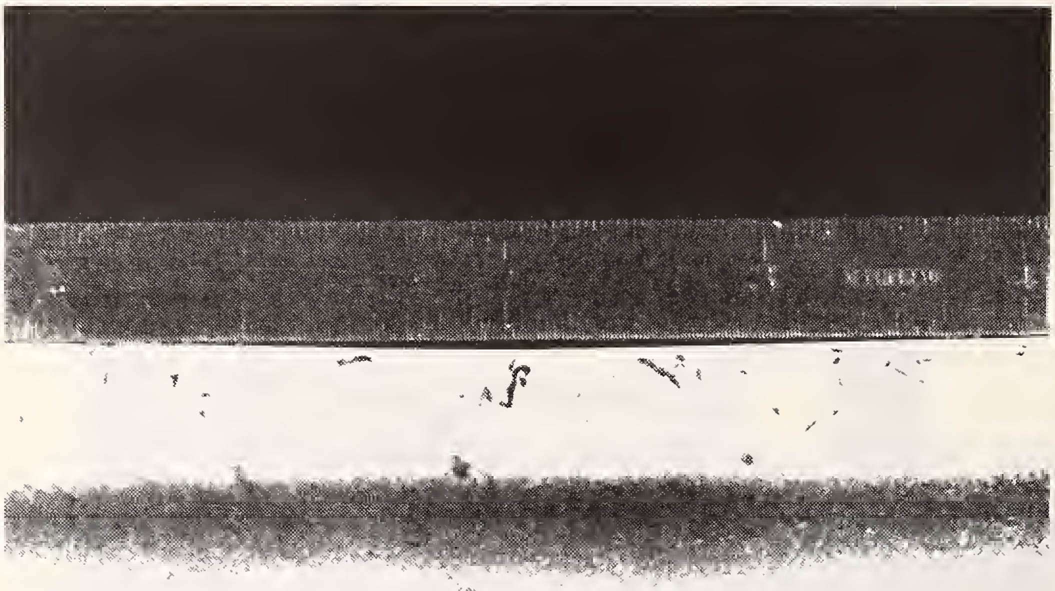

FIGURE 5.10 -- Metal Window Sill Dent.

intrusion of the impacting car caused substructure in the door to contact and effectively support the inside panel during head impact, with the main supporting component being a vertical metal rod about 6 inches behind the impact point. Broken window glass was between the metal and plastic at the imact point and became embedded in the plastic producing the bulge seen in Figure 5.8.

To reconstruct the accident, doors were placed in a framework designed for component test work (Figure 5.11). The supports were added to simulate the substructure effects mentioned above. No additional attempt was made to simulate the intrusion or door substructure crush.

The unknown variables adjusted in the reconstruction were the impact velocity and the angle of impact relative to the door. The occupant head contact point was on the right side of his head as evidenced by an abrasion over his right ear. This impact point could not be obtained with the FMHF. A point on the FMHF face which was the same distance vertically from the c.g. of the head as the occupant head impact point was used. This point on the FMHF lower forehead happened to be on a relatively flat portion of the dummy head, similar to the side of the head.

Each impact was judged by comparing the three aspects of the damage pattern mentioned above. Primary emphasis was placed on the dent in the metal window sill since it was considered the stiffest component. A summary of the reconstruction attempts is given in Table 5.4. The correctness of the pitch angle was most readily determined by observing the relative magnitude of the lateral and vertical components of the dent in the window sill. This proved to be an accurate means of determining the required pitch since a pitch of 41 degrees in Test S73105 produced a mainly vertical dent and a pitch of 30 degrees in Test S73108 was primarily lateral. All tests at 30 or 35 degrees pitch also gave

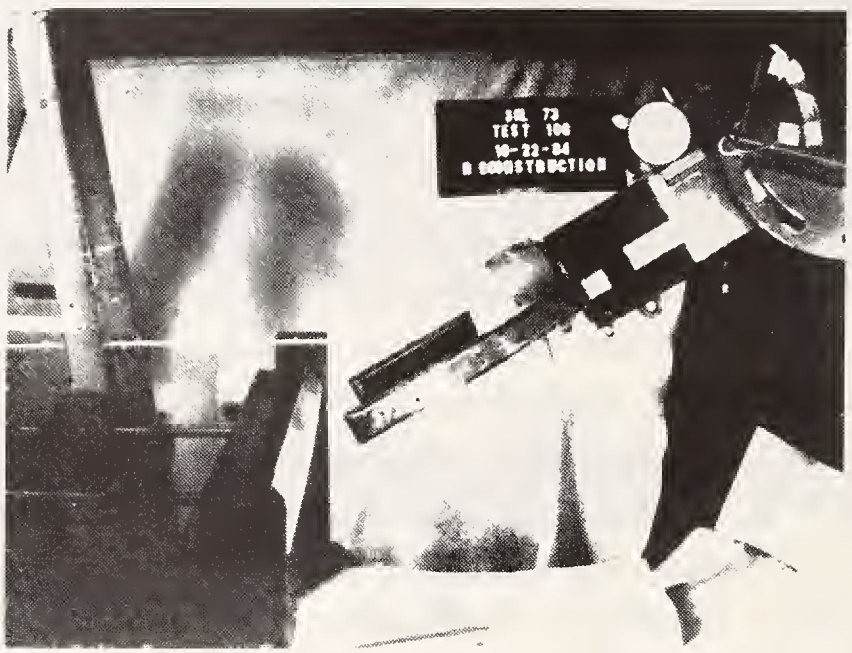

FIGURE 5.11 -- Duster Reconstruction Apparatus.

TABLE 5.4

Duster Reconstructions

Test Number	Velocity (mph)	Gun Pitch (deg)	HIC	Peak Resultant Rotational Acceleration (rad/s**2)	Comment
S73105	27.8	-41	3335	15320	Too severe, dent primarily down
S73106	16.5	-20	700	11880	Dent primarily in and too deep, no bend in support tab
S73107	16.9	-30	1212	9920	Same door as 106, support tab bent, no additional door damage
S73108	21.9	-30	2256	9330	Primarily inward, good depth
S73109	25.5	-35	3042	16490	Too severe, plastic crush, large dent
S73110	23.1	-35	2279	14900	Very close in all respects, but deeper than actual dent

reasonable bends in the plastic covering support tab. The hairline crack in the plastic covering was not well reproduced in any test, with the closest one being a 12 inch crack produced in Test S73110.

Two tests, S73108 and S73110 were judged to be reasonable reconstructions of the dent pattern. Figure 5.12 illustrates the contours of Tests S73108 -- S73110. Test S73108 was closest to the correct lateral depth but did not produce any vertical deformation. Test S73110 produced both lateral and vertical components but both were slightly larger than desired. However, considering the difference in deformation observed between Tests S73109 and S73110 for a 2.4 mph velocity change, it was judged that only a slightly lower velocity would have been required to make the dents in S73110 closer to the actual damage pattern. For this reason S73110 was also considered a good reconstruction. Due to the similarity in headform response between tests S73108 and S73110 the average value of these tests was used as the reconstruction result. (The acceleration responses for these two tests are contained in Appendix D.) The rather large relative difference in deformations between S73109 and S73110 (.12 in compared to .04 in) whose impact velocities differed by only 2.4 mph, also increased confidence in the reconstruction velocity accuracy. There was a large scale deformation of the door observed in all reconstruction attempts which was not apparent in the accident door (Figure 5.13). The apparent lack of such deformation in the accident door may have been due to the vehicle engagement causing a more distributed support to the door than in the reconstruction tests.

In summary, this accident reconstruction also required an assumption regarding the stiffness of the door component, which was altered due to the striking vehicle engagement. Given this condition and the fact that the FMHF was restricted to a frontal rather than side head impact, the reconstruction produced a damage pattern which reasonably represented that of the accident.

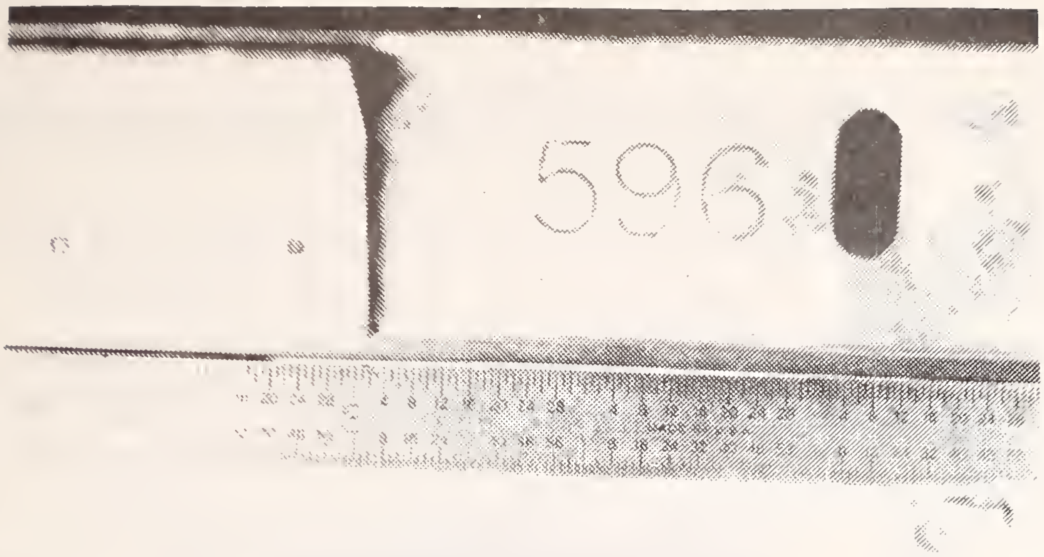

Test S73108, Horizontal Dent

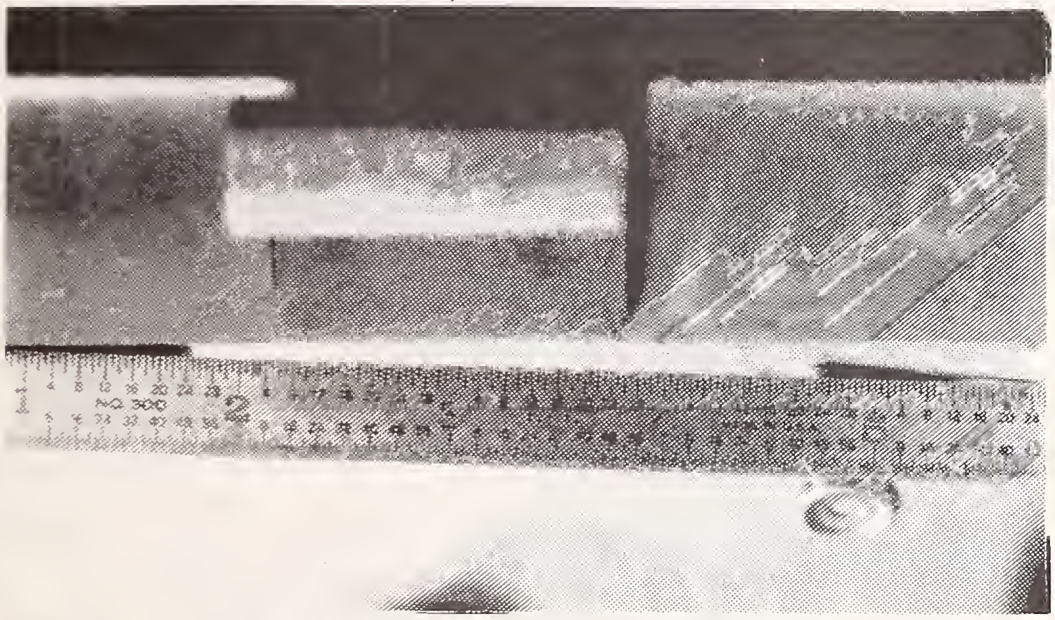

Test S73109, Horizontal Dent

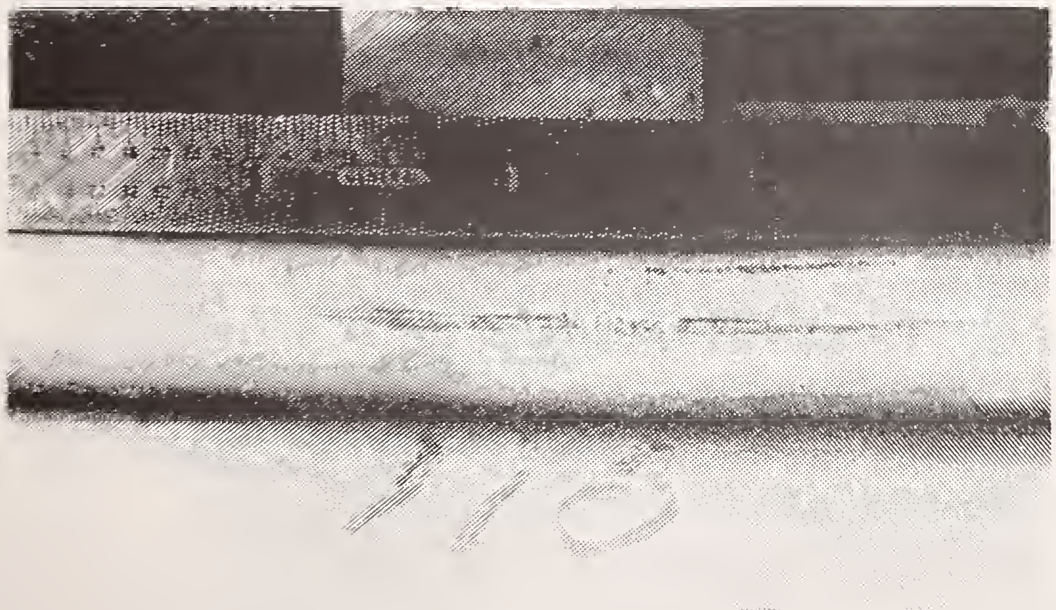

Test S73110, Vertical Dent

FIGURE 5.12 -- Duster Reconstruction Damage.

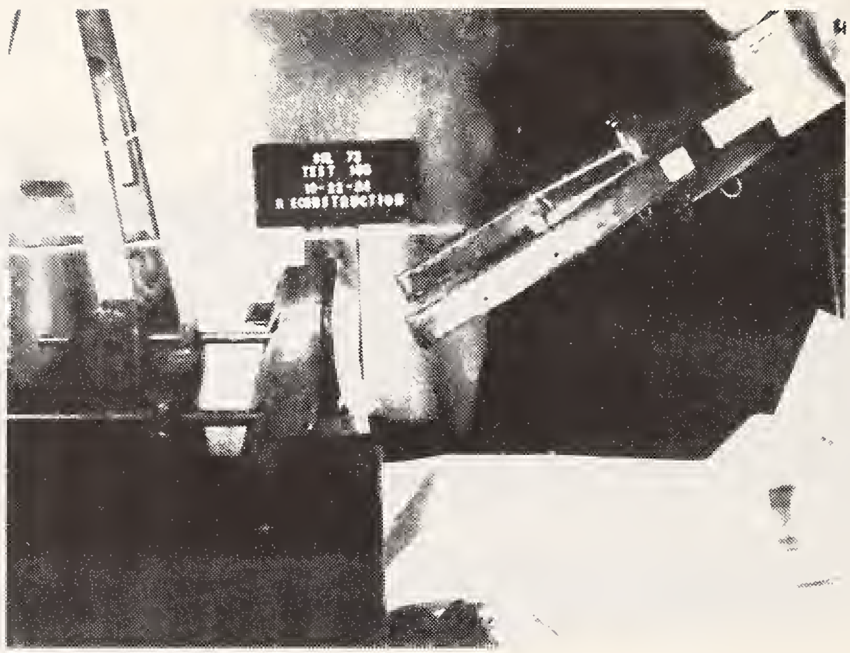

FIGURE 5.13 -- Duster Reconstruction - Large Scale Deformation.

5.4 Accident Reconstruction Summary and Discussion

The accident and reconstruction data are summarized in Table 5.5. Although the data are limited for this feasibility study, there appear to be some correlations between the accident head injuries and the component headform measurements. Note that the HIC increased for the more severe injuries. Somewhat suprising was the decreasing rotational acceleration with the increasing accident head injury. In two of the reconstructions (Aries and S-10), peak rotational accelerations resulted from short duration (3-4 ms) windshield impacts. Diffuse injuries normally associated with rotational effects are considered to require greater time durations. However, even when the initial 3 msec of the windshild impact is disregarded for the Aries and S-10 reconstructions and the maximum rotational accelerations occuring after that time are used, the trend, though changed, still does not correlate with the occupant injury severity.

A further discussion of the correlation results require consideration of the types of head injuries observed in the accidents since different correlations may exist for different types of head injuries. The specific injuries are described in Table 5.1. The Aries occupant suffered a mild concussion with brief unconsciousness; a diffuse type of injury thought to be associated primarily with rotational acceleration. The S-10 occupant's more severe injuries were the frontal lobe contusion and associated cerebral edema which are contact phenomena related to the size of the impacting structure and the magnitude of the force. These injuries are normally correlated to the linear acceleration of the head during impact. The Duster occupant had injuries related to rotational acceleration (corpus callosum hematoma, subarachnoid hemorrhage, ventricle bleed) and contact phenomena (basilar skull fracture, cerebral contusions) with the former being more serious. Because of these distinctions in the injury mechanism, the S-10 (contact injury mechanism) reconstruction correlation to the accident injury might be different than

TABLE 5.5

Summary of Reconstruction Results

ACCIDENT DATA			RECONSTRUCTION RESULTS			
Accident Case	Crash Delta-V (mph)	Head AIS	Velocity (mph)	HIC	Peak Resultant Rotational Acceleration (rad/s^2) (neglecting first 3 msec)	Peak Resultant Rotational Velocity (rad/s)
Dodge Aries	14	2	22.9	290	55410 (3800)	93.0
Chevy S-10*	44	3	36.4	1791	38920 (18300)	84.9
Duster*	25	5	22.5	2268	12115	28.7

*Average values

the other two cases. Additional accident reconstructions are necessary before a possible correlation could be established, but it is interesting to note the wide headform HIC and rotational acceleration response difference for the Aries and Duster diffuse head injuries.

6.0 CONCLUSIONS AND RECOMMENDATIONS

A free motion headform (FMHF) has been developed and evaluated for purposes of determining:

1) General performance characteristics of the free-motion headform in vehicle interior component tests.

2) The ability to reconstruct vehicle occupant head impacts with the free-motion headform.

The conclusions for the general performance characteristics of the free-motion headform in vehicle interior component tests were that:

- Repeatable head impact velocities were achieved with the current test apparatus.

- Headform response was sensitive to relatively small velocity changes.

- The headform response was adequate in demonstrating a significant difference between components.

- Based upon neck pendulum tests, the nine-accelerometer rotational acceleration array mounting and software was found to produce reasonably good angular position and velocity versus time results, implying reasonable rotational acceleration measurement.

- Varying impact location on the head was critical to the HIC and rotational acceleration response, with the glancing impacts having a higher rotational acceleration and a lower HIC.

- The free-motion headform response for windshield impacts compared very well to a full Hybrid III dummy crash test head response.

The conclusions for the accident reconstruction testing with the FMHF were:

- Damage patterns were reproduced satisfactorily for the three accident reconstructions. HIC values for the reconstructions increased with increasing injury level.

- One of the three accident reconstructions was of a diffuse head injury (Aries concussion). The highest peak rotational acceleration was also experienced for this case, the result of initial, short duration spikes.

- The availability of the damaged vehicle component was very useful, if not essential, to the accident reconstructions.

The following areas of further investigation and development are recommended on the basis of the results of this study:

- The rotational head injury criterion needs further refinement to determine the significance of short time duration pulses. The windshield impacts indicated such effects. However, the diffuse injuries normally associated with rotational effects are considered to require time durations greater than the initial 3-4 msec spikes of the windshield impacts. This may indicate that the rotational acceleration criterion can neglect the higher frequency pulses. Subdural hematoma head injuries are thought to be related to acceleration onset rate (i.e., higher frequencies), but little research has been done to develop a criterion for them.

- Incorporation of computer simulation of the accident case into the reconstruction process would improve the understanding of probable occupant kinematics and contact velocities. Note, for example, that the S-10 and Duster reconstructions both required impact velocities which were less than the vehicle delta-V. This appears to be reasonable based upon crash test results with unrestrained occupants which indicate that the relative occupant head contact velocities are from 75-90% of the vehicle delta-V. For the Aries case, however, a velocity which was higher than the delta-V was required to reconstruct the damage pattern with the component device. This result might be expected if the occupant had rotated slightly, impacted the windshield with the top of his head, and had a greater effective mass due to the neck compressive load. A computer simulation of the Aries case was made at NHTSA headquarters subsequent to the reconstruction testing. The simulation indicated an occupant head impact orientation which would have resulted in neck compressive loading.

- Development of a unified method of identifying and documenting occupant contact damage patterns is recommended. Again, for the S-10 and Duster reconstructions, the damaged vehicle components were available and accurate duplication of the damage patterns was possible. For the Aries, the windshield damage documentation consisted of only photographic information which could not easily be used to quantify the damage. A unified approach would allow not only better documentation of the contact damage, but also a method for more widespread data collection from accident investigation teams.

- Finally, improvements to the component headform which would allow it to simulate a wider variety of accident occupant head impacts would be desirable. The current design is limited to frontal impacts. Design modifications could be made to simulate other impact orientations (such as side) or to attain a variable mass headform.

Despite these areas in which the accident reconstruction methodology can be improved, the results of this head component reconstruction feasibility study indicated that information obtained directly from the accident environment can be valuable in the refinement and development of human injury criteria, and that the approach should continue to be pursued. The free motion headform component test device also appears to provide a realistic and economic approach for obtaining head injury predictions for vehicle interior component impacts with potential applications to vehicle component design and safety standard development.

REFERENCES

1. "Head Injury -- Hope Through Research," U.S. Department of Health and Human Services, Public Health Service National Institutes of Health, Publication No. 84-2478, August 1984.

2. Side Interior Stiffness Event Report SRL-66, Vehicle Research and Test Center, East Liberty, Ohio, 1984.

3. Searle, J.A., "Headform Impact Tests on the Interior Surfaces of Two of the Renault 5 Vehicles," Motor Industry Research Association, Report No. K4320/R5, 1981.

4. Robbins, D.H., Melvin, J.W., Heulke, D.F., Sherman, H.W., "Biomechanical Accident Investigation Methodology," The University of Michigan Transportation Research Institute, 1983.

5. Walker, L.B., Harris, E.H., Pontius, U.R., "Mass, Volume, Center of Mass, Moment of Inertia of Head and Neck of Human Body," The 17th Stapp Car Crash Conference, 1973.

6. Goodman, L.E. and Robinson, R.A., "Effect of Finite Rotations on Gyroscopic Sensing Devices," Journal of Applied Mechanics, 25, No. 2 (1958), p. 210.

7. Beebe, M., "1980 Ford Mustang to Fixed Load Cell Barrier," Report Number DOT-HS-806 726, Project SRL-98, Vehicle Research and Test Center, January 1985.

8. Head and Neck Injury Case Report No. HNN-28-207(074), Management Engineers Incorporated, Reston, Virginia, 1983.

9. Head and Neck Injury Study Report No. 146-020484, Calspan Field Service, Inc., Arlington, Virginia, 1984.

10. Head and Neck Injury Study Report No. 133-111983, Calspan Field Service, Inc., Arlington, Virginia, 1983.

APPENDIX A

Rotational Acceleration Calculation

The purpose of this Appendix is to demonstrate how the angular acceleraton of a rigid body in general three-dimensional motion may be calculated using a nine accelerometer array shown in Figure 2.4.

The relative motion of any two points in space is illustrated in Figure A.1. The relative motion equations are:

$$r = R + \rho \qquad (1)$$

$$\dot{r} = \dot{R} + \dot{\rho} \qquad (2)$$

$$\ddot{r} = \ddot{R} + \ddot{\rho} \qquad (3)$$

where $(\dot{\ })$ represents the time derivative with respect to the XYZ coordinates. Consider the coordinates (XYZ) to be fixed and the moving (x,y,z) system to have an angular velocity ω and an angular acceleration α. Assume ρ is defined with respect to the moving coordinates and does not change with respect to them. For such a case the vector ρ may be represented in terms of the (x,y,z) system angular velocity, angular acceleration, and vector as

$$\ddot{\rho} = \alpha x \rho + \omega x(\omega x \rho)$$

Thus, equation (3) becomes

$$\ddot{r} = \ddot{R} + \alpha x \rho + \omega x(\omega x \rho)$$

or

$$A_p = A_o + \alpha x \rho + \omega x(\omega x \rho) \qquad (4)$$

where:

A_p = acceleration of point P with respect to (XYZ)

A_o = acceleration of point 0 with respect to (XYZ)

α = angular acceleration of (xyz) with respect to (XYZ)

ω = angular velocity of (x,y,z) with respect to (XYZ)

p = position vector of P defined in (xyz) coordinates.

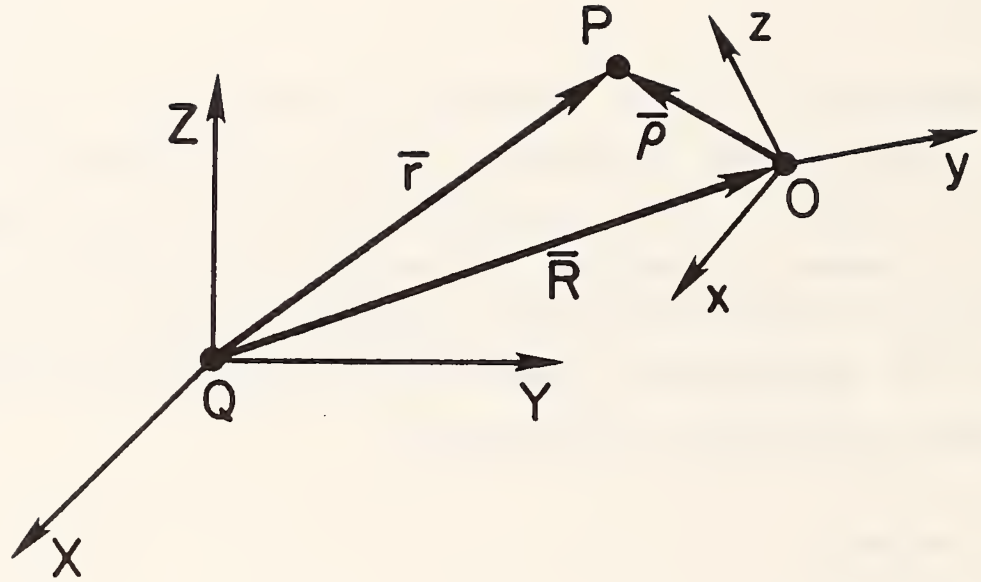

FIGURE A.1 -- Position Vectors Describing Headform Motion

We can now write every term in equation (4) as the sum of its components in the (xyz) system and expand the equation to

$$\begin{bmatrix} (A_p)_x \\ (A_p)_y \\ (A_p)_z \end{bmatrix} = \begin{bmatrix} (A_o)_x \\ (A_o)_y \\ (A_o)_z \end{bmatrix} + \begin{bmatrix} -(\omega_y^2+\omega_z^2) & (\omega_y\omega_x-\alpha_z) & (\omega_z\omega_x+\alpha_y) \\ (\omega_x\omega_y+\alpha_z) & -(\omega_x^2+\omega_z^2) & (\omega_z\omega_y-\alpha_x) \\ (\omega_x\omega_z-\alpha_y) & (\omega_y\omega_x+\alpha_x) & -(\omega_x^2+\omega_y^2) \end{bmatrix} \begin{bmatrix} \rho_x \\ \rho_y \\ \rho_z \end{bmatrix} \quad (5)$$

Equation (5) gives the components of the acceleration of P with respect to (XYZ) along the directions of (xyz). The quantities on the left of equation (5) represent the acceleration an accelerometer would measure if fixed at point P in the x, y or z direction.

By inserting the position vector for each accelerometer of the nine-accelerometer array into equation (5) and noting whether it is oriented in the x, y, or z direction, the measured acceleration can be related to the unknowns α_x, α_y, α_z $(A_o)_x$, $(A_o)_y$, $(A_o)_z$. A summary of results is shown below.

Accelerometer	Position Vector	Result of Substitution Into (5)
HD1XG	$p_4 i+p_1 j$	HD1XG= $-p_4(\omega_y^2+\omega_z^2)+p_1(\omega_x\omega_y-\alpha_z)+(A_o)_x$
HD1ZG	$p_1 j+p_4 k$	HD1ZG= $-p_4(\omega_x^2+\omega_y^2)+p_1(\omega_y\omega_z+\alpha_x)+(A_o)_z$
HD2YG	$p_2 i+p_4 j$	HD2YG= $-p_4(\omega_x^2+\omega_z^2)+p_2(\omega_x\omega_y+\alpha_z)+(A_o)_y$
HD2ZG	$p_2 i+p_4 k$	HD2ZG= $-p_4(\omega_x^2+\omega_y^2)+p_2(\omega_x\omega_z-\alpha_y)+(A_o)_z$

HD3XG	$p_4 i + p_3 k$	HD2XG= $-p_4(\omega_y^2+\omega_z^2)+p_3(\omega_x\omega_y+\alpha_y)+(A_o)_x$
HD3YG	$p_4 j + p_3 k$	HD3YG= $-p_4(\omega_x^2+\omega_z^2)+p_3(\omega_y\omega_z-\alpha_x)+(A_o)_y$
HEDXG	$p_4 i$	HEDXG= $-p_4(\omega_y^2+\omega_z^2)+(A_o)_x$
HEDYG	$p_4 j$	HEDYG= $-p_4(\omega_x^2+\omega_z^2)+(A_o)_y$
HEDZG	$p_4 k$	HEDZG= $-p_4(\omega_x^2+\omega_y^2)+(A_o)_z$

(Equations 6 -- 14 above)

In the above nine equations (6-14) there are nine unknowns: three translational accelerations (A_p), three rotational accelerations (α), and three rotational velocities (ω). One could solve for these unknowns using nine equations, but the solution is not straight forward due to the rotational velocity terms. These nine equations, however, can be manipulated to give the relationships between the measured translational accelerations and the three desired rotational accelerations without explicit determination of the rotational velocities as follows:

$$\alpha_x = \frac{(HD1ZG - HEDZG)}{2\ p_1} - \frac{(HD3YG - HEDYG)}{2\ p_3} \qquad (15)$$

$$\alpha_y = \frac{(HD3XG - HEDXG)}{2\ p_3} - \frac{(HD2ZG - HEDZG)}{2\ p_2} \qquad (16)$$

$$\alpha_z = \frac{(HD2YG - HEDYG)}{2\ p_2} - \frac{(HD1XG - HEDXG)}{2\ p_1} \qquad (17)$$

Several important comments should be made regarding these equations:

1. Although it was initially implied in equation (2) that the general acceleration of point 0 would be required in the calculation of rotational acceleration (something physically impossible due to the size of accelerometers) this is actually not the case as the terms $(A_0)_x, (A_0)_y, (A_0)_z$ in equations 6 -- 14 can be eliminated in favor of HEDXG, HEDYG, and HEDZG.

2. In performing the substitution mentioned above, all terms involving p_4 also drop out of the equations, thus the offset of the accelerometers from the coordinate axis has no effect on the accuracy of the calculated rotational accelerations.

3. No products of angular velocity appear in the final equations, allowing calculation of angular acceleration by algebraic manipulation of linear accelerations.

The values obtained (α_x, α_y, α_z) are the components of the rotational acceleration of the rigid body with respect to the inertial coordinates (X,Y,Z) projected on the body fixed x, y, and z axes. It is important to note that the angular velocity in any body fixed direction may be computed by the ordinary integration of the scalar component of angular acceleration in that direction - just as though the body fixed direction were space fixed as well. However, since three dimensional finite rotations do not obey the communicative law and thus cannot be treated as vectors, one cannot, in general, integrate body fixed velocities and obtain an angle which represents the rotation of a body about that axis (5). A simple example illustrates this idea. Given a rigid body rotating about a stationary axis OA with speed ω, axis OA can be regarded as both body fixed and space fixed.

For any body fixed axis OB inclined a constant angle β from axis OA the angular velocity is $\omega \cos \beta$. This is the constant quantity a rate gyro would measure if attached having its sensitive axis along OB. If we integrate this value over the period of one revolution ($T = 2\pi/\omega$), we obtain:

$$\int_0^T \omega\cos\beta \, dt = 2\pi\cos\beta$$

However, it is apparent that during that time interval every line in the rigid body has returned to its original position. Since the integration of the body fixed angular velocity indicates there is some amount of "rotation" other than 0 or 2π, it is apparent that direct physical significance cannot be placed in it. This effect is one possible source of the errors observed in the angle versus time comparisons made in the head-neck extension and flexion tests.

A problem with the nine accelerometer method of measuring rotational acceleration in impact situations can result when taking the difference of two large accelerations with similar magnitude. To help visualize this problem, the raw data from a 19 mph A-pillar test is presented in Figures A.2-A.7 by pairs according to their appearance in equations (15), (16), and (17). For a forehead impact such as this there is a significant difference (100 g's) between channels measuring y rotational acceleration (Figures A.2, A.3), while the differences for those measuring x (A.4 and A.5) and z (A.6 and A.7) rotational accelerations are smaller (typically less than 20 g). The larger this nominal difference is, the more accurate the rotational accelerations will be. In this case, the differences were significant enough to insure a fairly accurate measurement of rotational acceleration. The resulting rotational accelerations are shown in Figures A.8 -- A.10 as well as the resultant rotational acceleration (Figure A.11) and velocity (Figure A.12). By comparing the resultant rotational acceleration (Figure A.11) and the raw data (Figures A.2 - A.7), it appears that both quantities have similar forms and the maximum values for both quantities occur at the same time. From the Figures A.8 - A.10 one can observe a 150-200 r/s^2 noise in the rotational acceleration output. This occurs in all the rotational accelerations and is a direct result of the random 1-2 g noise in the accelerometer output. This is not considered a critical problem since, at typical levels, the noise is very small (1 to 3 percent of the maximum values).

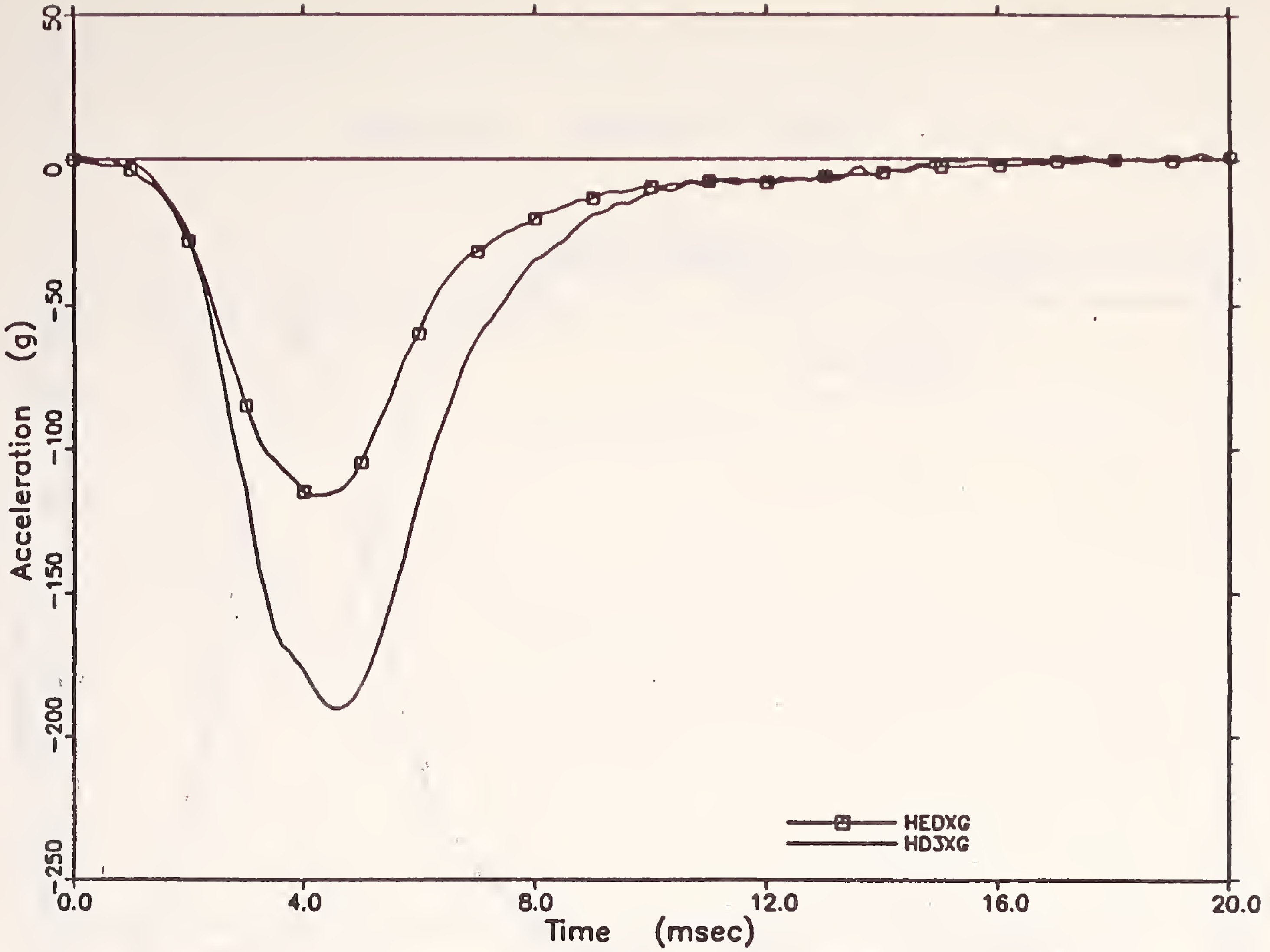

Figure A2 Raw Data for S73039

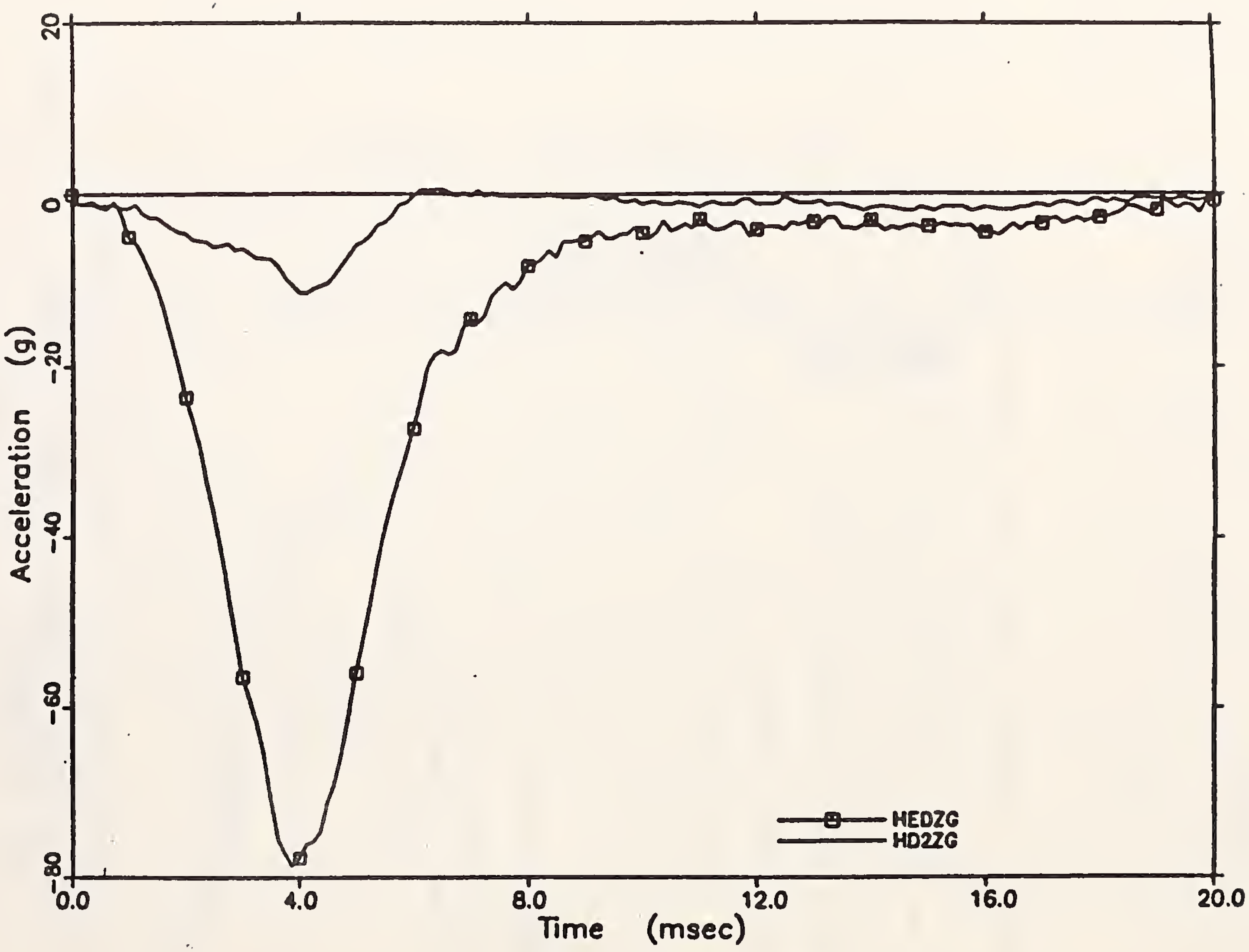

Figure A3 Raw Data for S73039

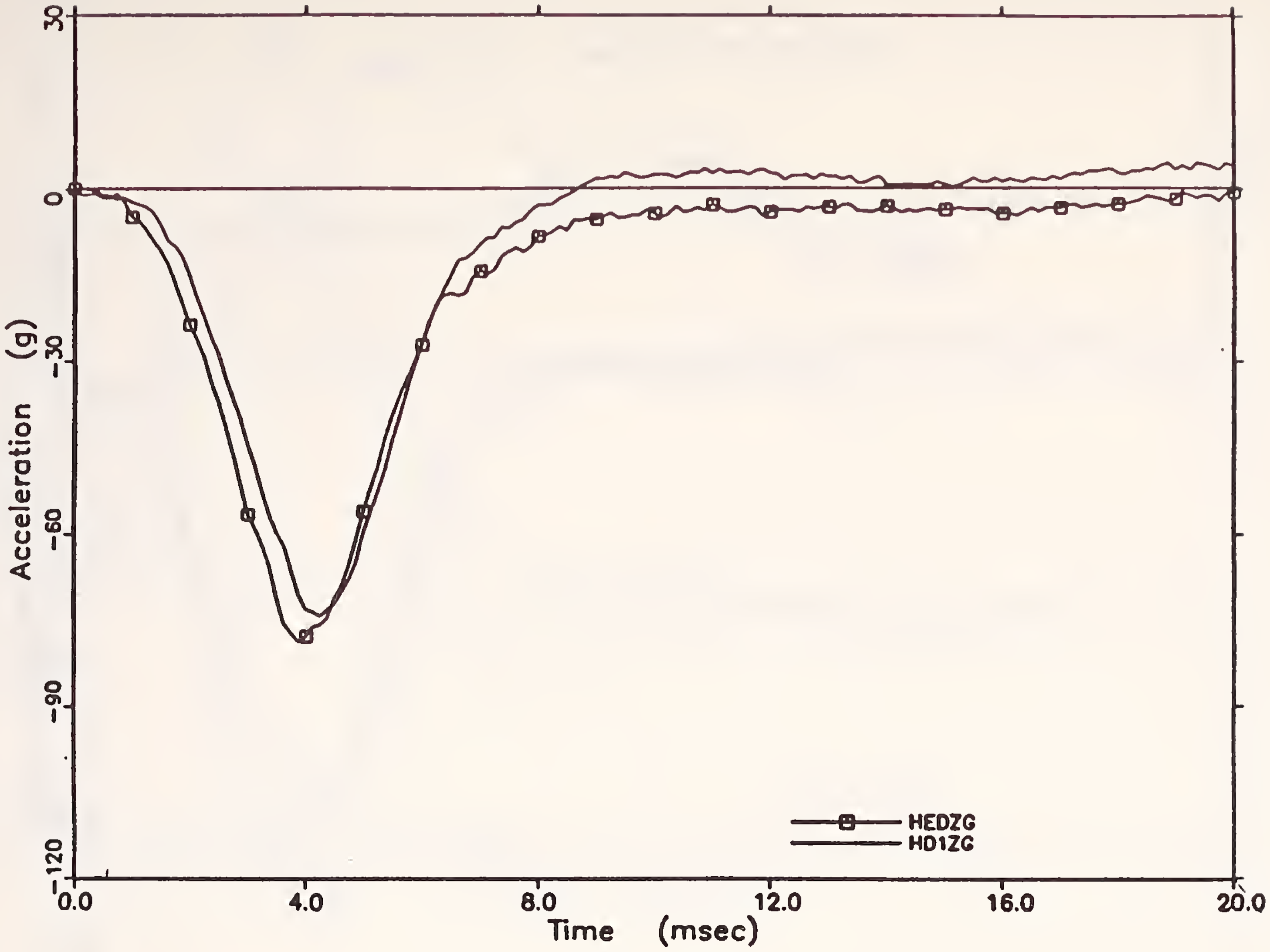

Figure A4 Raw Data for S73039

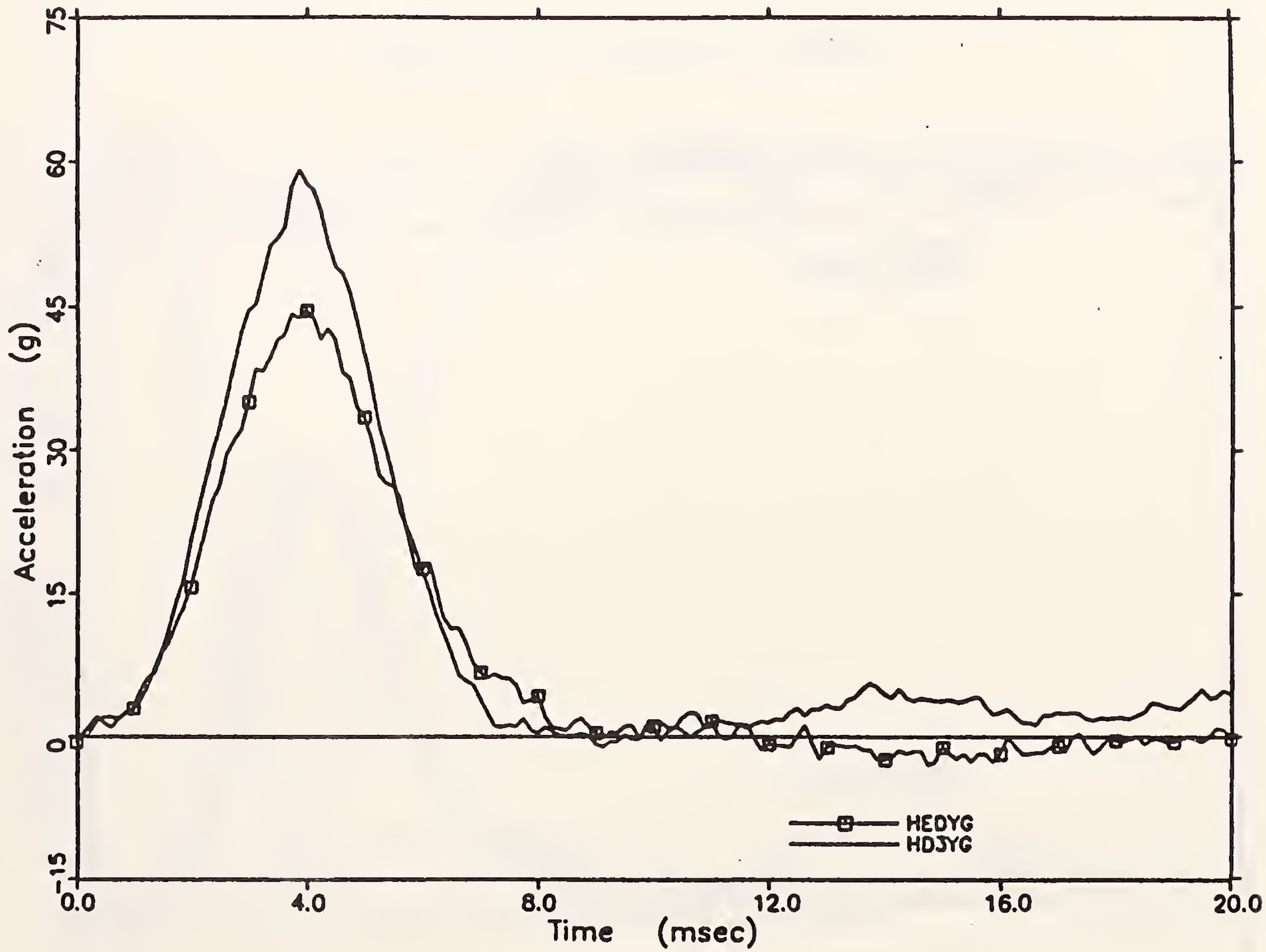

Figure A5 Raw Data for S73039

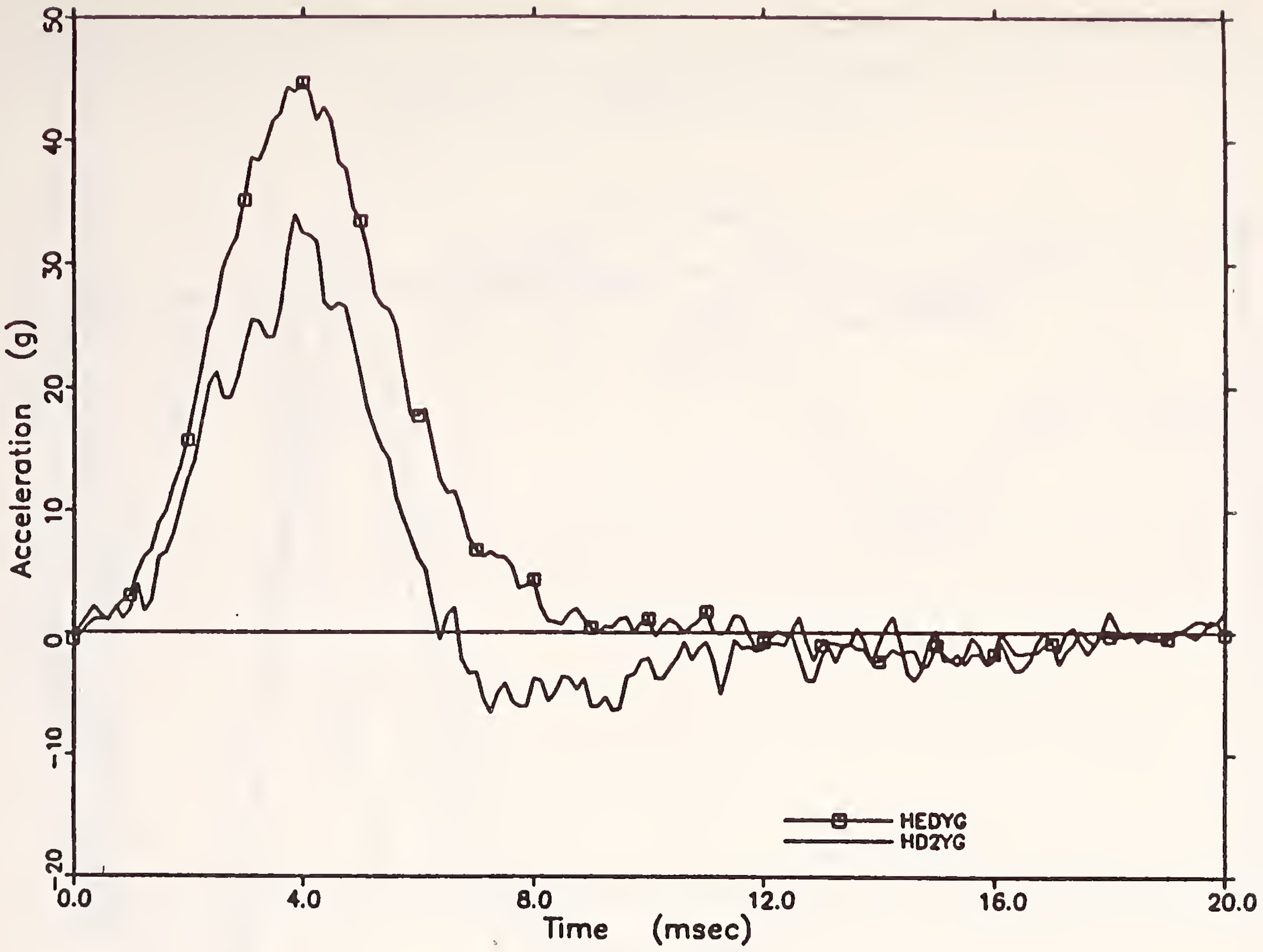

Figure A6 Raw Data for S73039

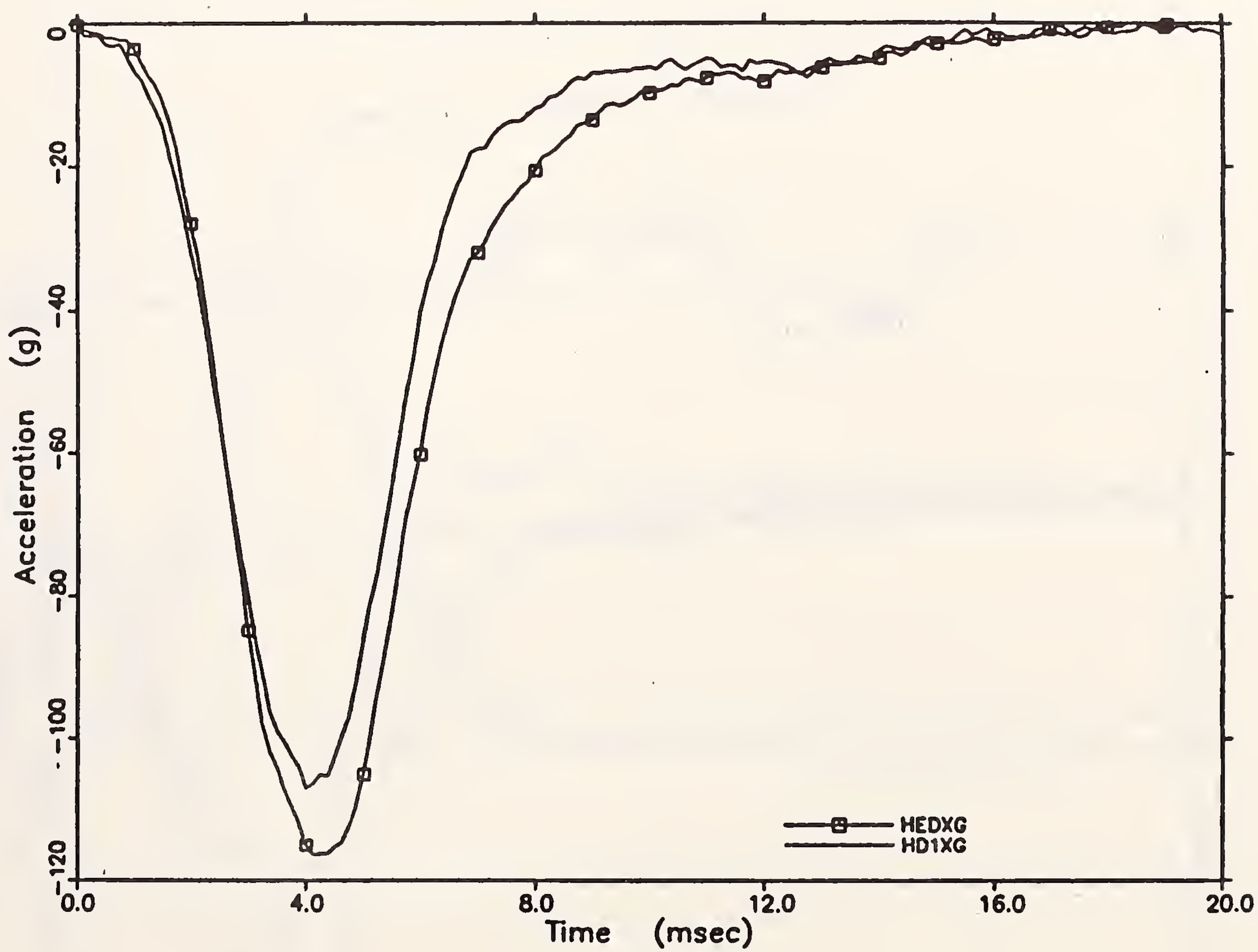

Figure A7 Raw Data for S73039

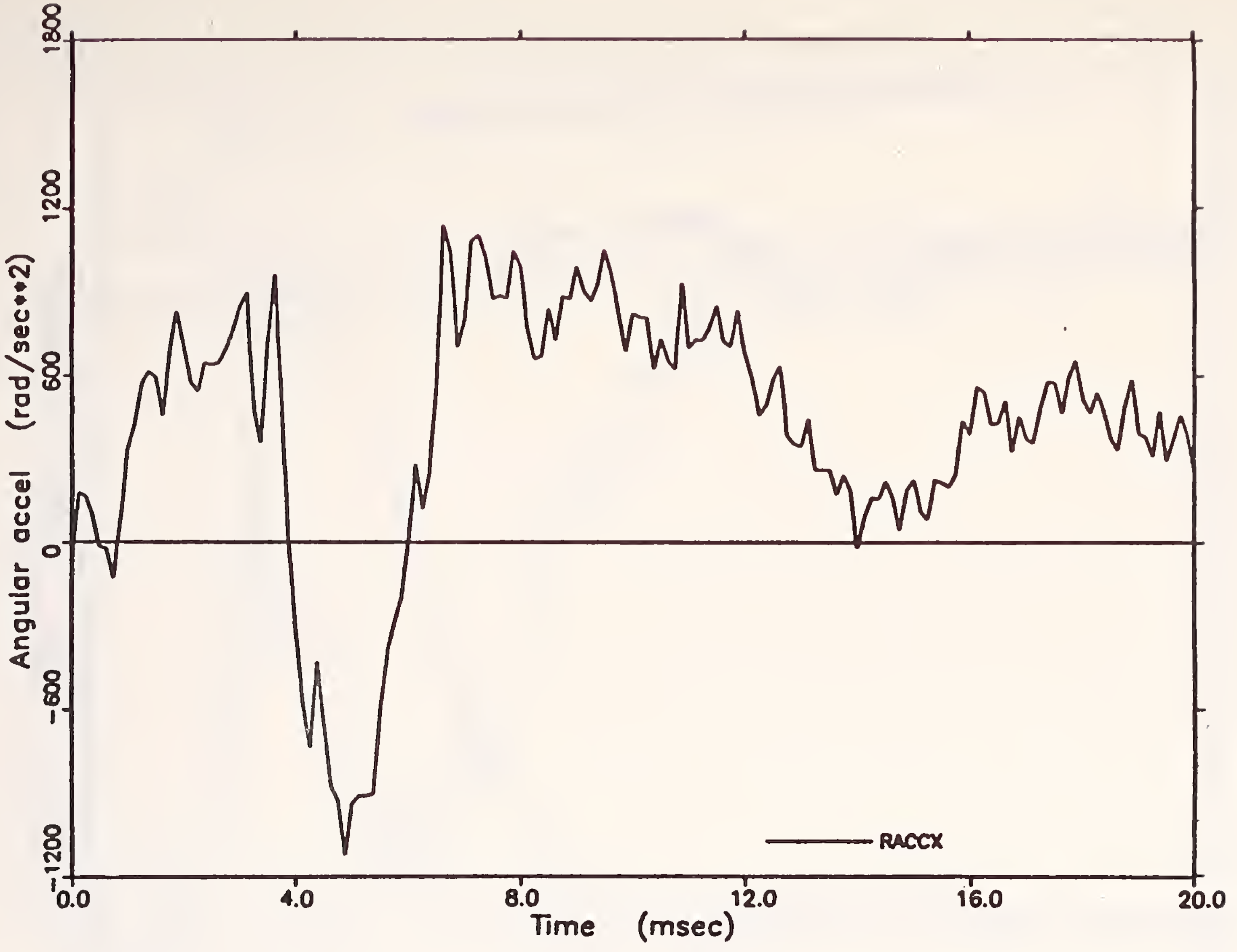

Figure A8 x-Axis Rotational Acceleration-S73039

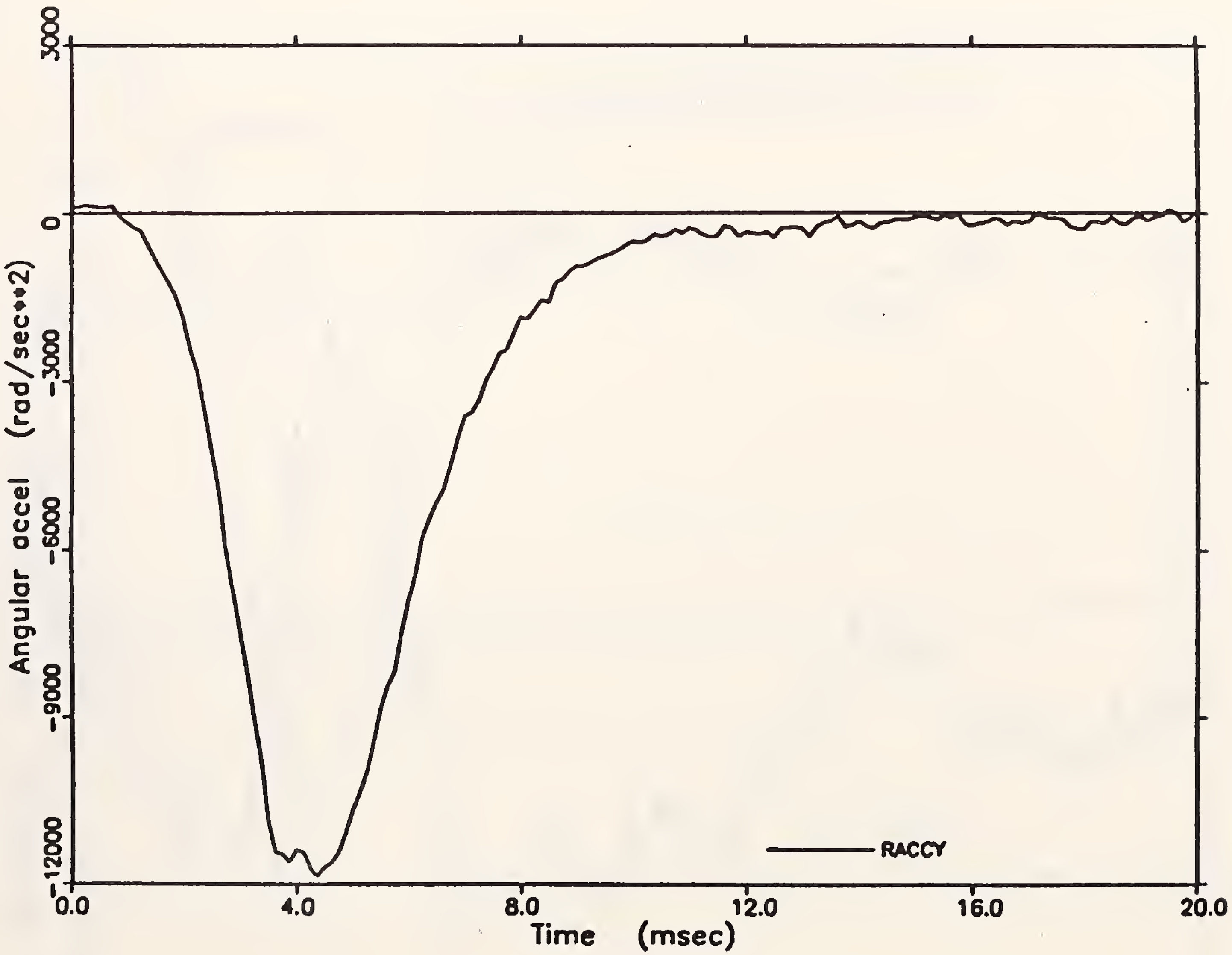

Figure A9 y-Axis Rotational Acceleration-S73039

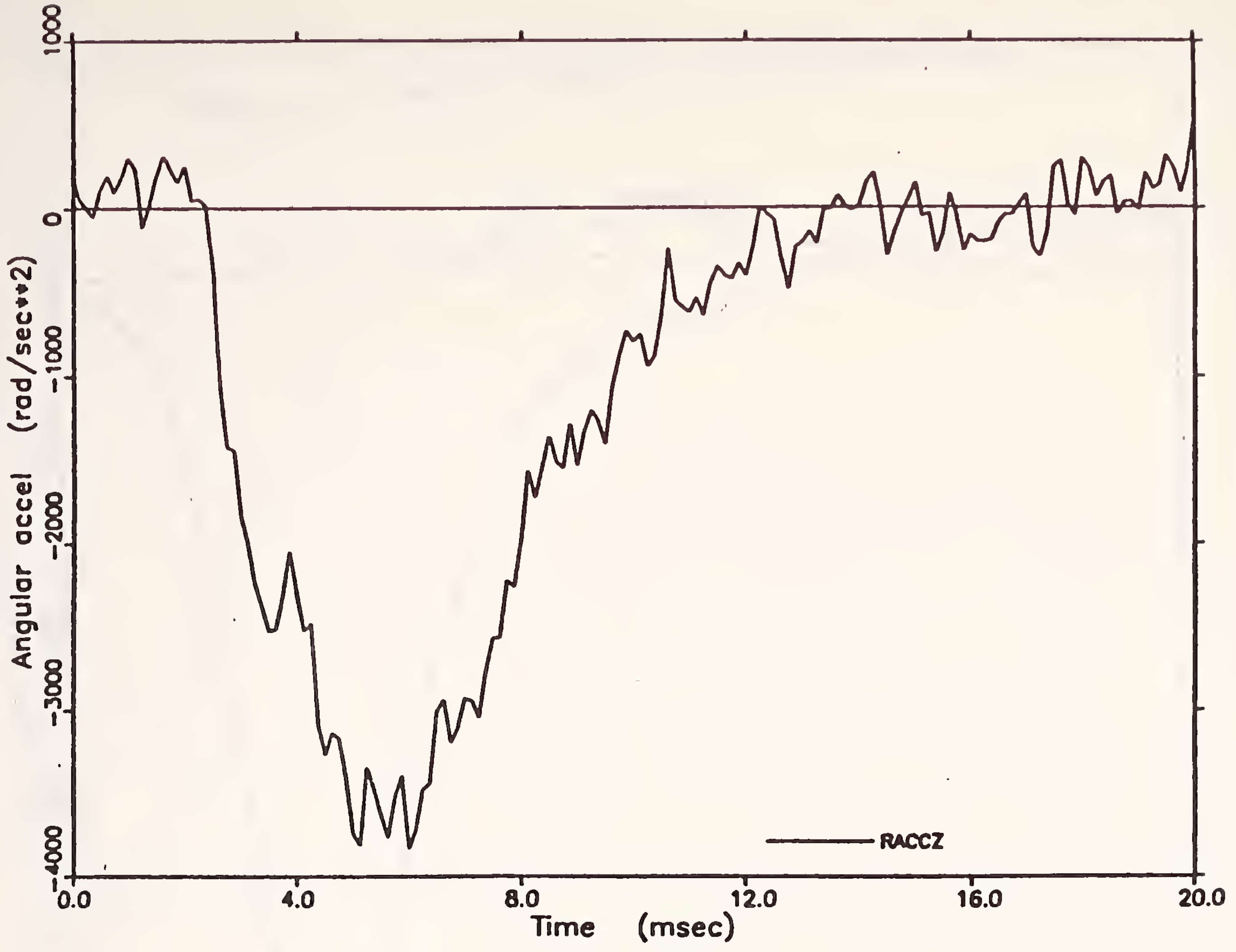

Figure A10 z-Axis Rotational Acceleration-S73039

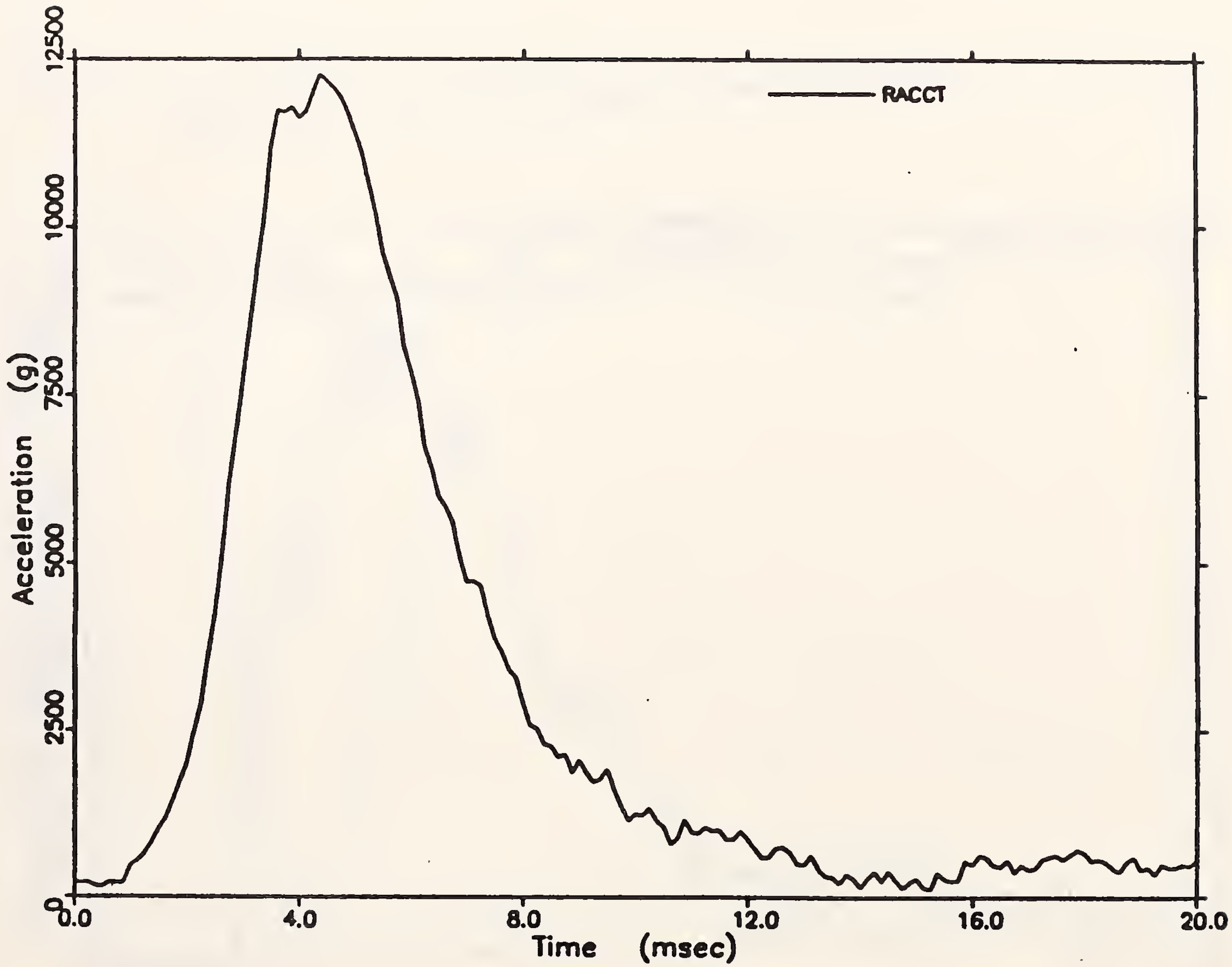

Figure A11 Resultant Rotational Acceleration-S73039

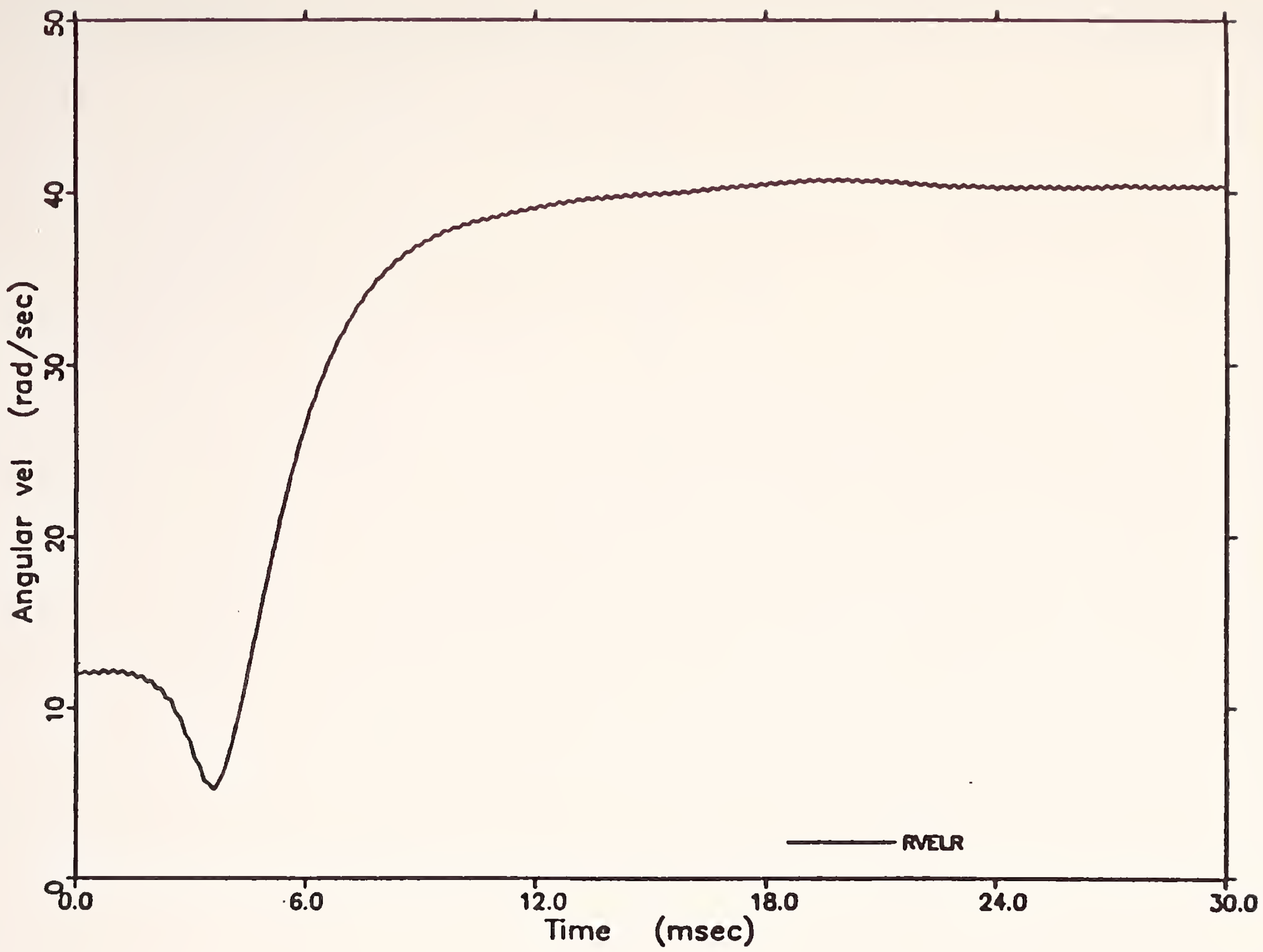

Figure A12 Resultant Rotational Velocity-S73039

APPENDIX B

Aries Reconstruction Data for Test Number S73097

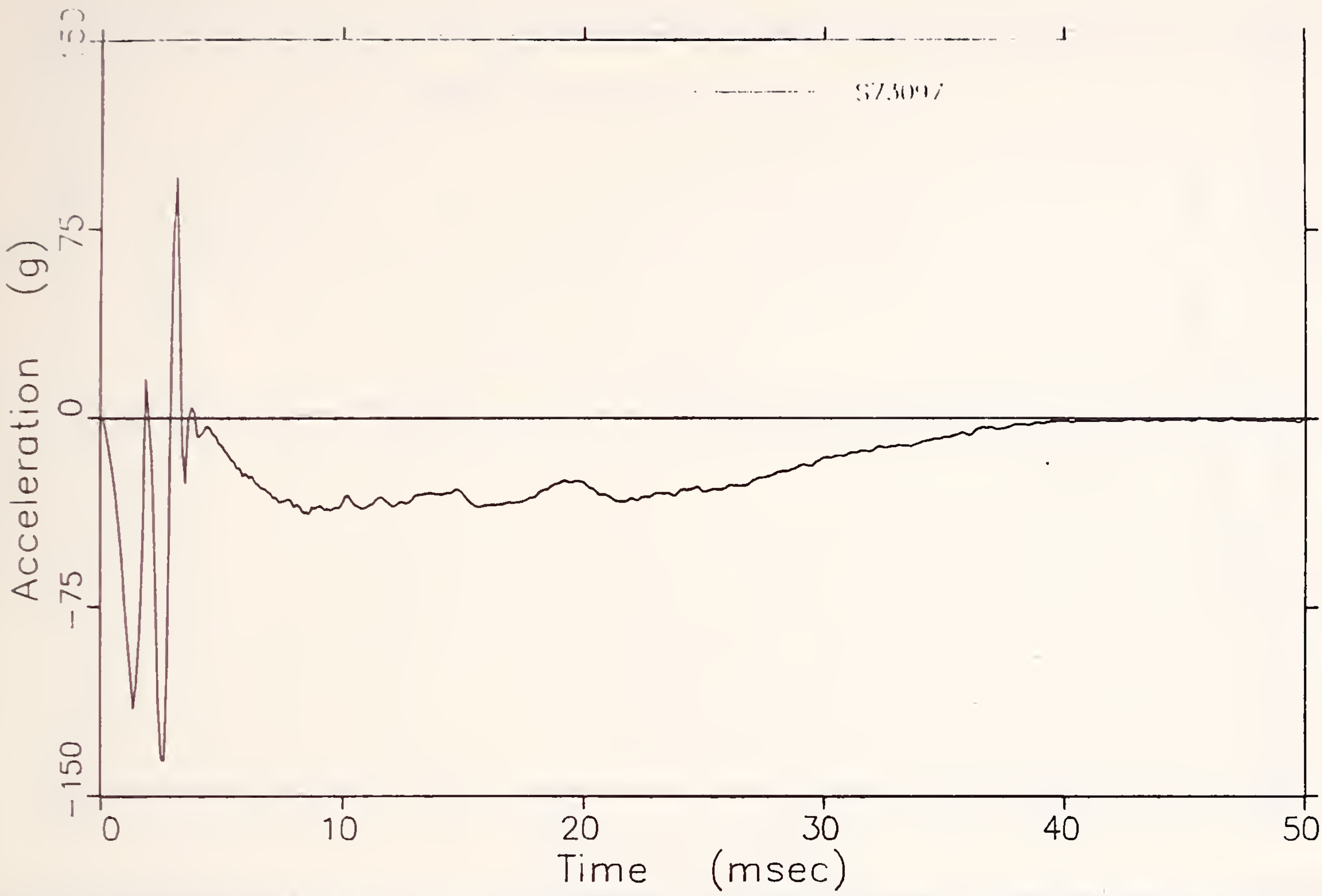

FIGURE B.1 -- Aries Reconstruction: Head C.G. X-Axis Acceleration

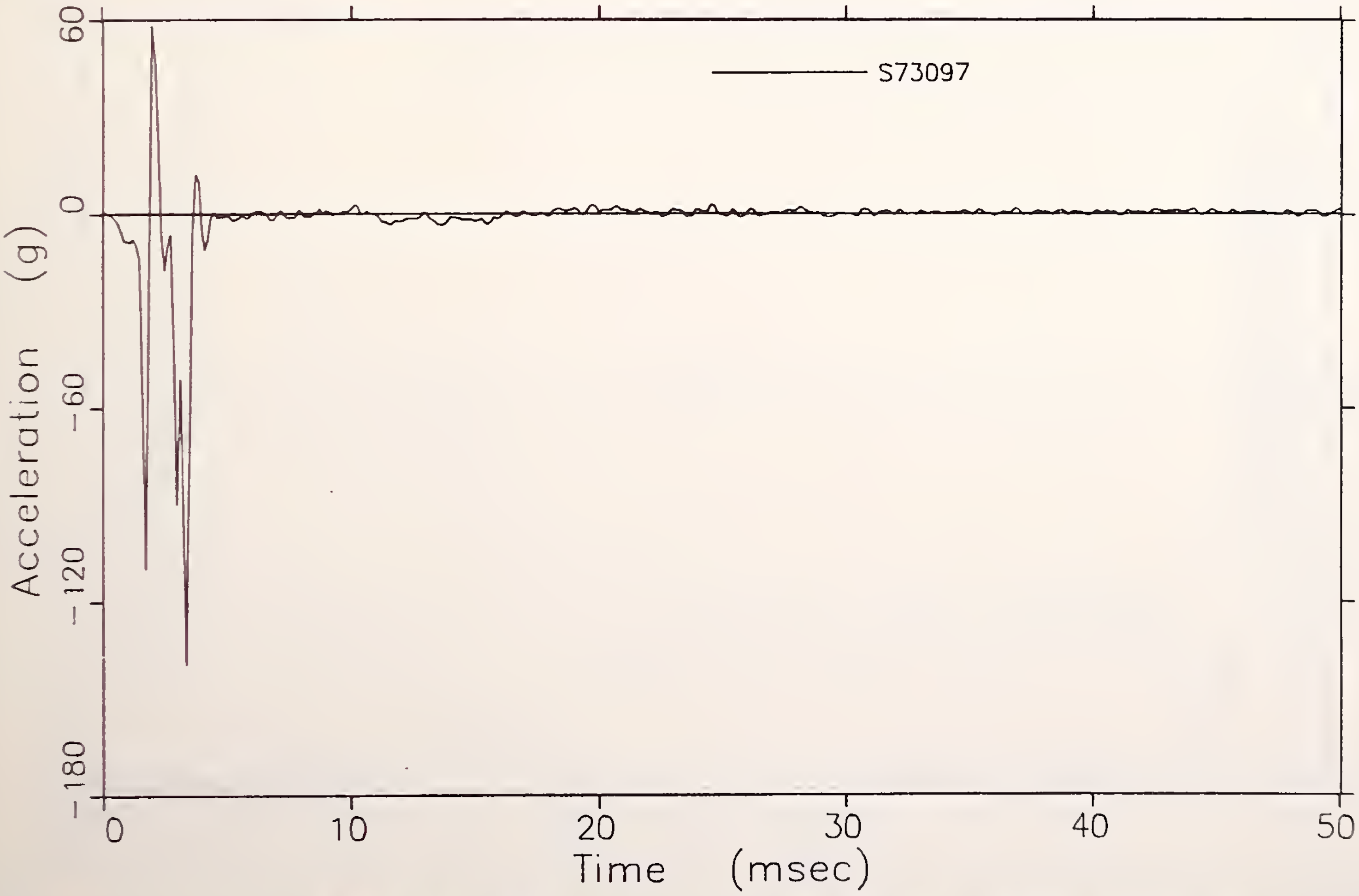

FIGURE B.2 -- Aries Reconstruction: Head C.G. Y-Axis Acceleration

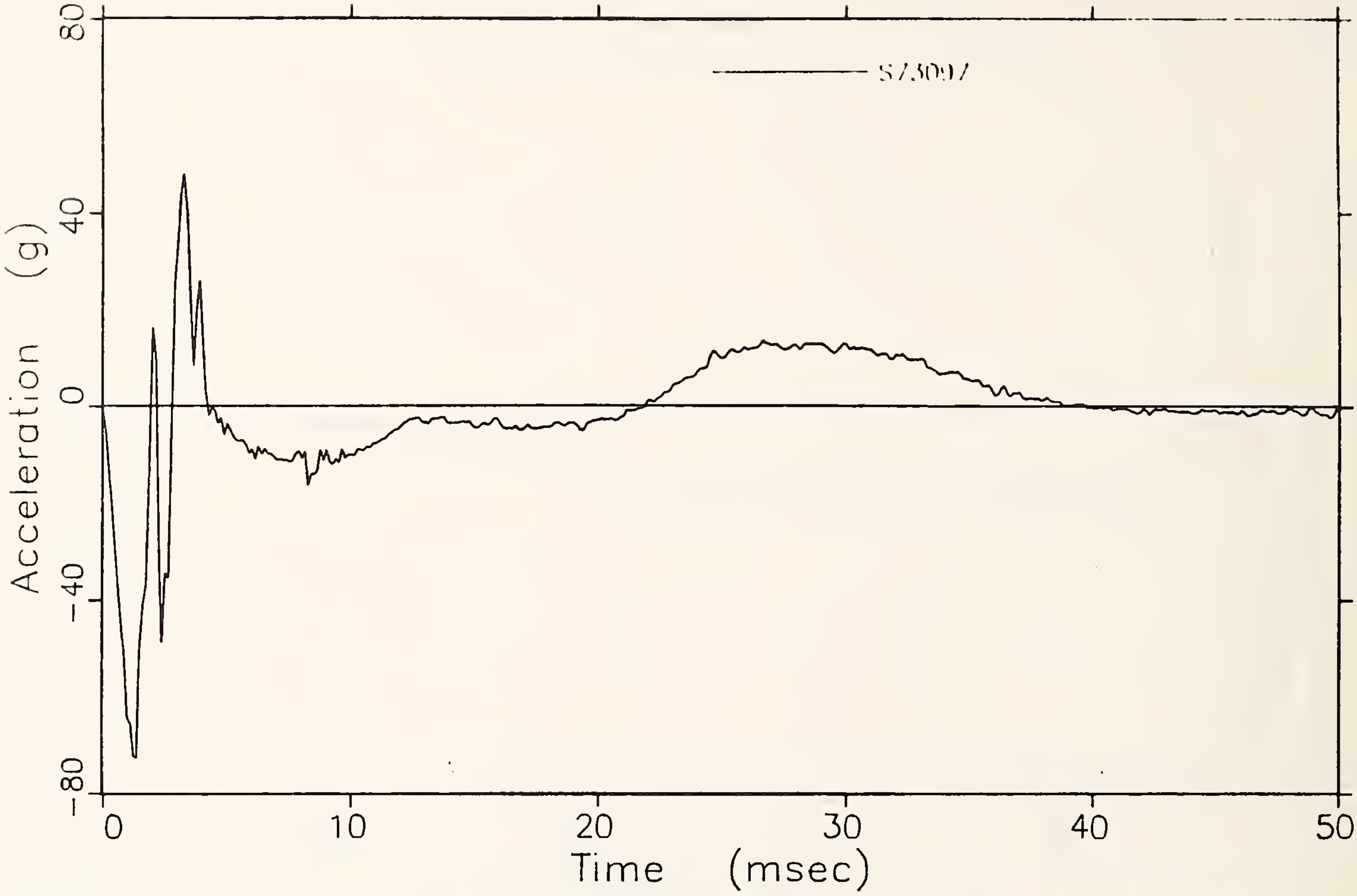

FIGURE B.3 -- Aries Reconstruction: Head C.G. Z-Axis Acceleration

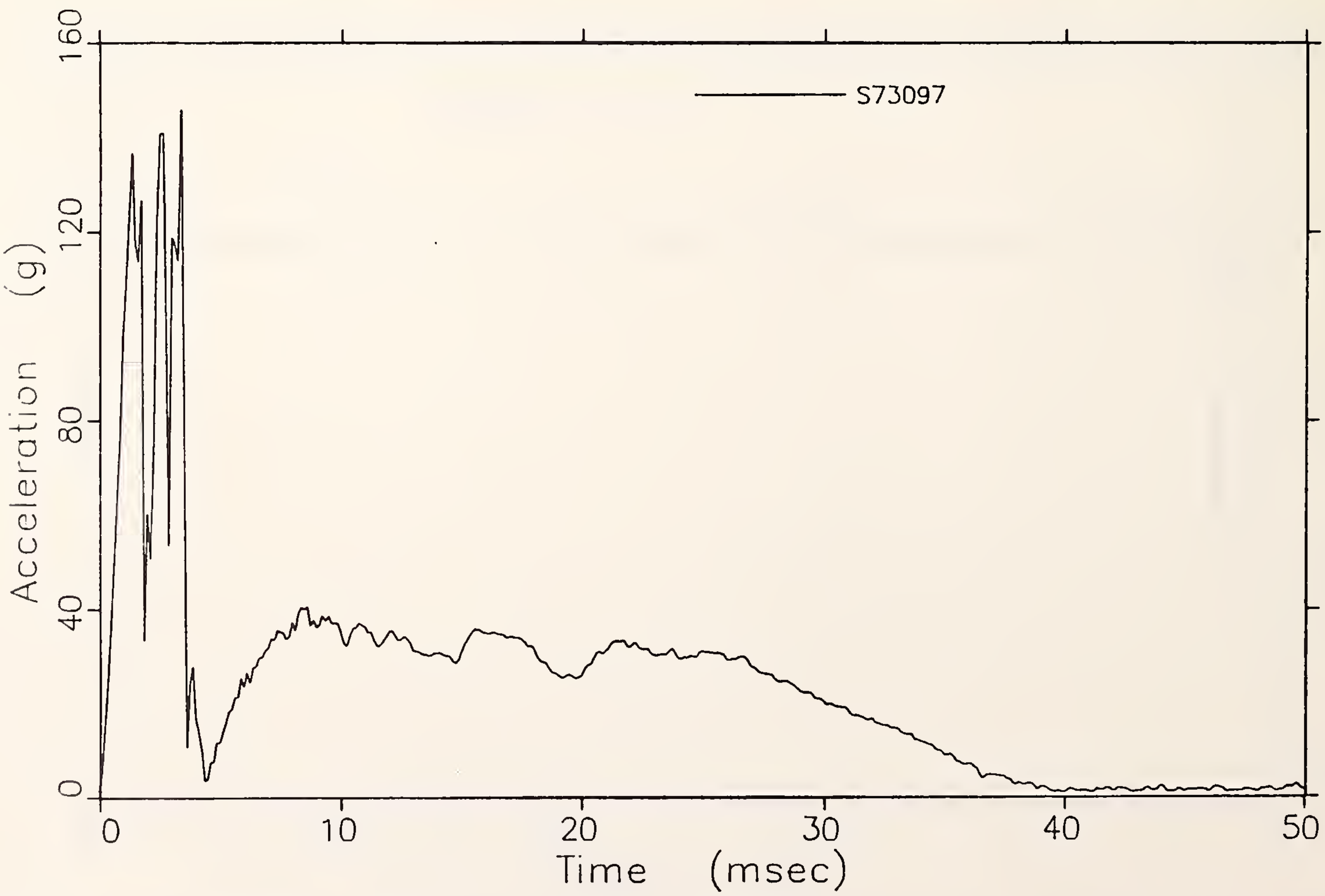

FIGURE B.4 -- Aries Reconstruction: Head C.G. Resultant Acceleration

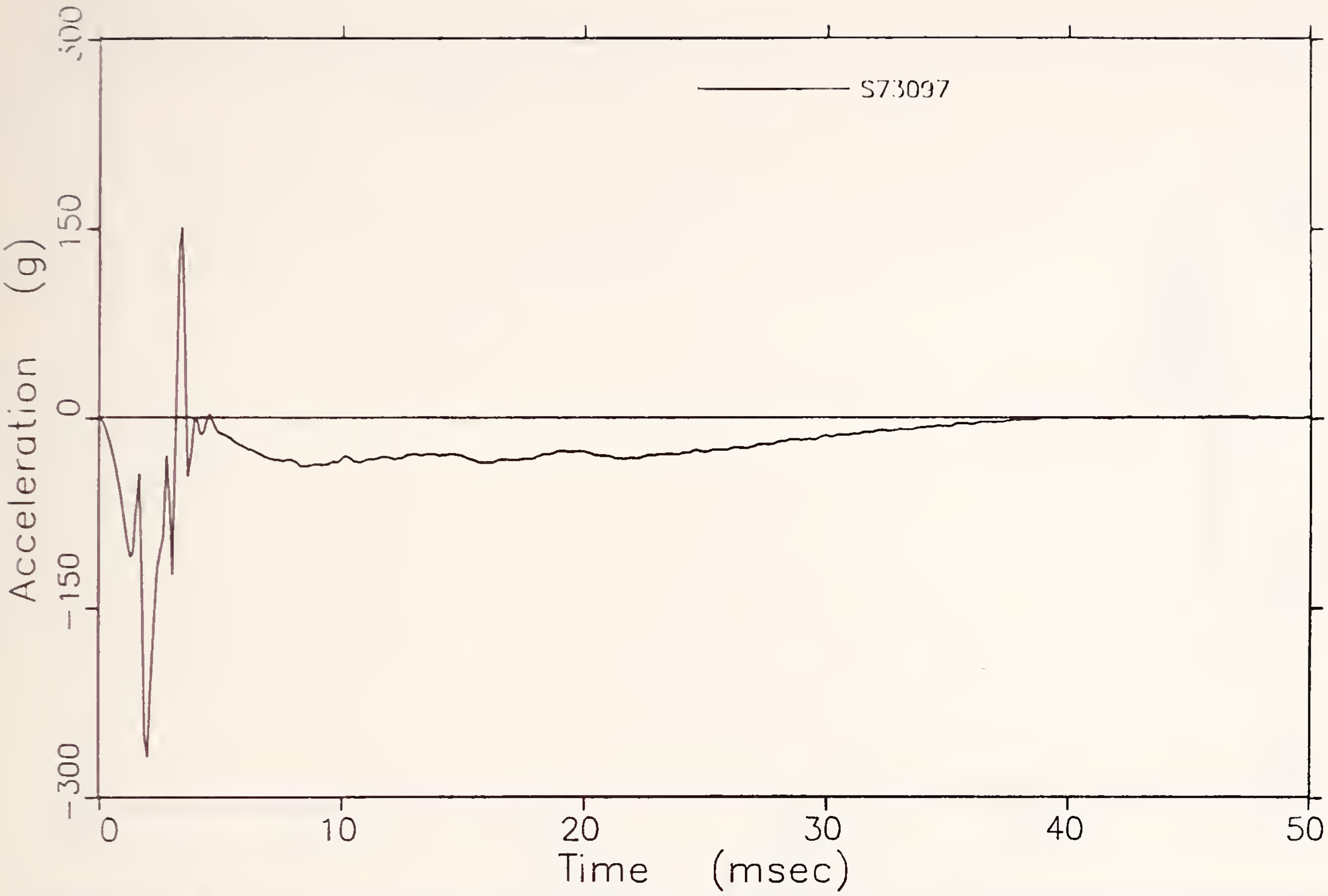

FIGURE B.5 -- Aries Reconstruction: X-Direction Acceleration at Array Position Number 1

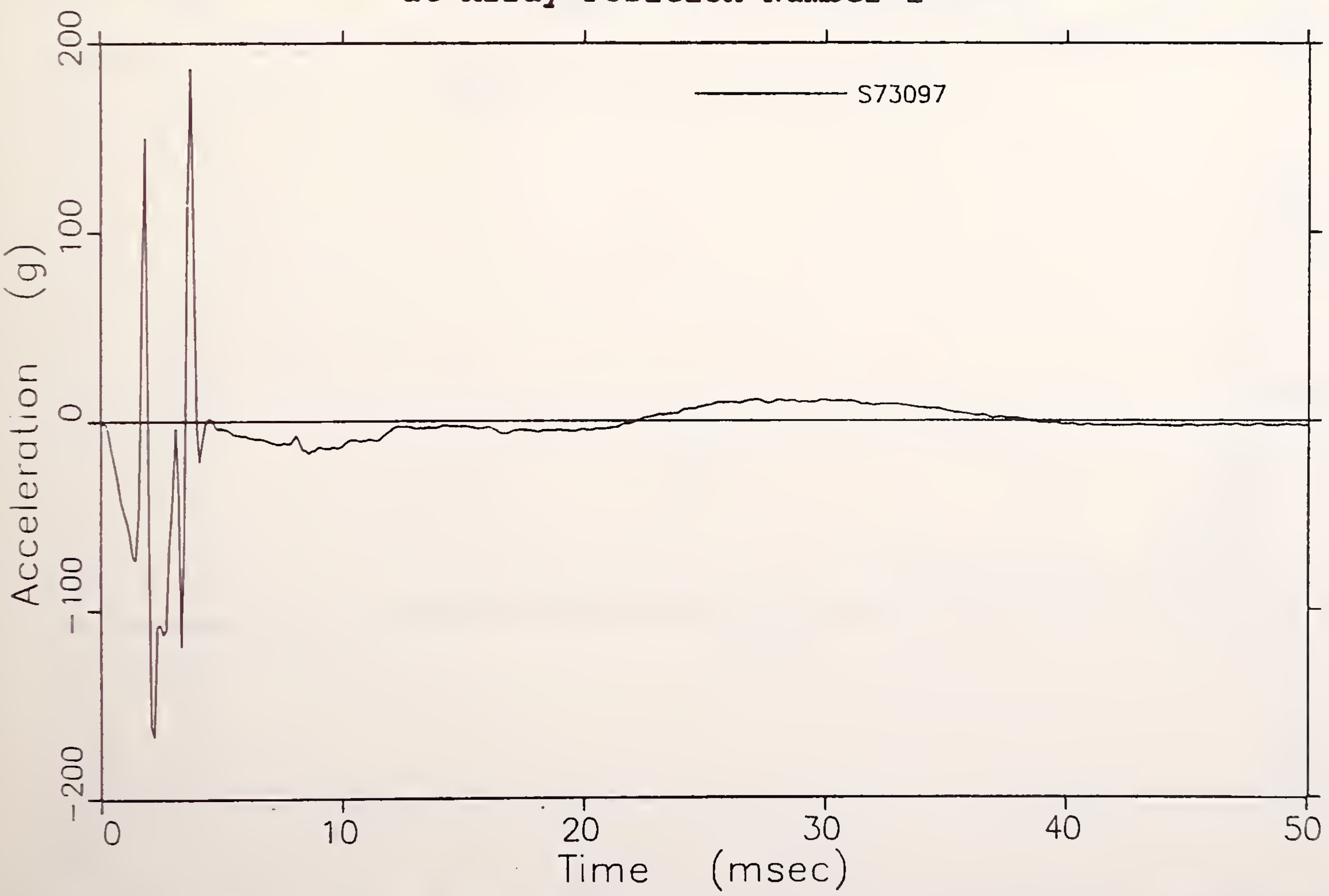

FIGURE B.6 -- Aries Reconstruction: Z-Direction Acceleration at Array Position Number 1

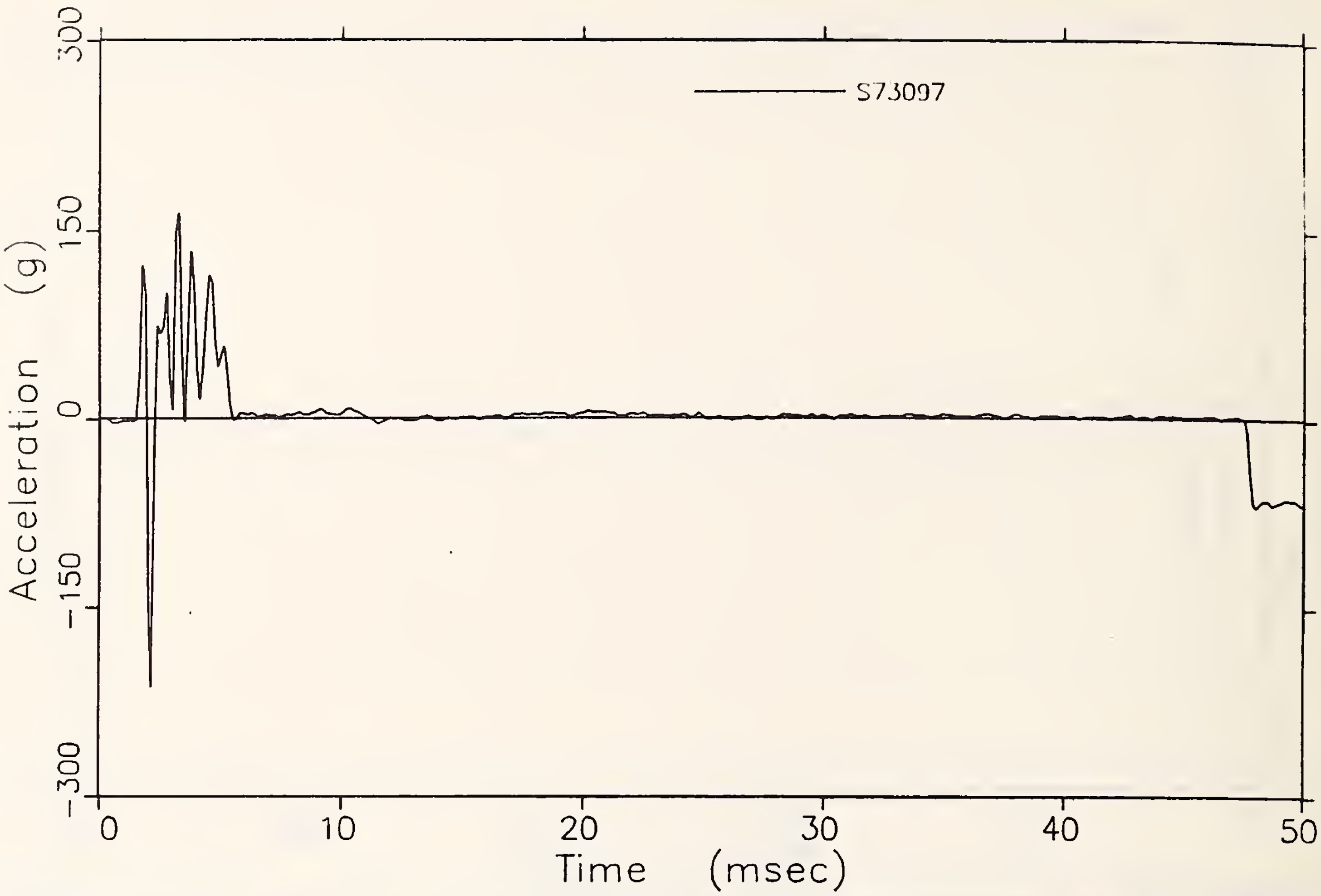

FIGURE B.7 -- Aries Reconstruction: Y-Direction Acceleration at Array Position Number 2

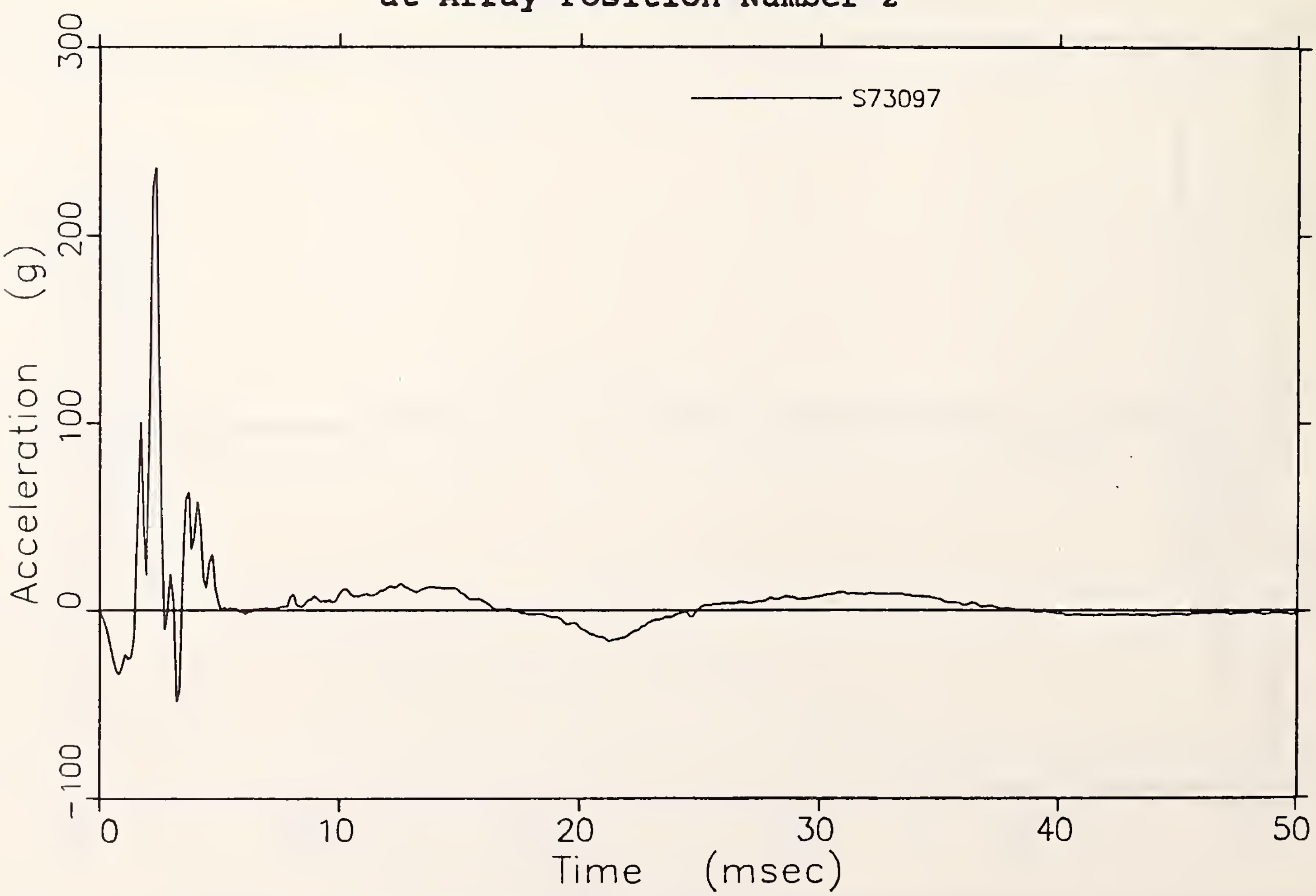

FIGURE B.8 -- Aries Reconstruction: Z-Direction Acceleration at Array Position Number 2

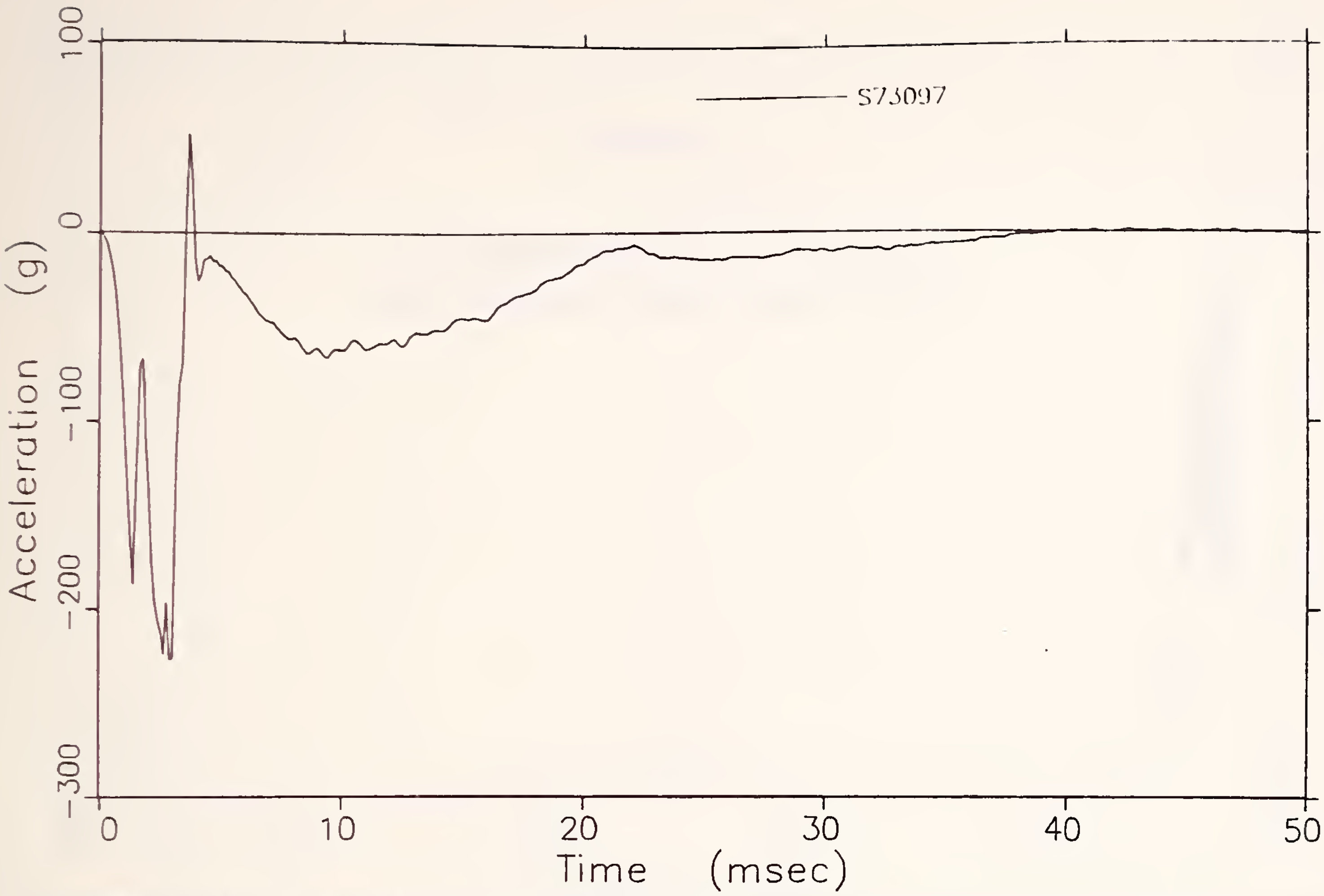

FIGURE B.9 -- Aries Reconstruction: X-Direction Acceleration at Array Position Number 3

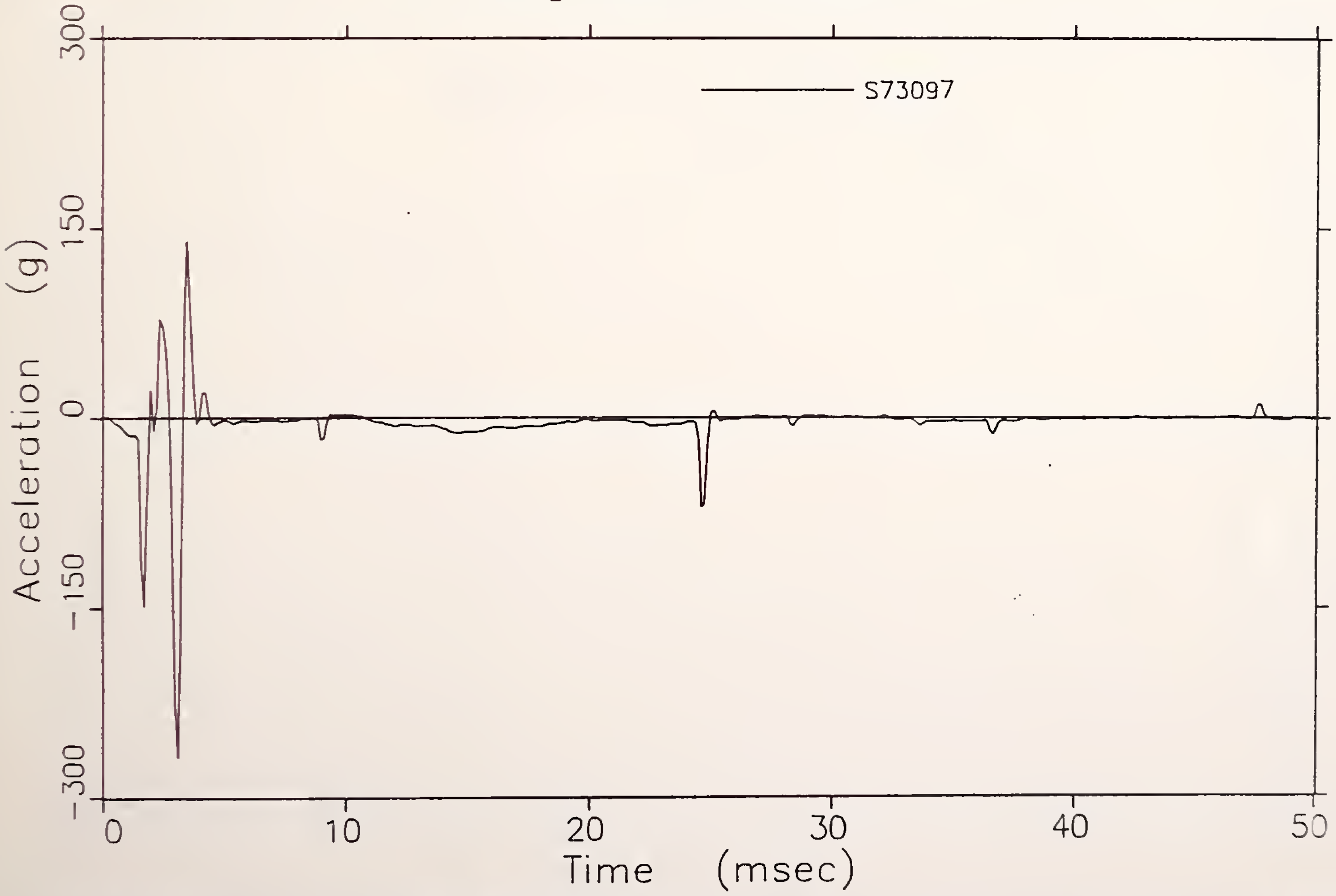

FIGURE B.10 -- Aries Reconstruction: Y-Direction Acceleration at Array Position Number 3

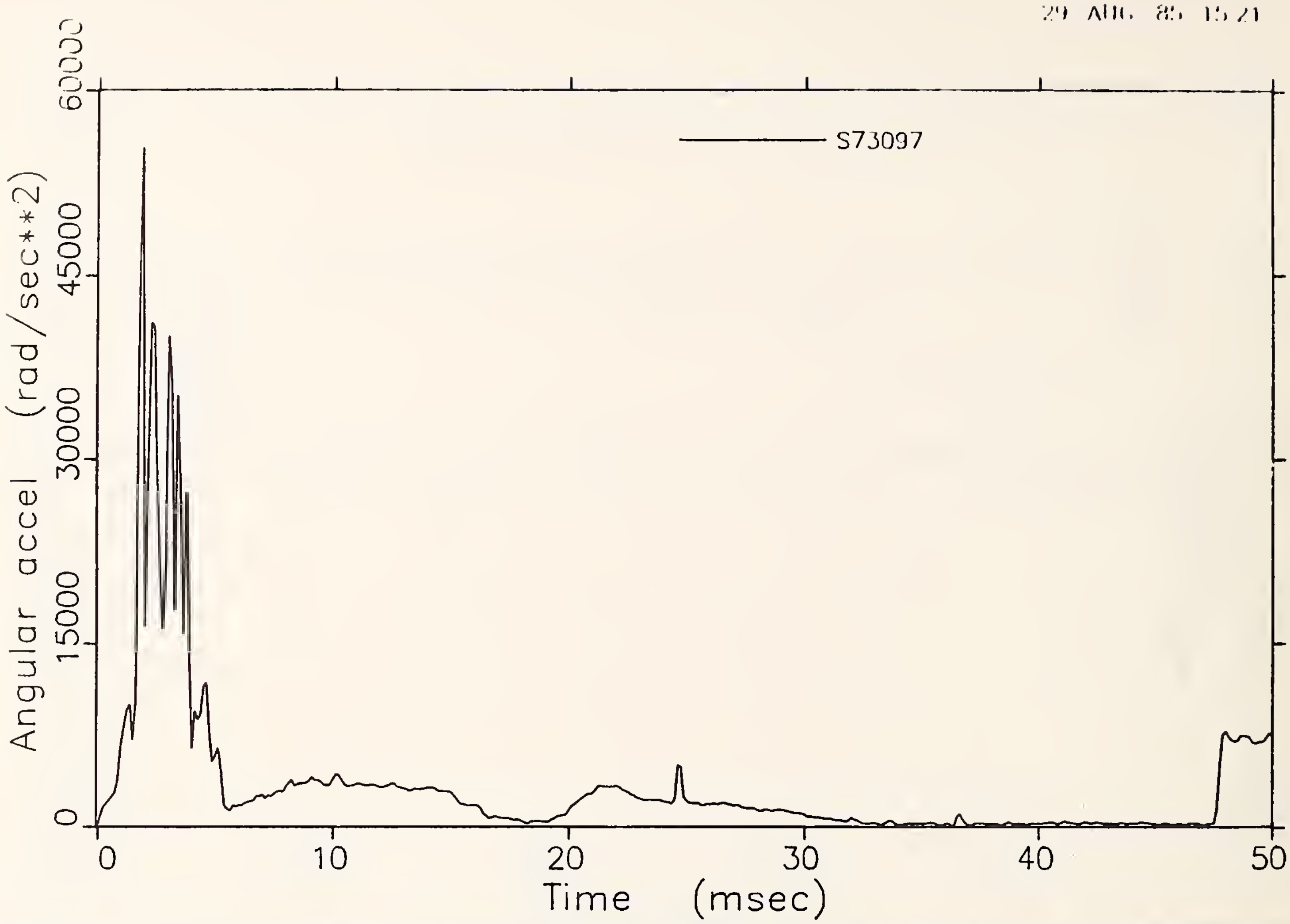

FIGURE B.11 -- Aries Reconstruction: Resultant Rotational Acceleration

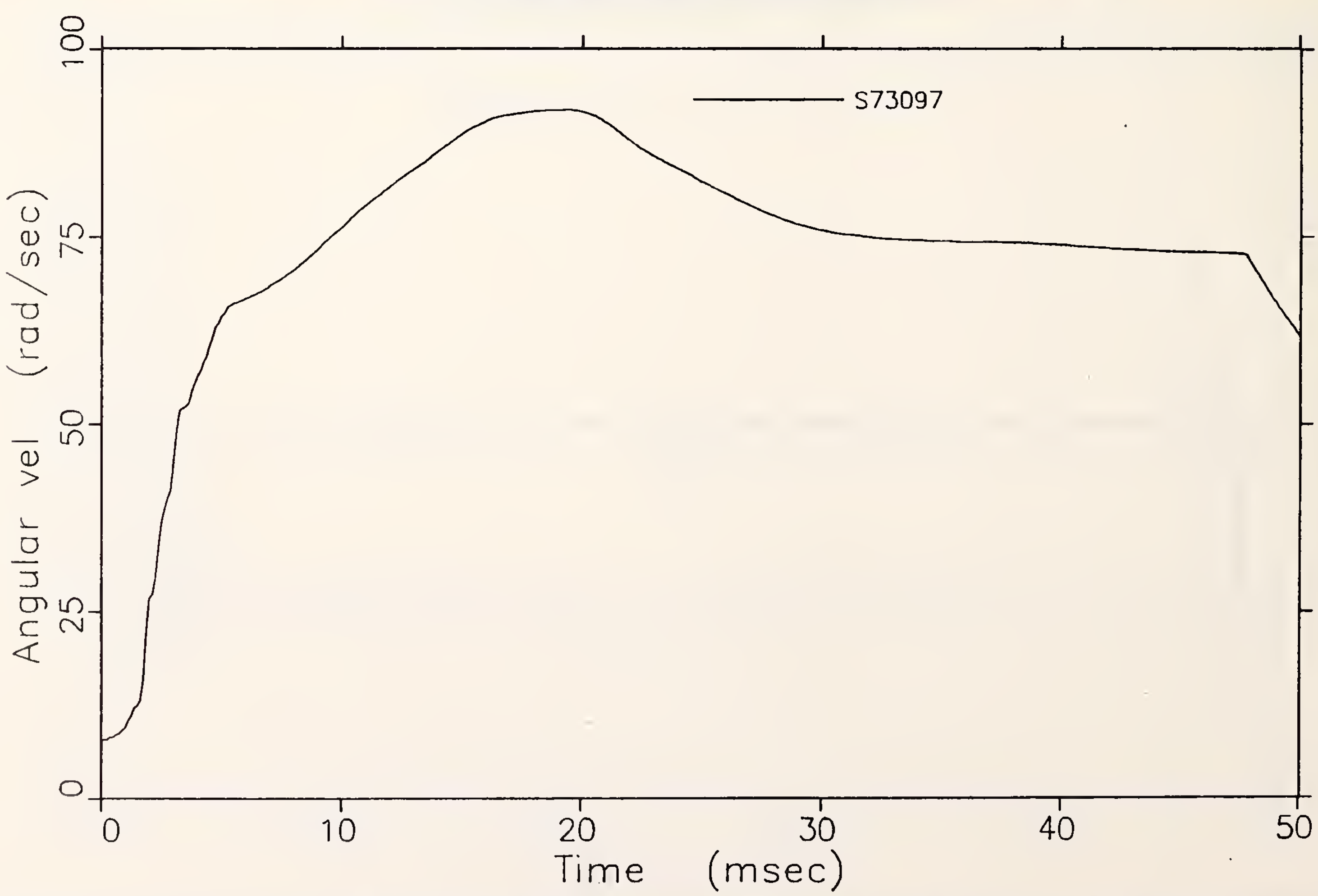

FIGURE B.12 -- Aries Reconstruction: Resultant Rotational Velocity

APPENDIX C

S-10 Reconstruction Data for Test Numbers S73103 and S73104

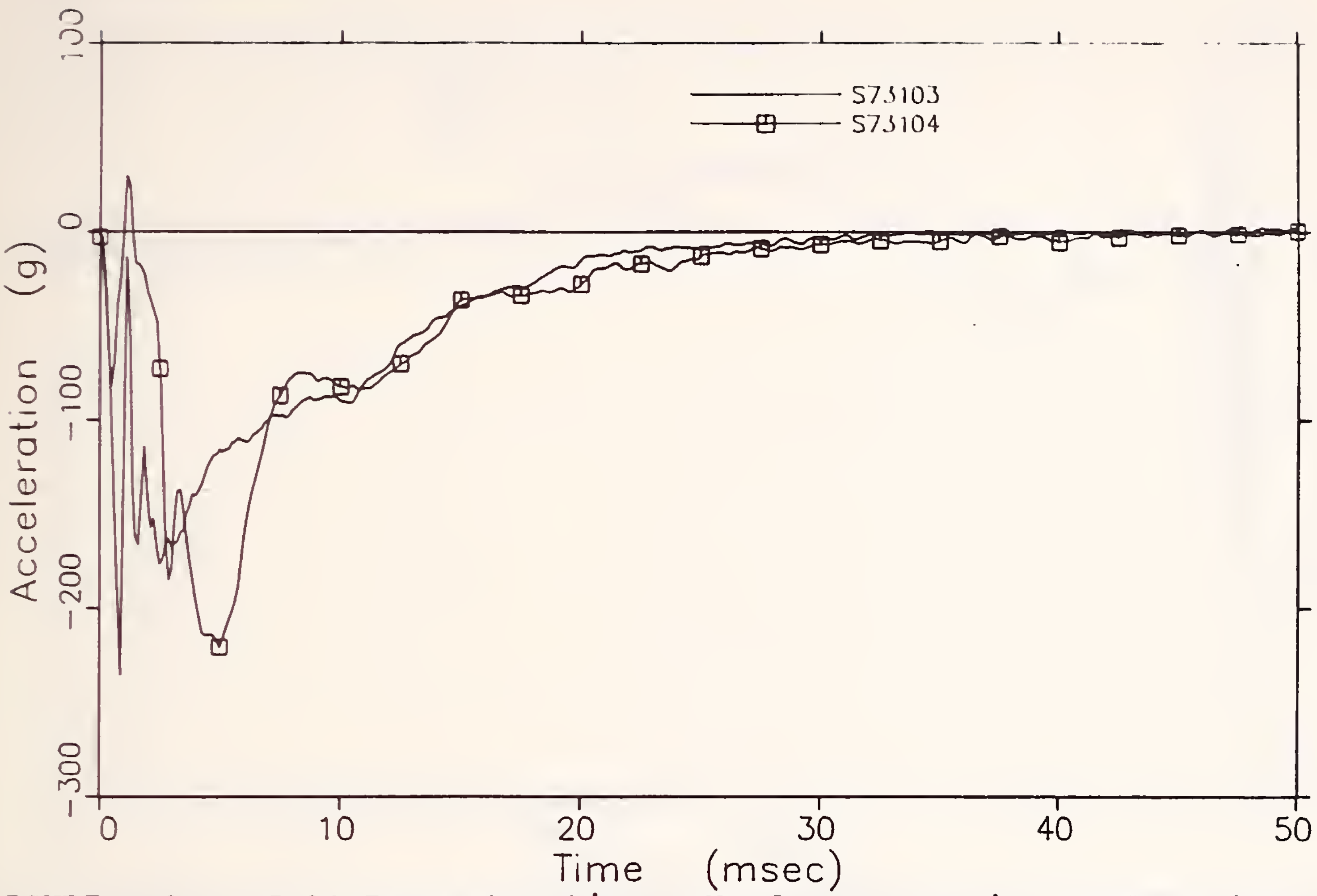

FIGURE C.1 -- S-10 Reconstruction: Head C.G. X-Axis Acceleration

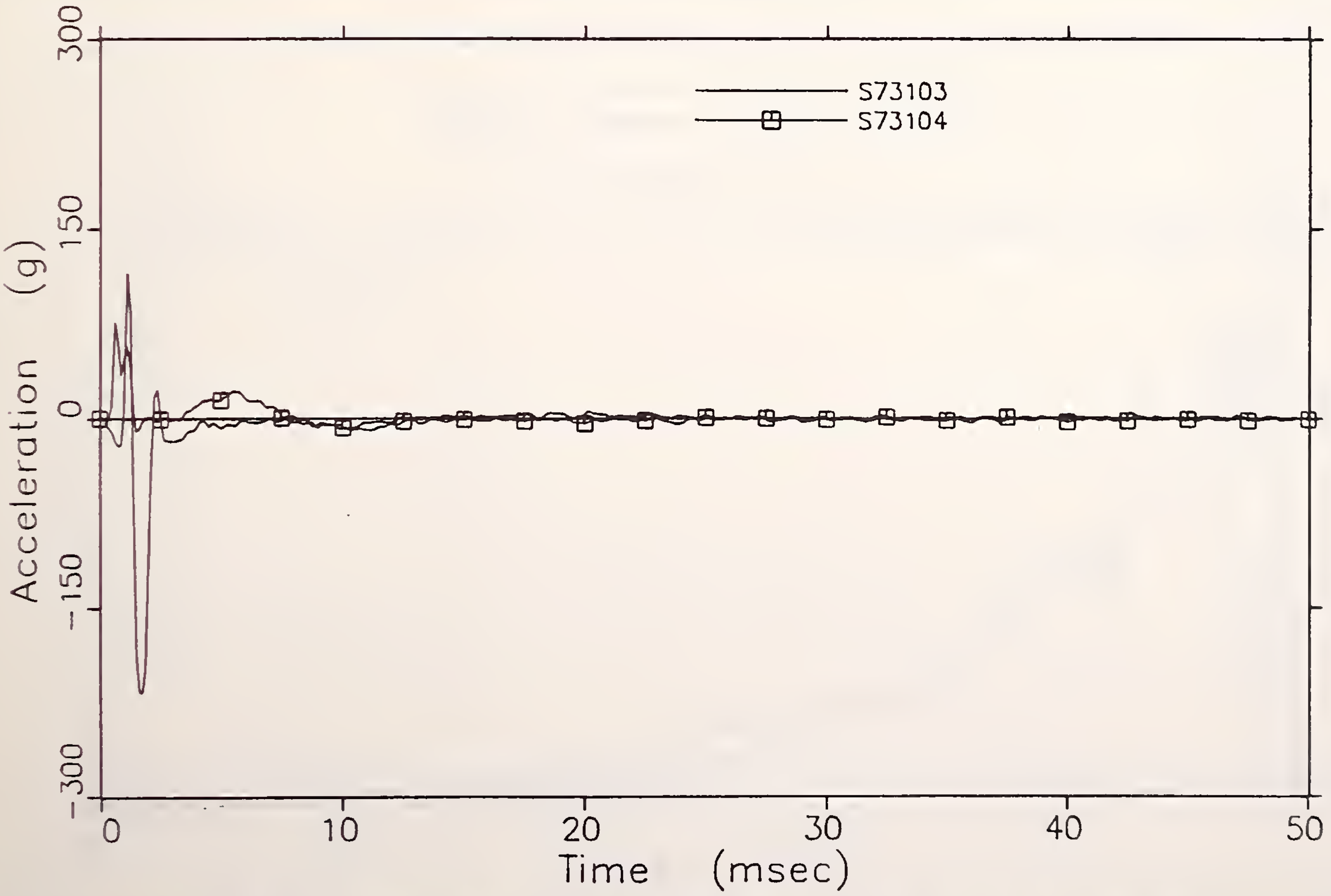

FIGURE C.2 -- S-10 Reconstruction: Head C.G. Y-Axis Acceleration

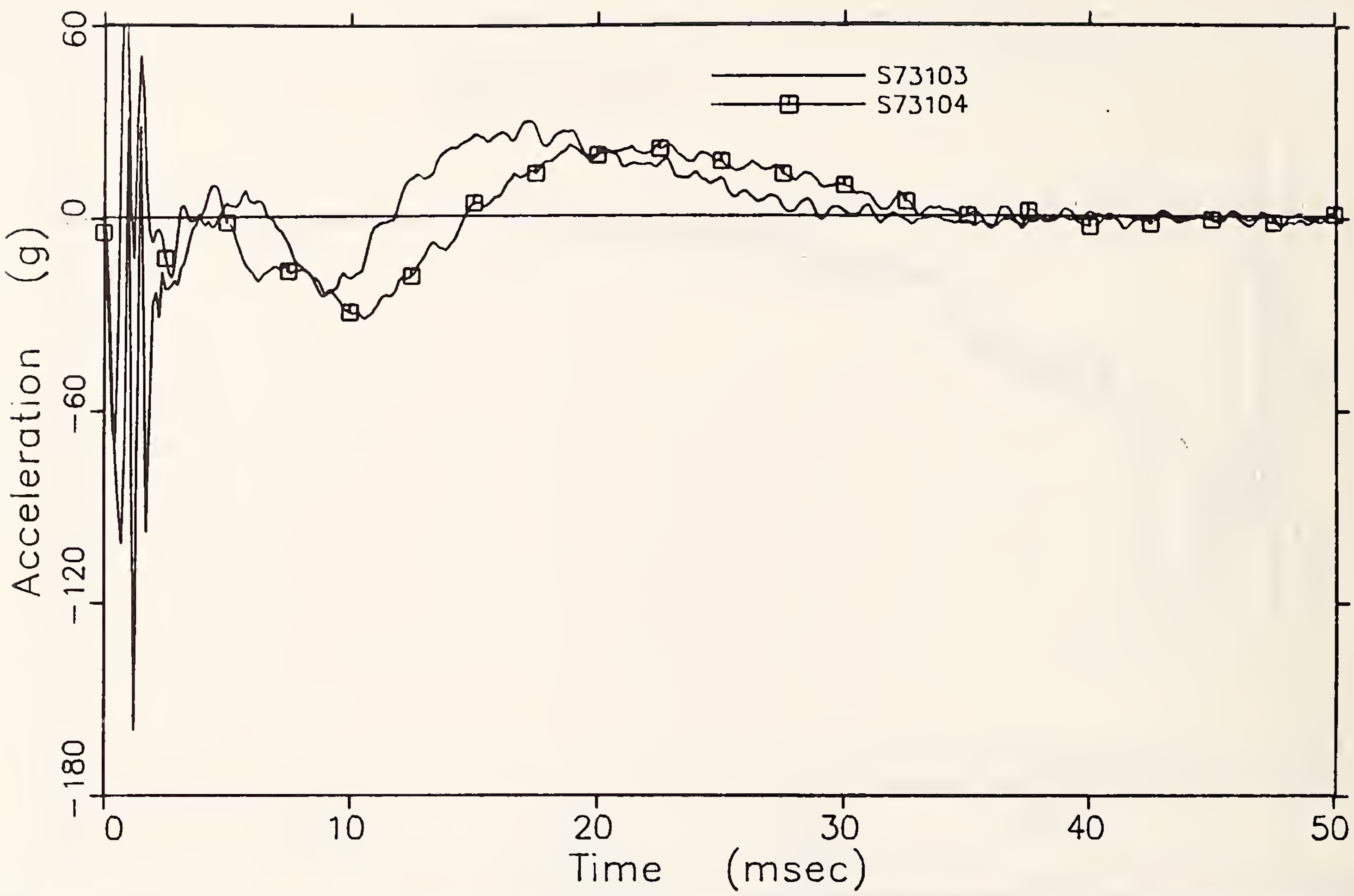

FIGURE C.3 -- S-10 Reconstruction: Head C.G. Z-Axis Acceleration

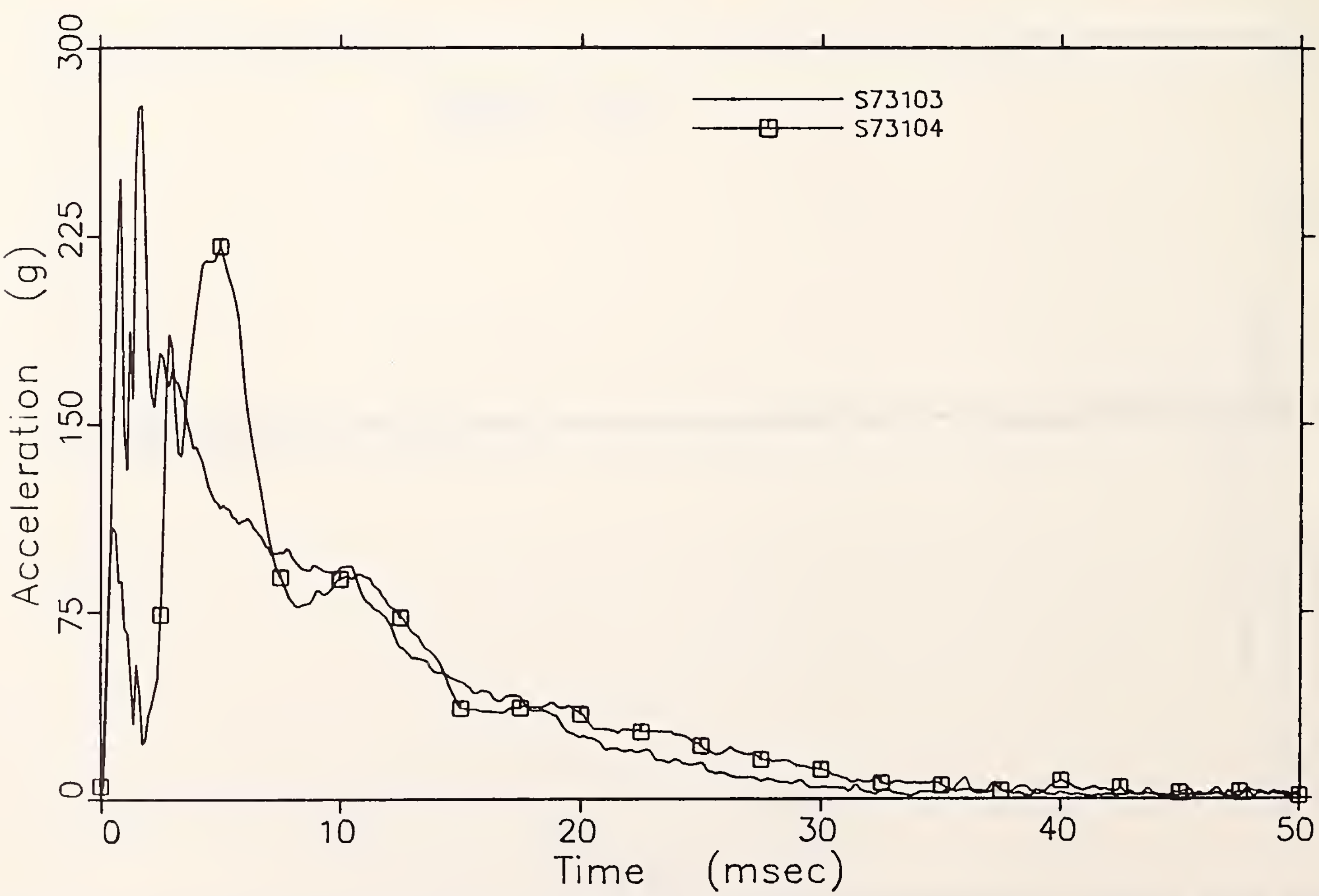

FIGURE C.4 -- S-10 Reconstruction: Head C.G. Resultant Acceleration

30-AUG-85 13:28

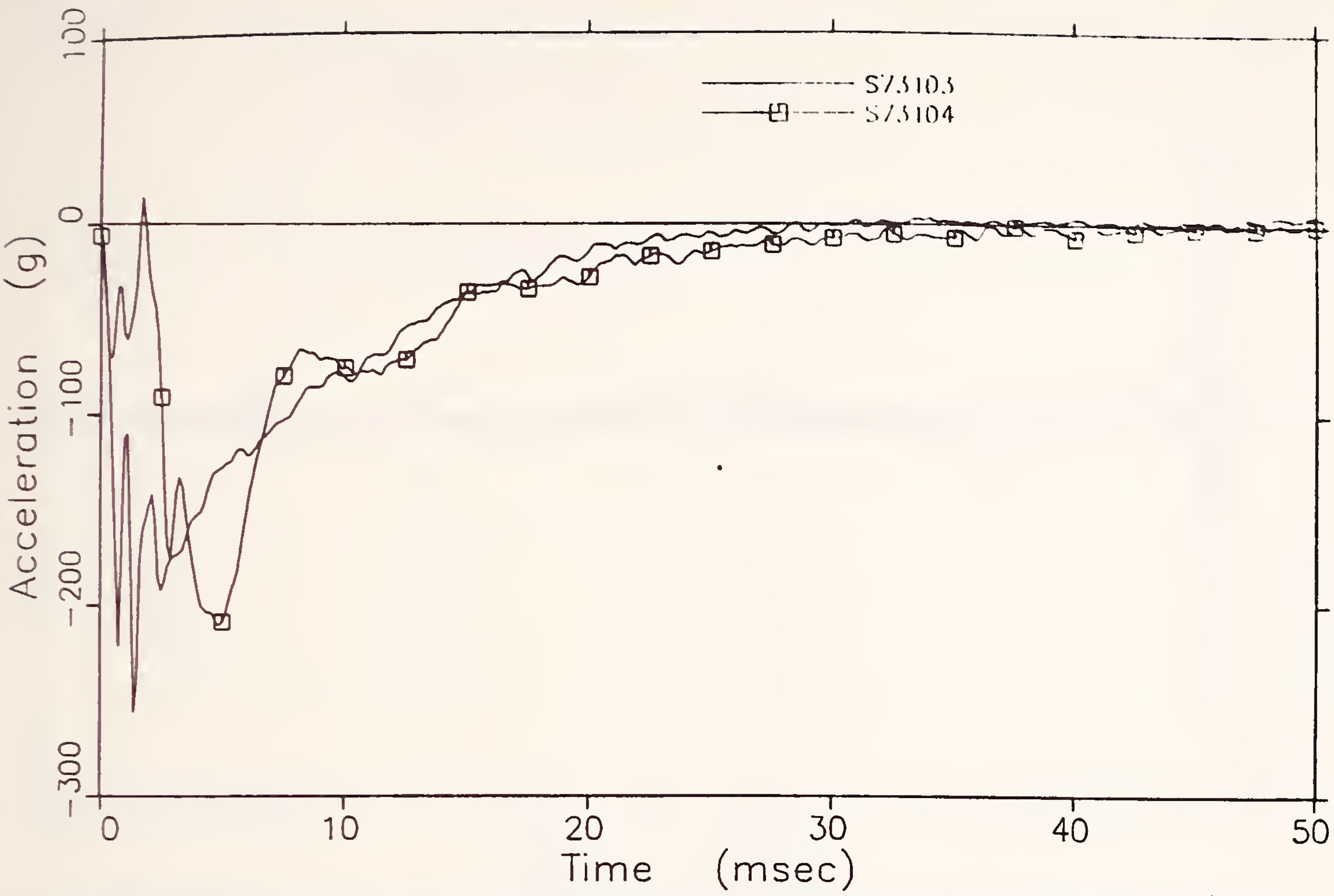

FIGURE C.5 -- S-10 Reconstruction: X-Direction Acceleration at Array Position Number 1

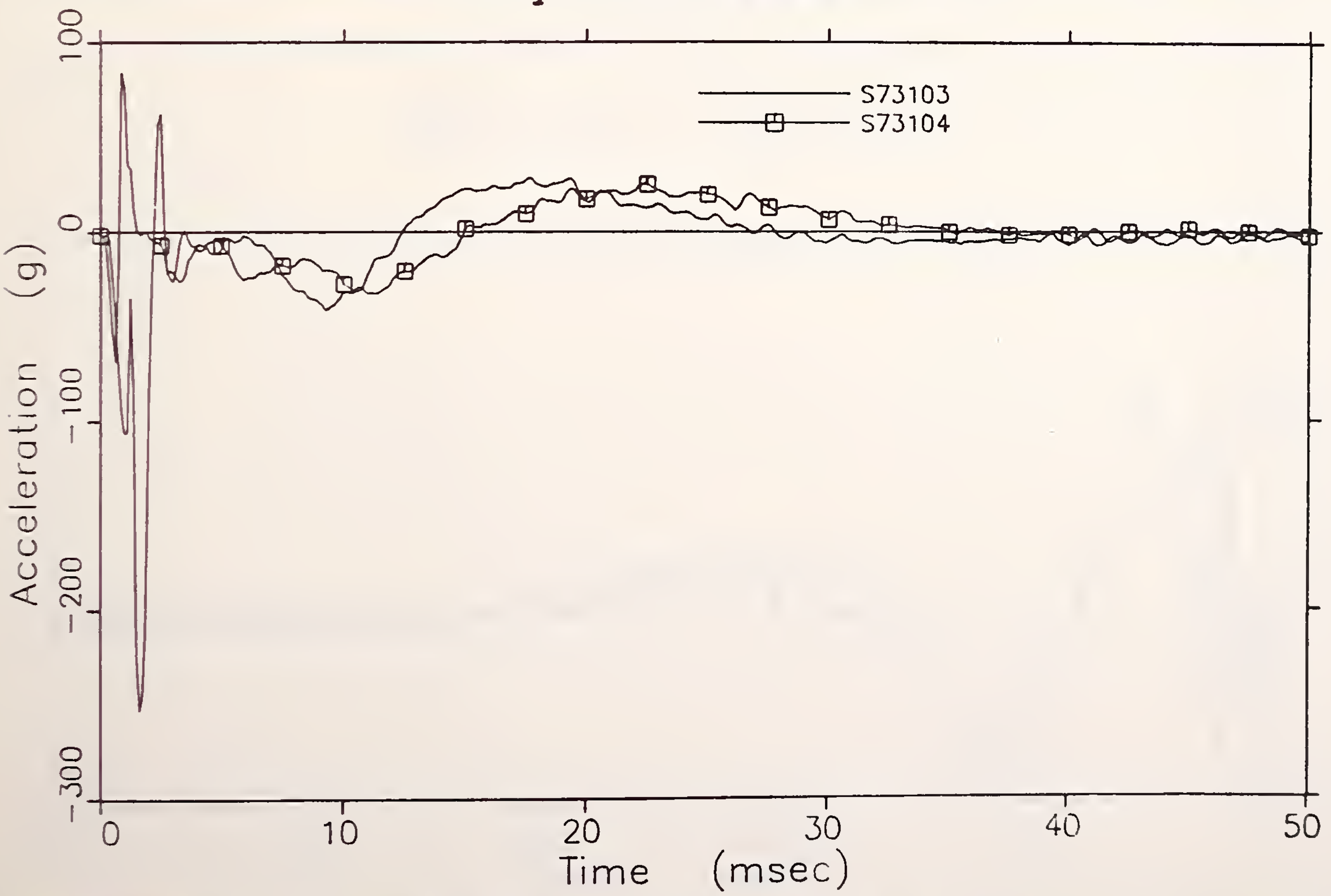

FIGURE C.6 -- S-10 Reconstruction: Z-Direction Acceleration at Array Position Number 1

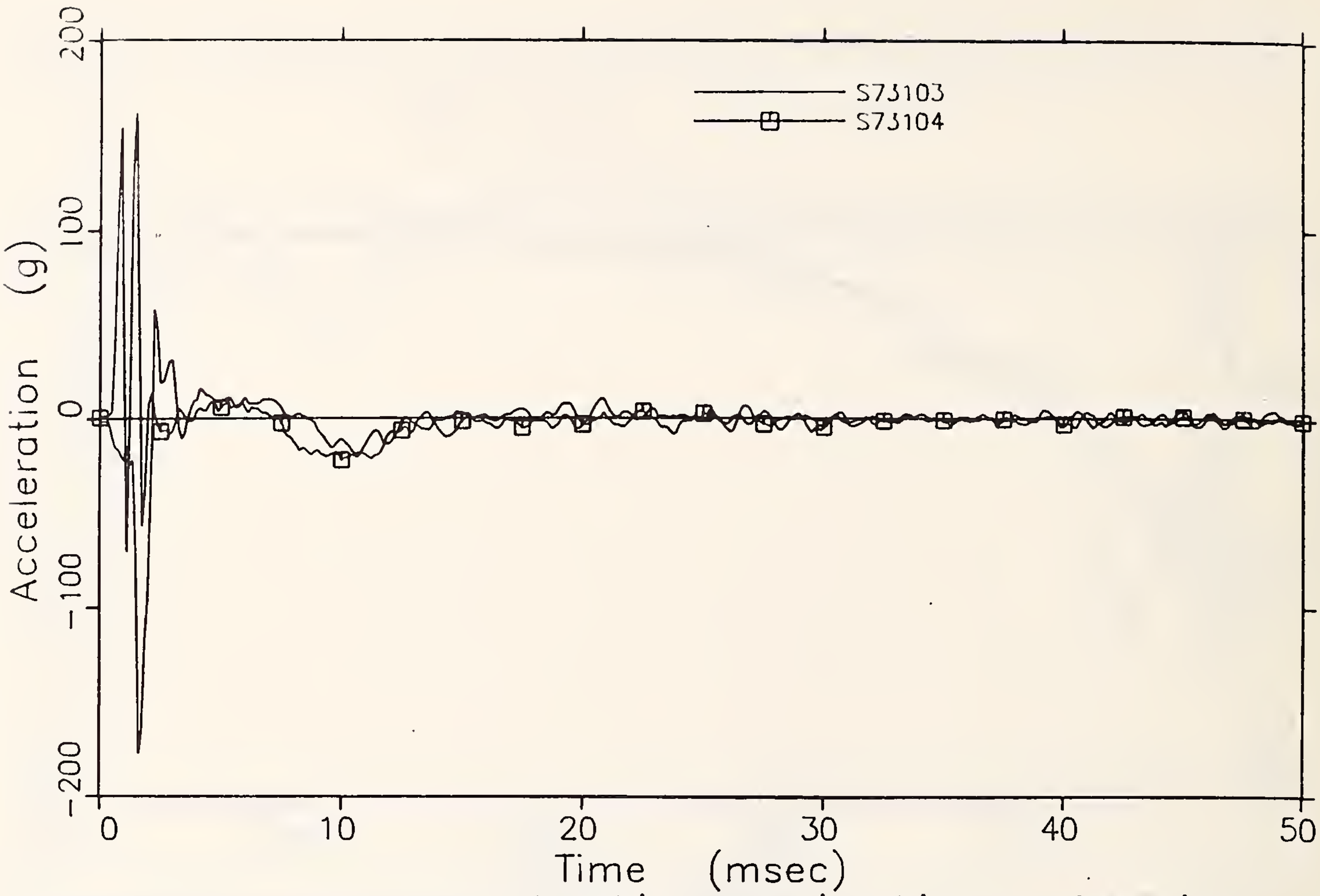

FIGURE C.7 -- S-10 Reconstruction: Y-Direction Acceleration at Array Position Number 2

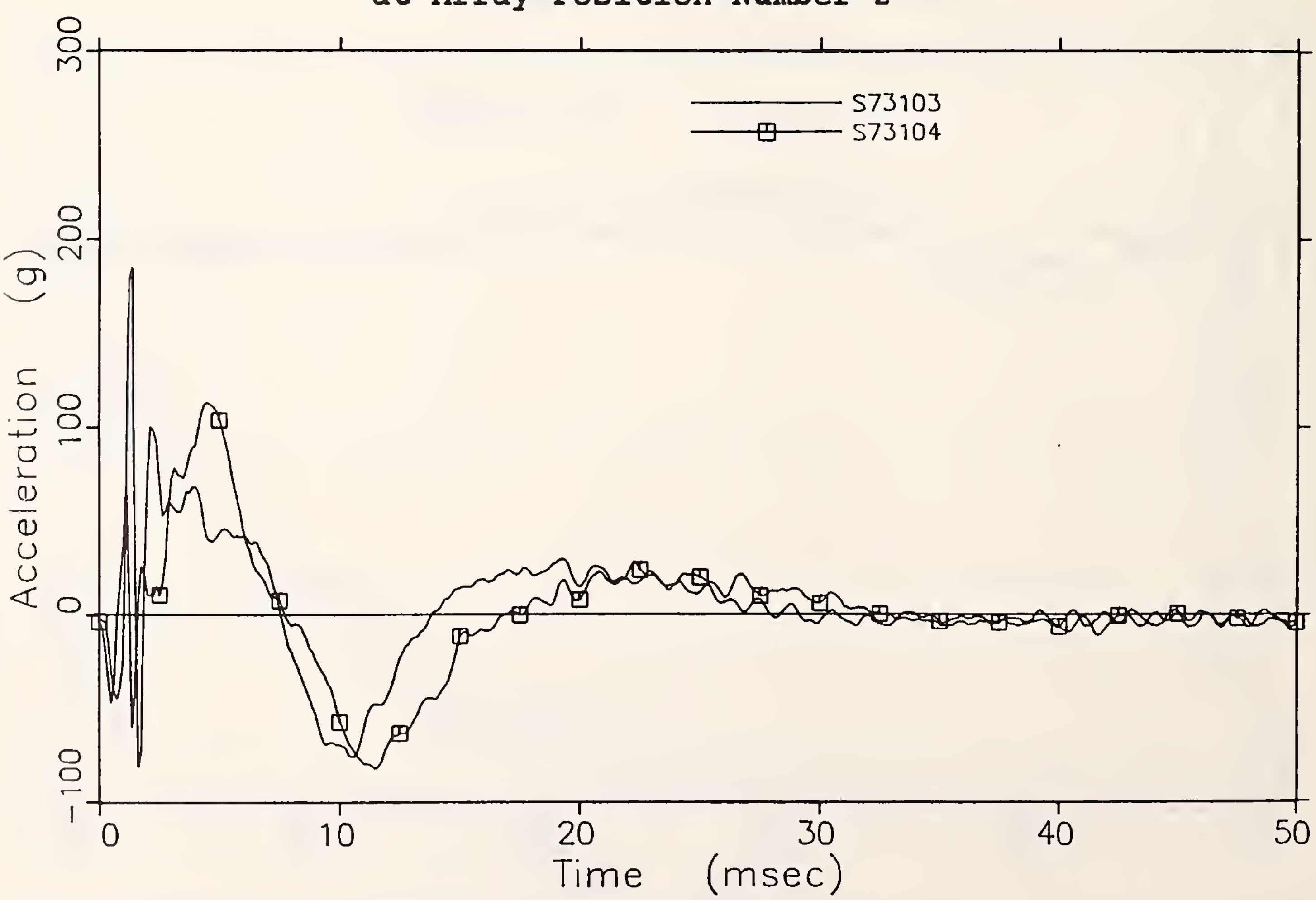

FIGURE C.8 -- S-10 Reconstruction: Z-Direction Acceleration at Array Position Number 2

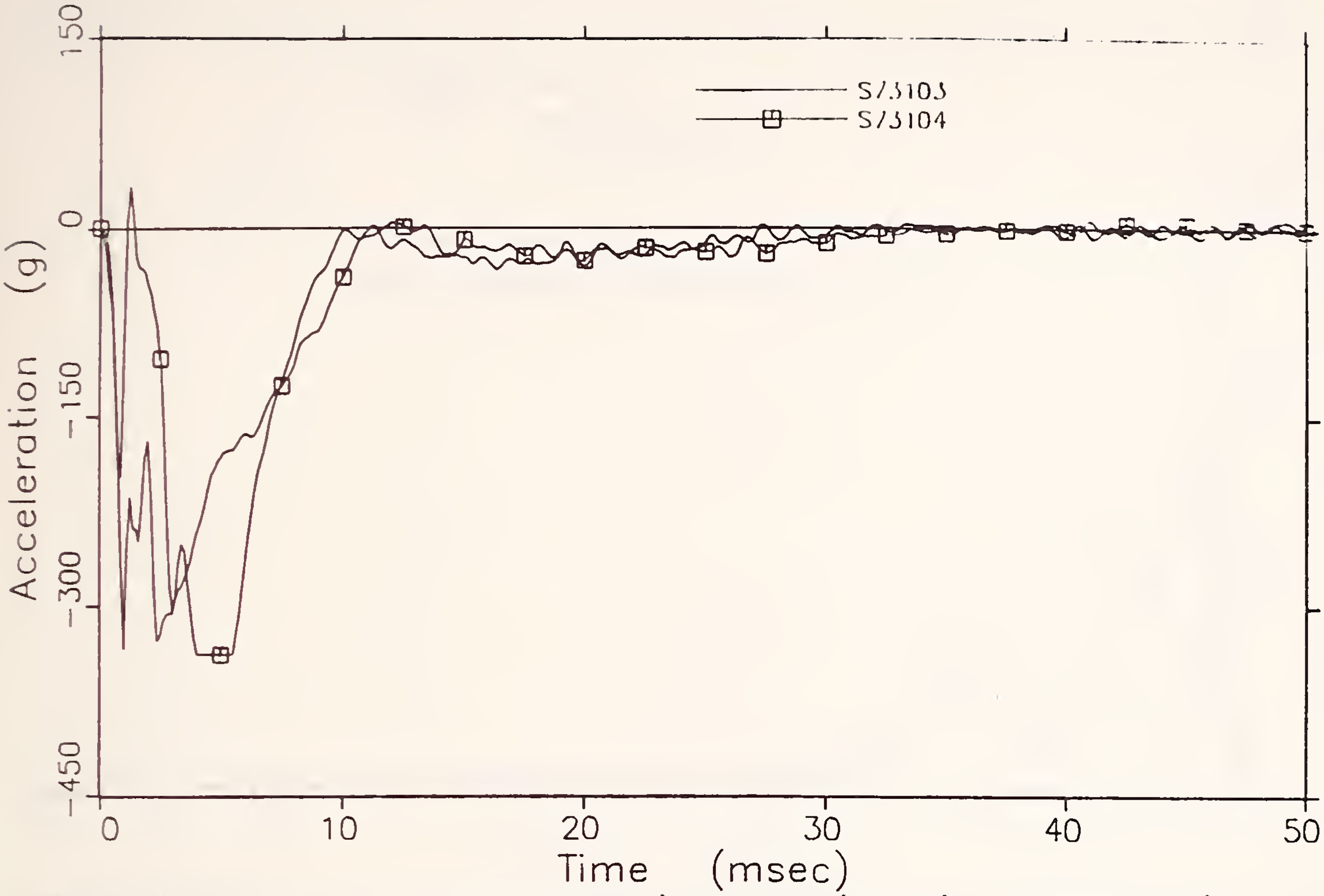

FIGURE C.9 -- S-10 Reconstruction: X-Direction Acceleration at Array Position Number 3

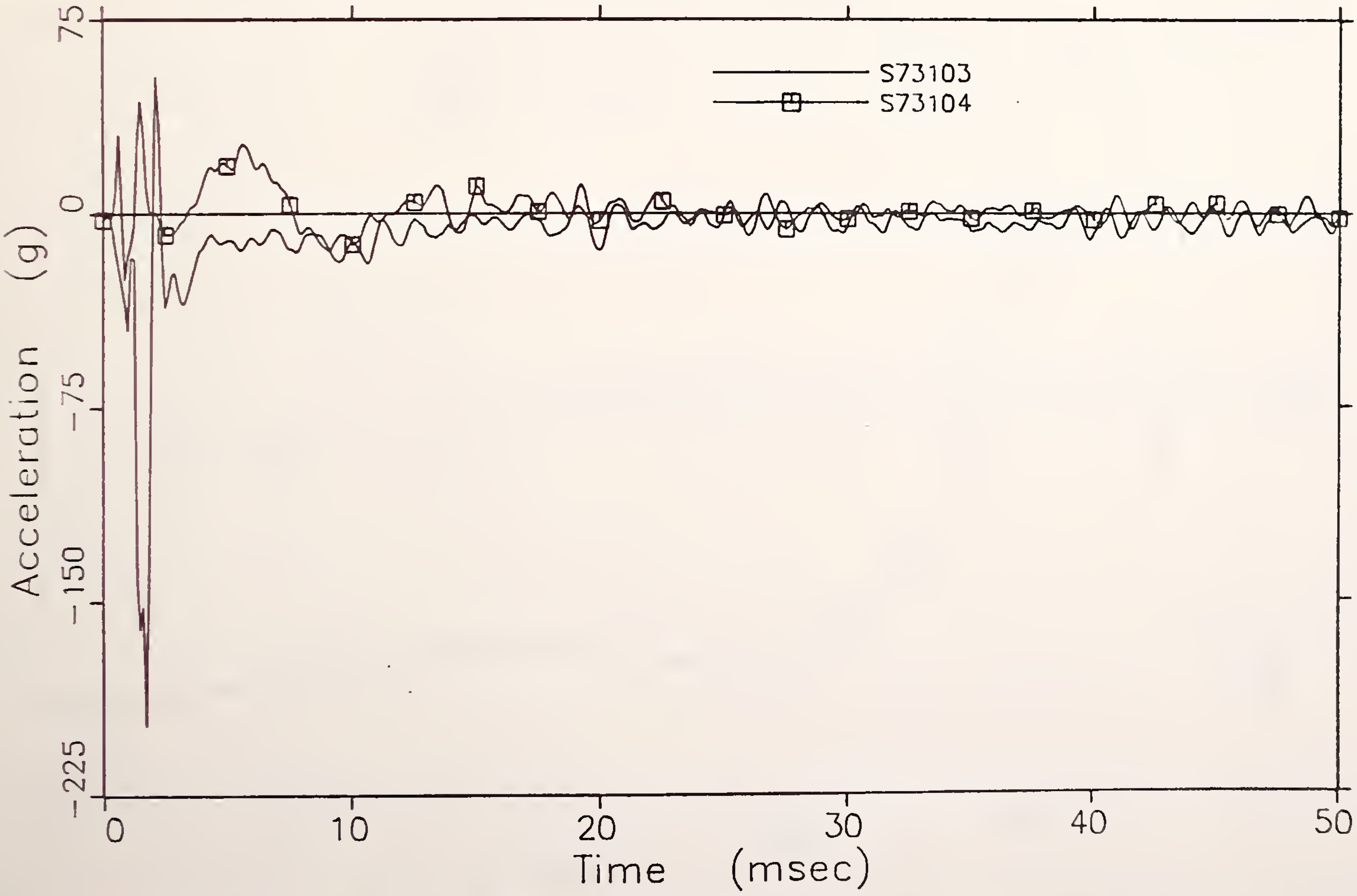

FIGURE C.10 -- S-10 Reconstruction: Y-Direction Acceleration at Array Position Number 3

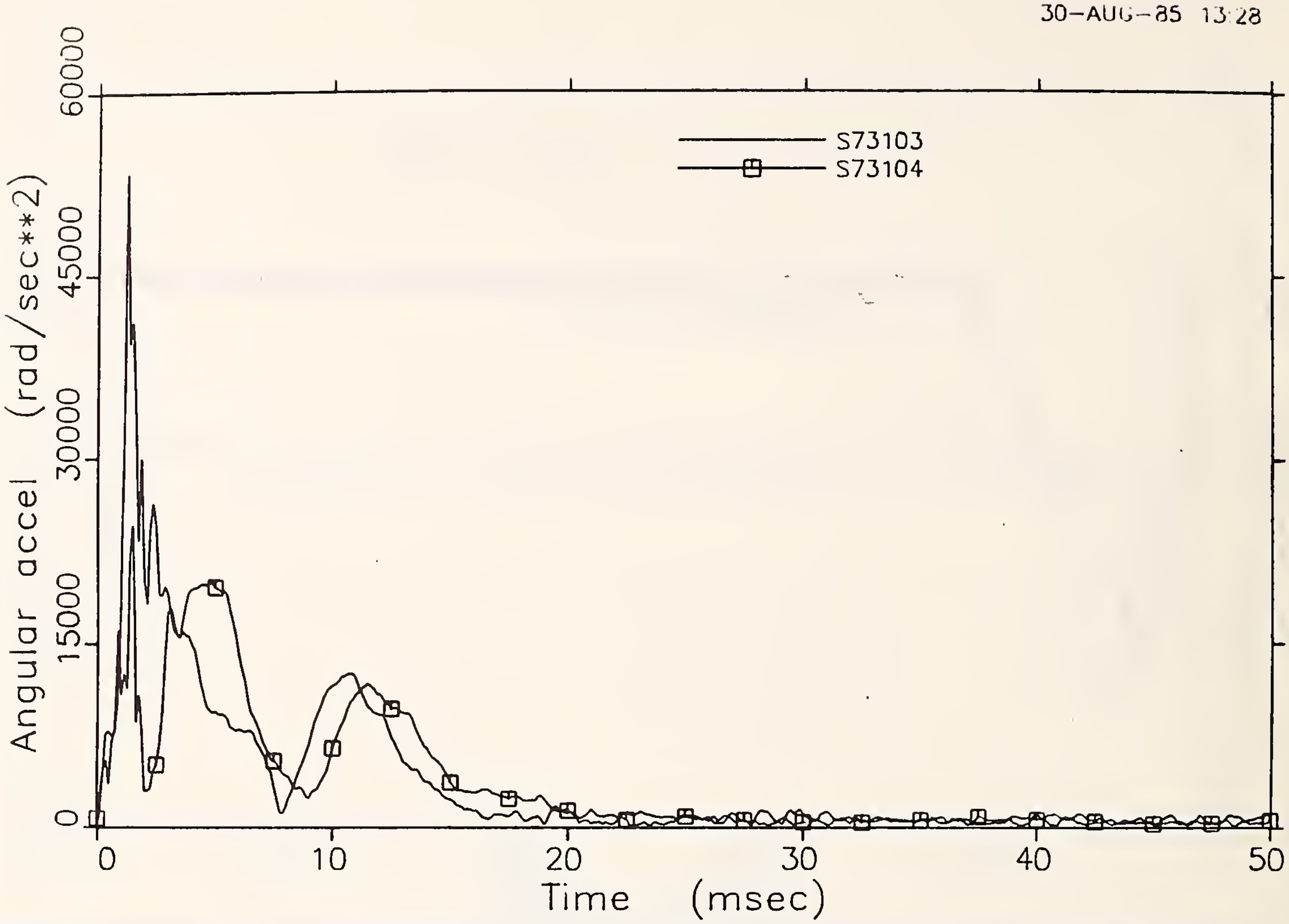

FIGURE C.11 -- S-10 Reconstruction: Resultant Rotational Acceleration

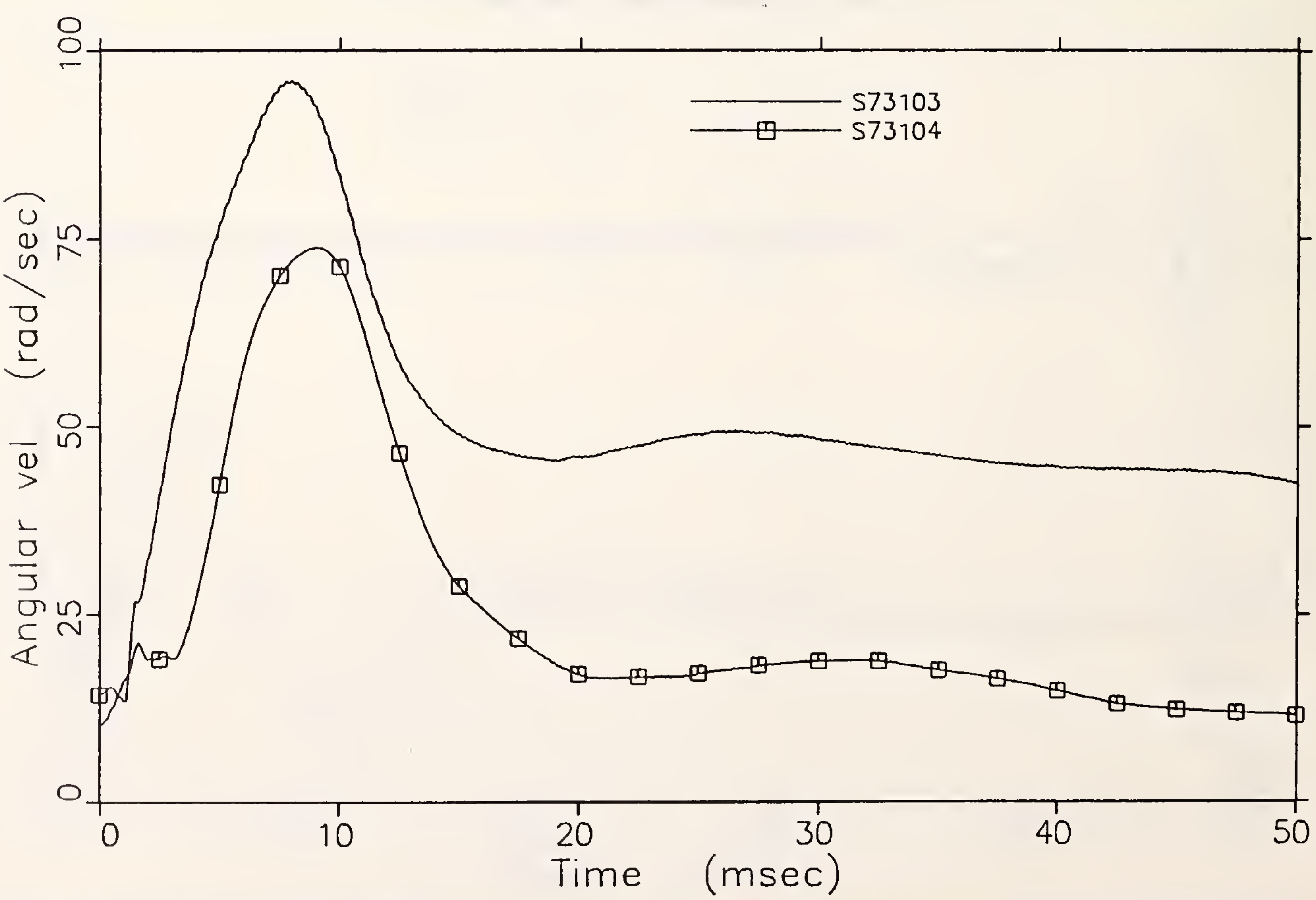

FIGURE C.12 -- S-10 Reconstruction: Resultant Rotational Velocity

APPENDIX D

Duster Reconstruction Data for Test Numbers S73108 and S73110

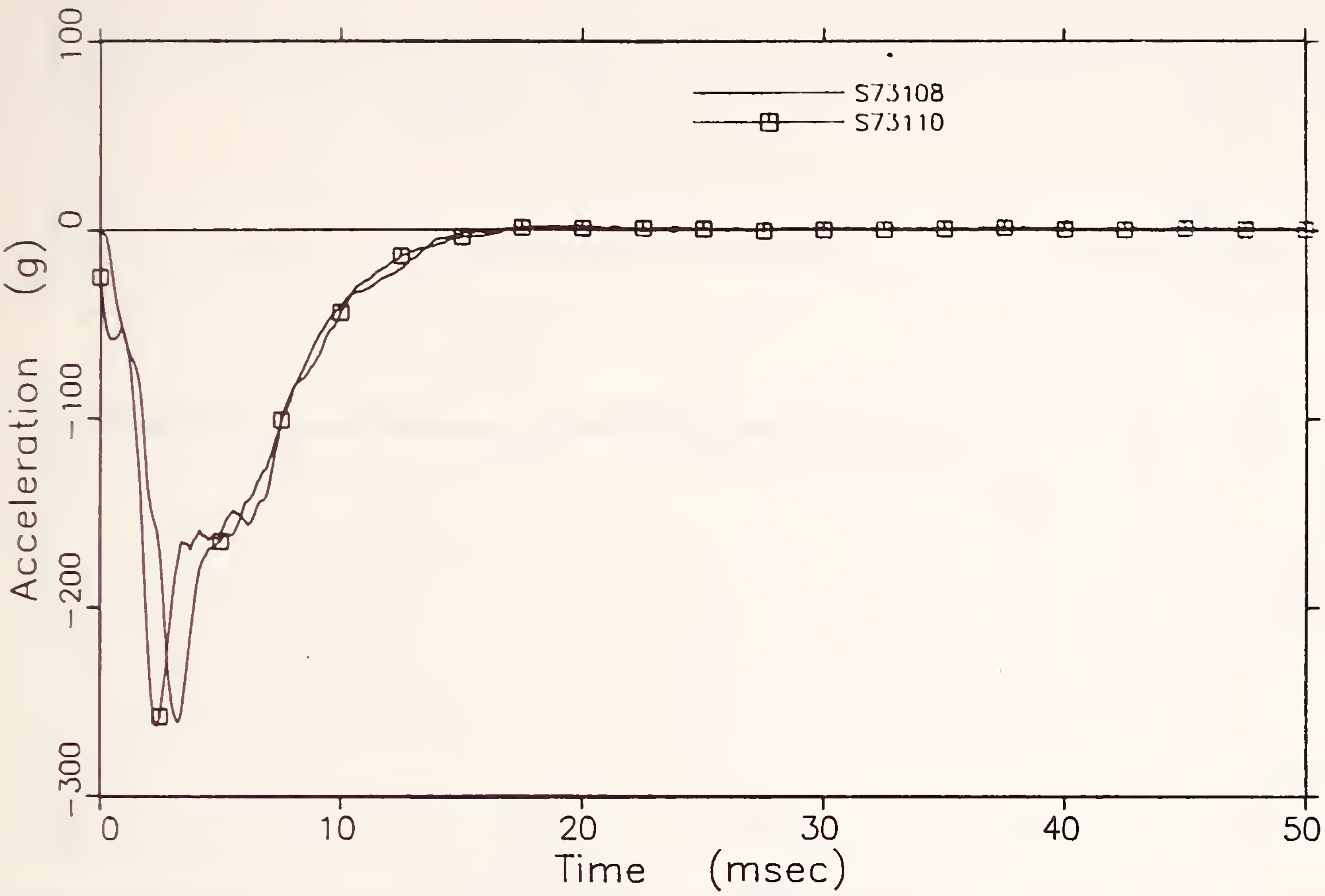

FIGURE D.1 -- Duster Reconstruction: Head C.G. X-Axis Acceleration

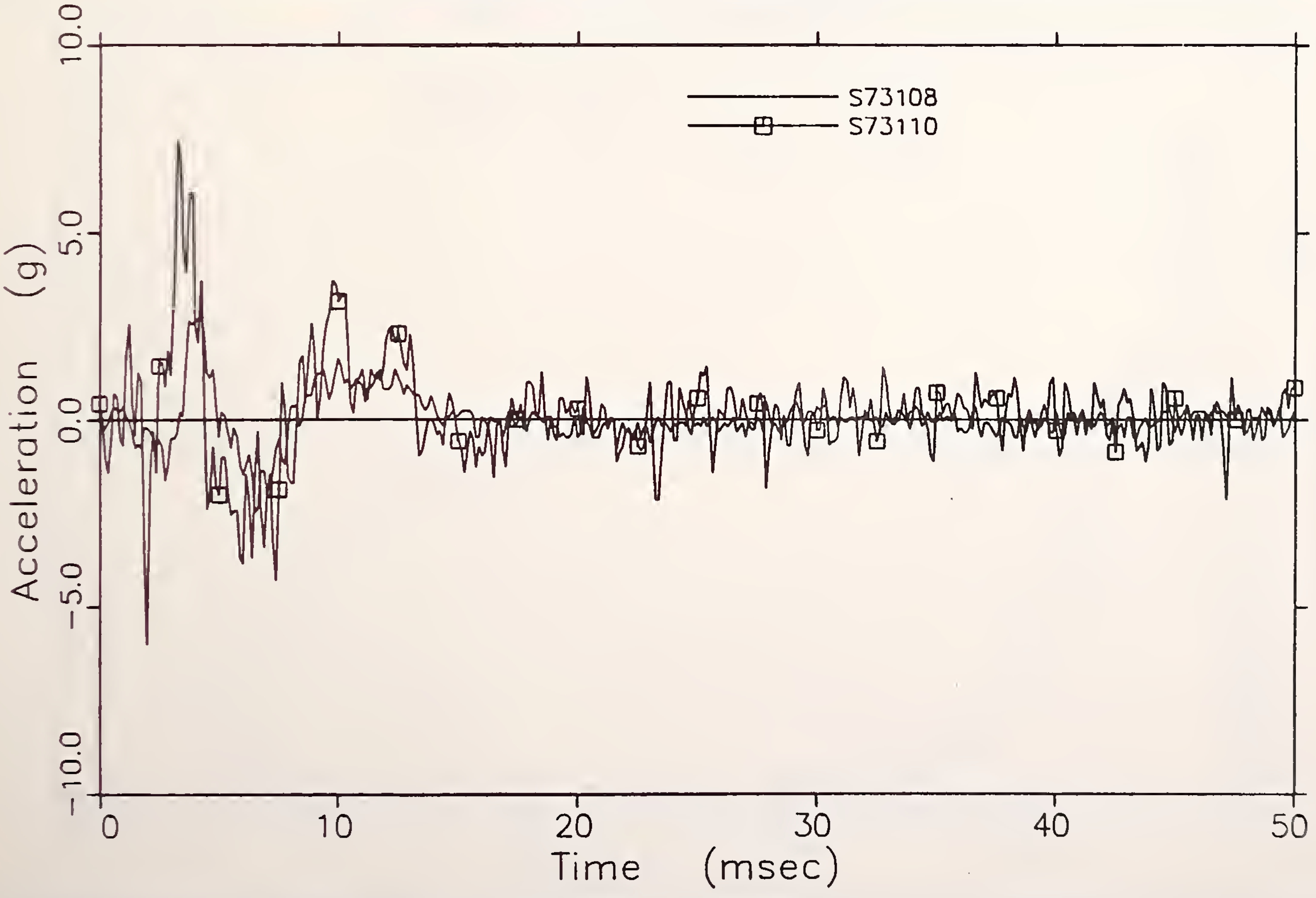

FIGURE D.2 -- Duster Reconstruction: Head C.G. Y-Axis Acceleration

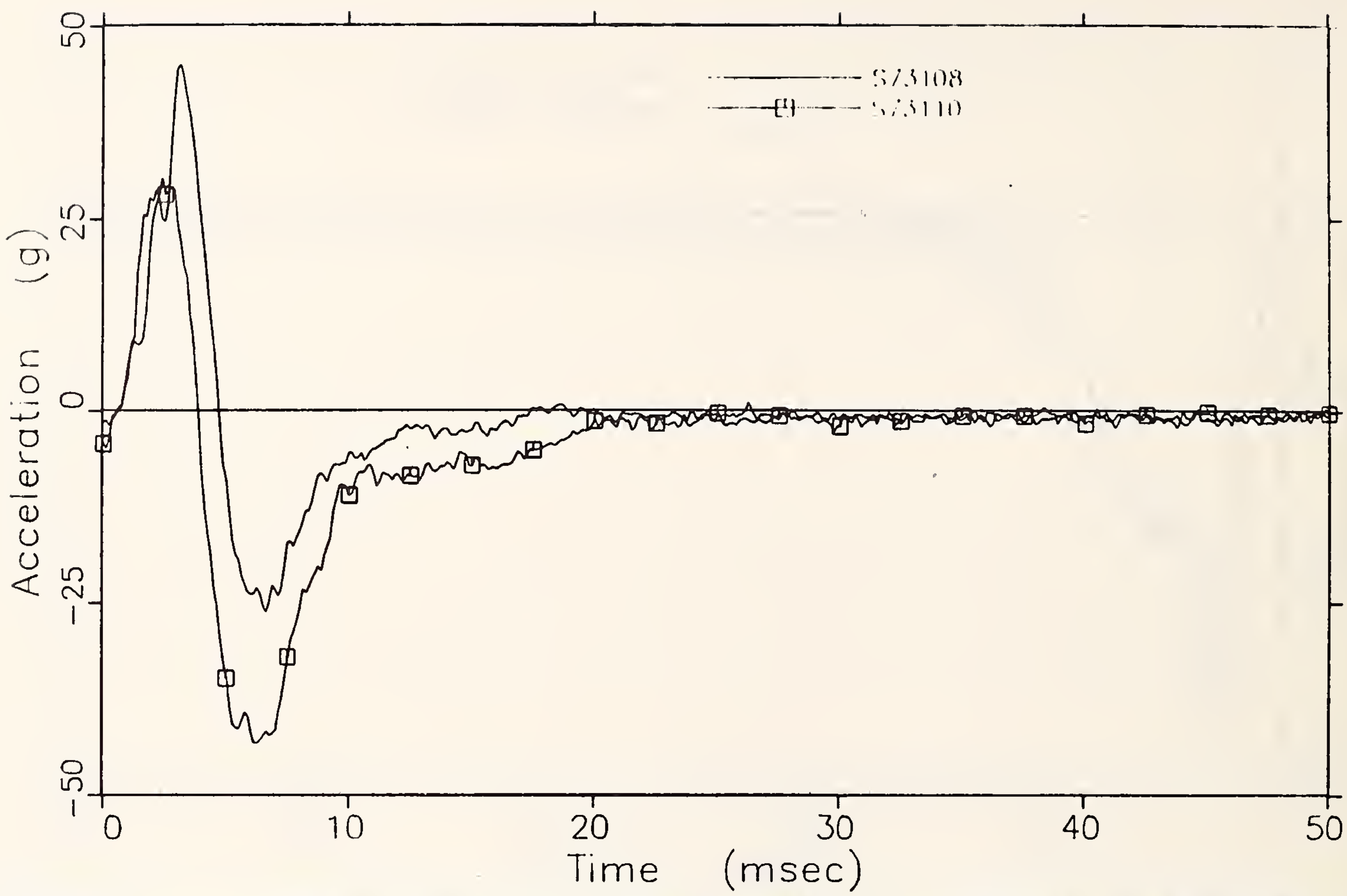

FIGURE D.3 -- Duster Reconstruction: Head C.G. Z-Axis Acceleration

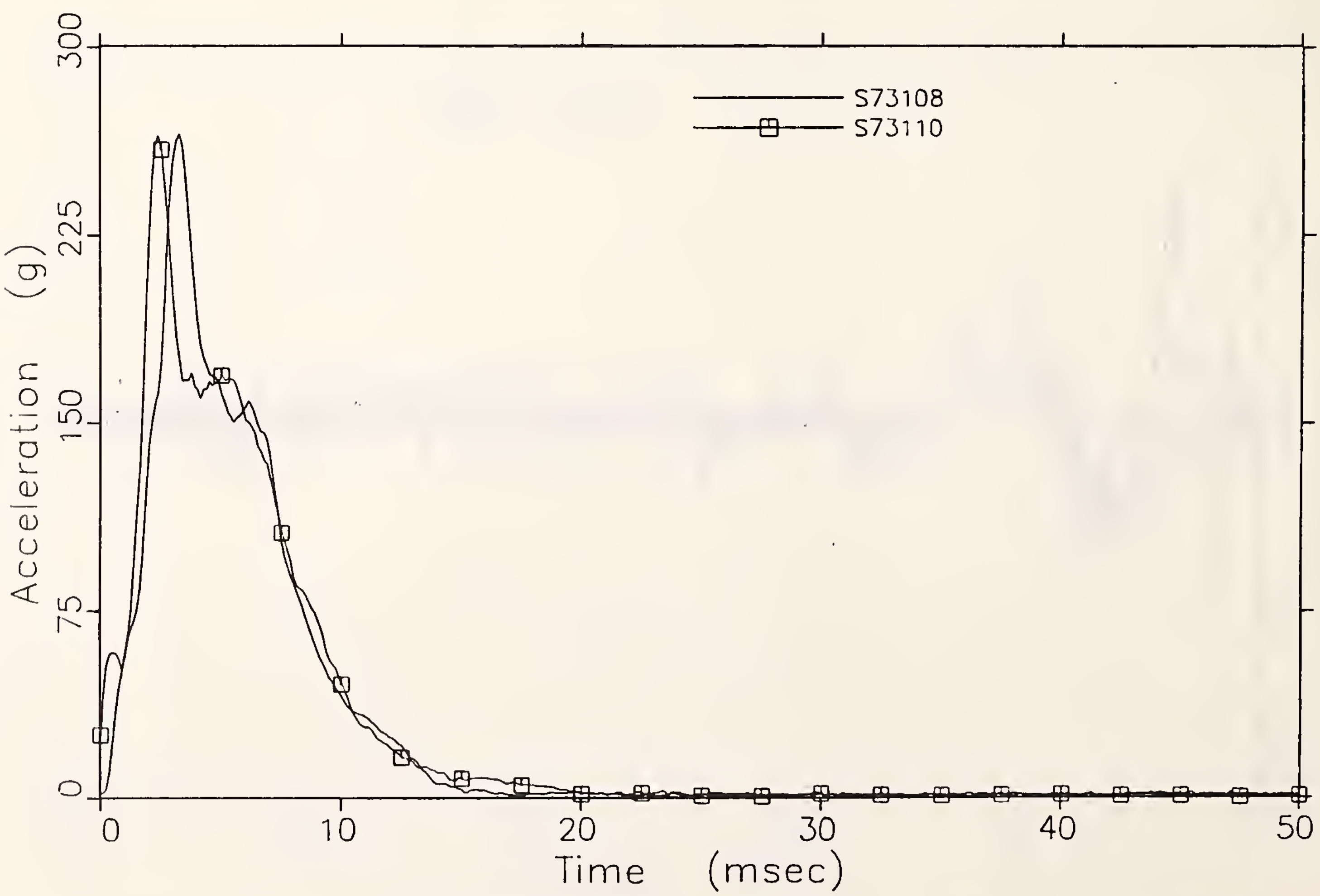

FIGURE D.4 -- Duster Reconstruction: Head C.G. Resultant Acceleration

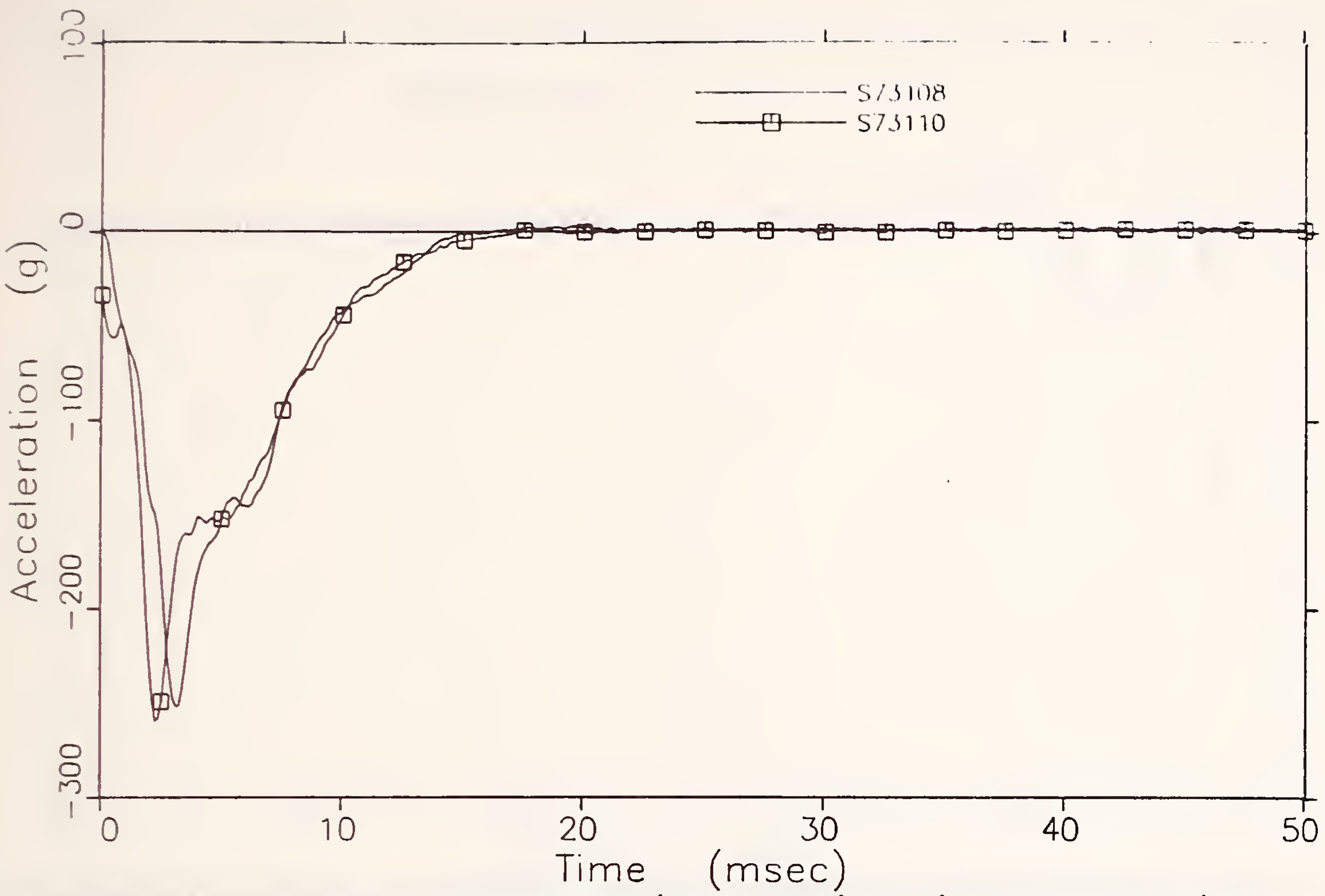

FIGURE D.5 -- Duster Reconstruction: X-Direction Acceleration at Array Position Number 1

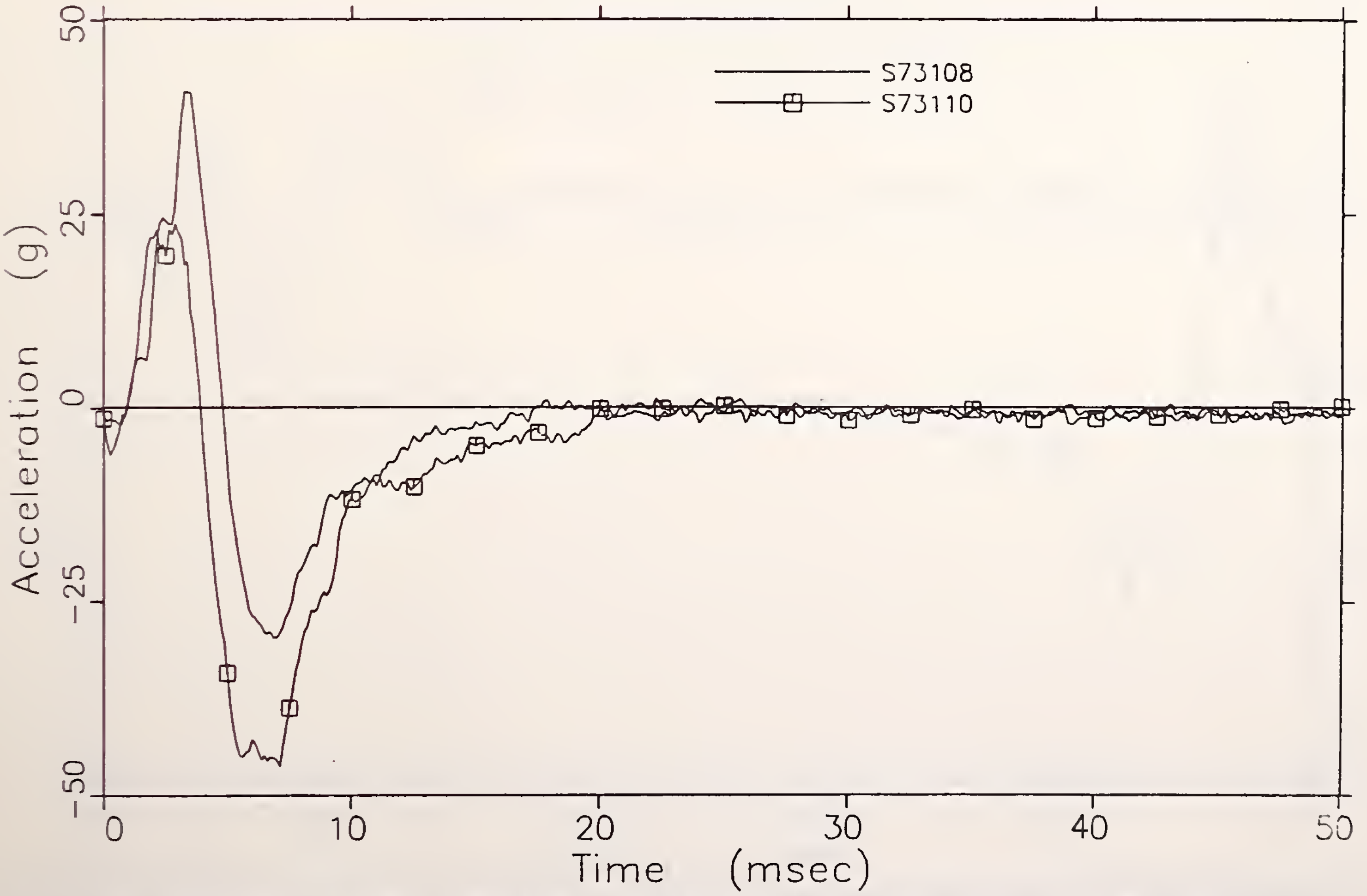

FIGURE D.6 -- Duster Reconstruction: Z-Direction Acceleration at Array Position Number 1

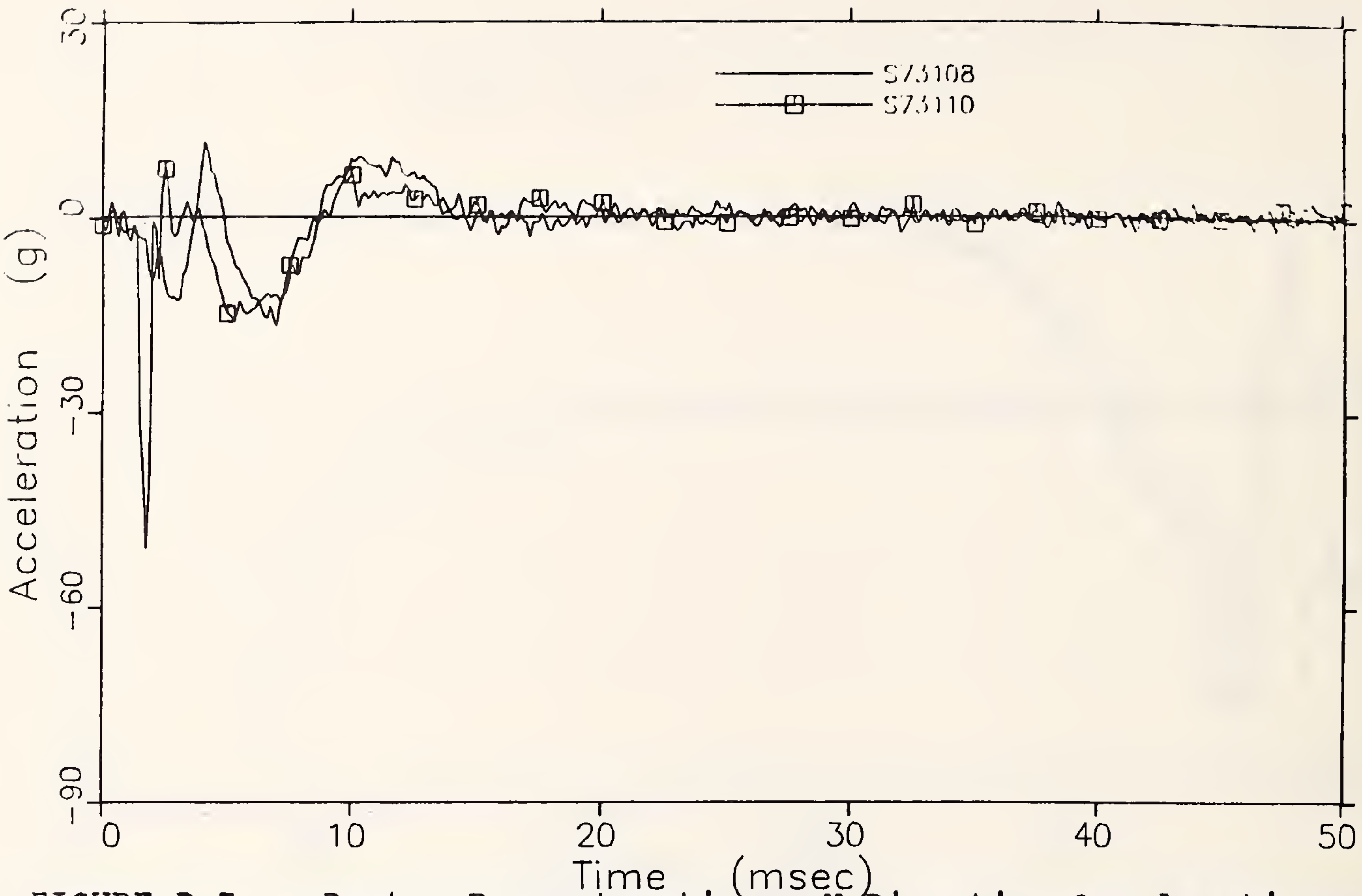

FIGURE D.7 -- Duster Reconstruction: Y-Direction Acceleration at Array Position Number 2

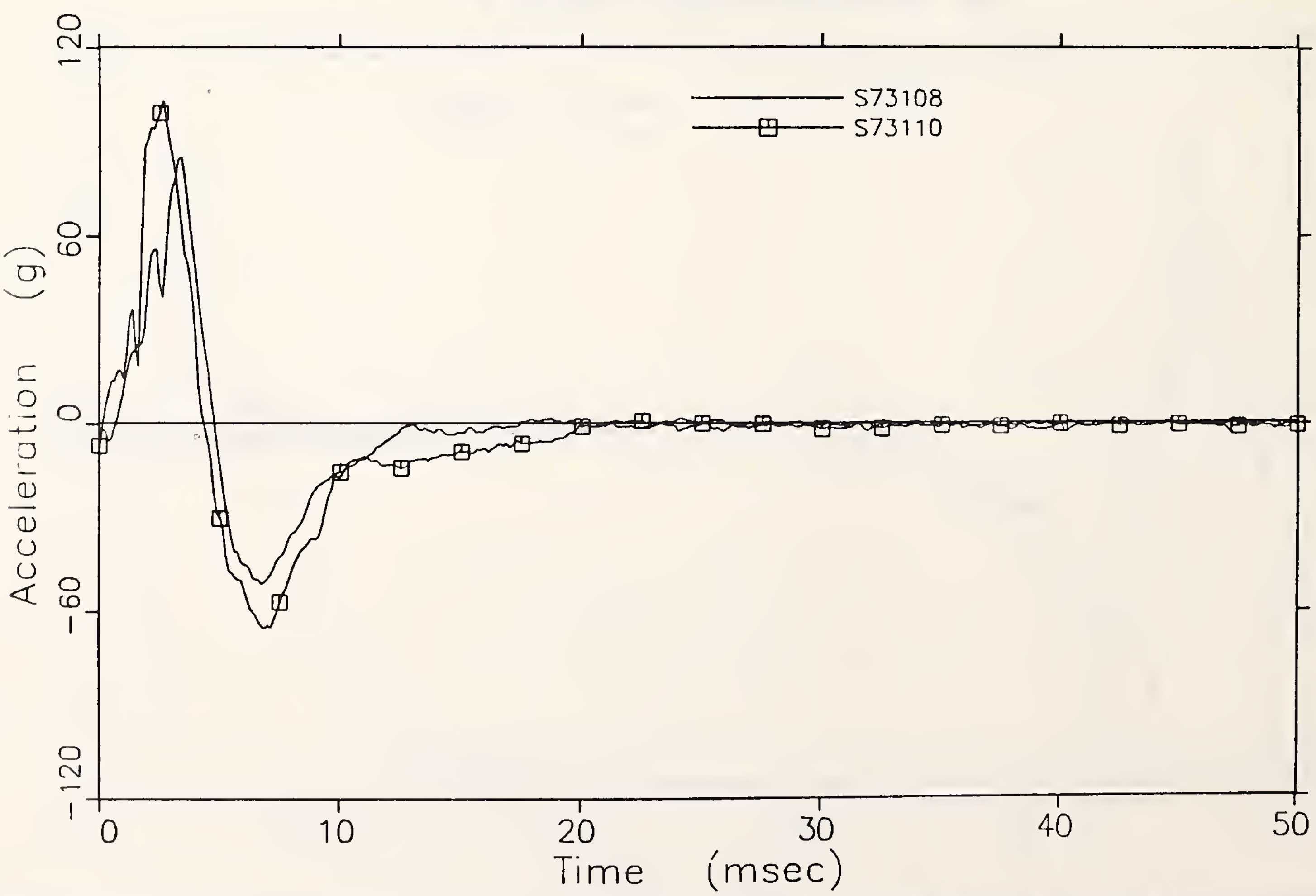

FIGURE D.8 -- Duster Reconstruction: Z-Direction Acceleration at Array Position Number 2

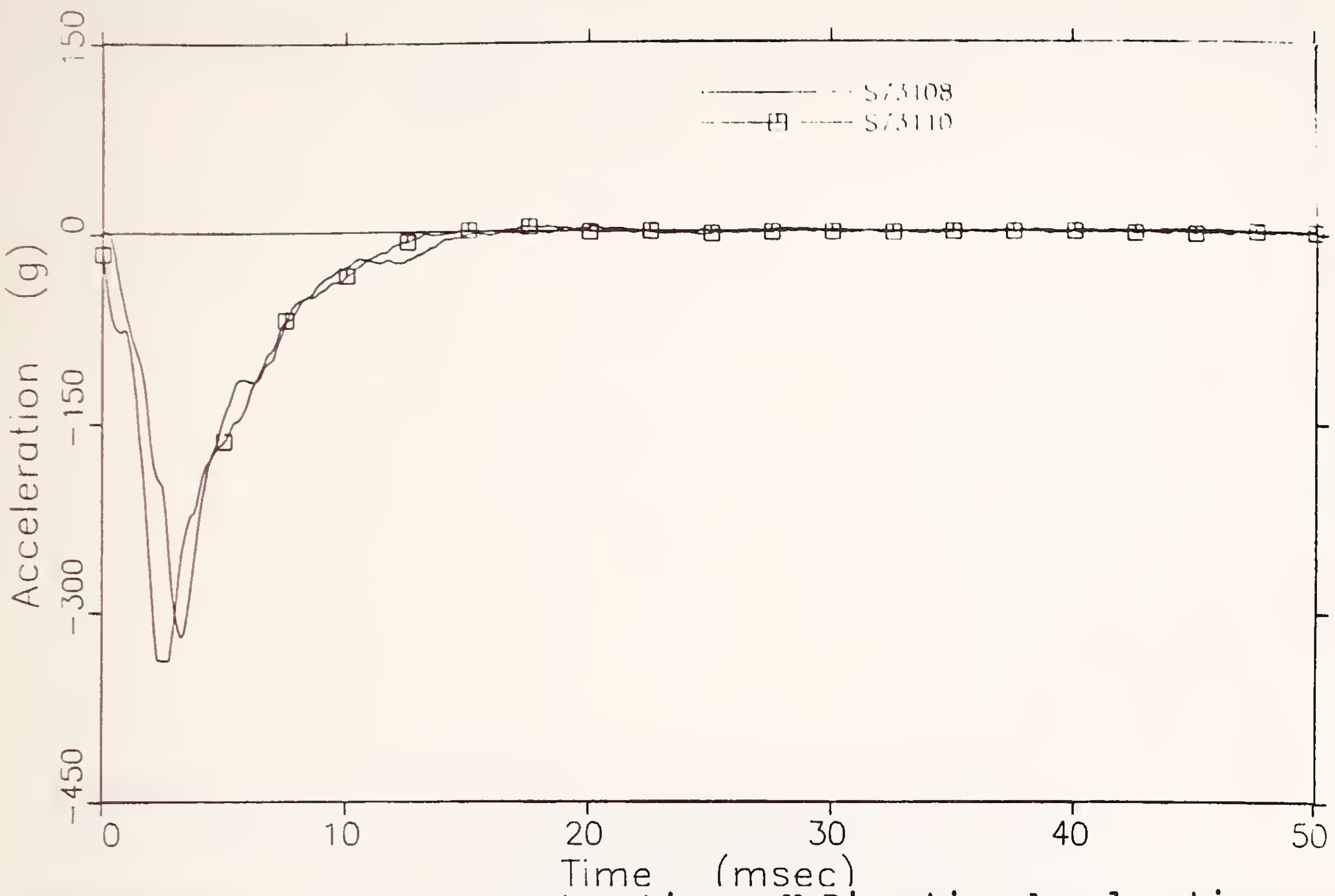

FIGURE D.9 -- Duster Reconstruction: X-Direction Acceleration at Array Position Number 3

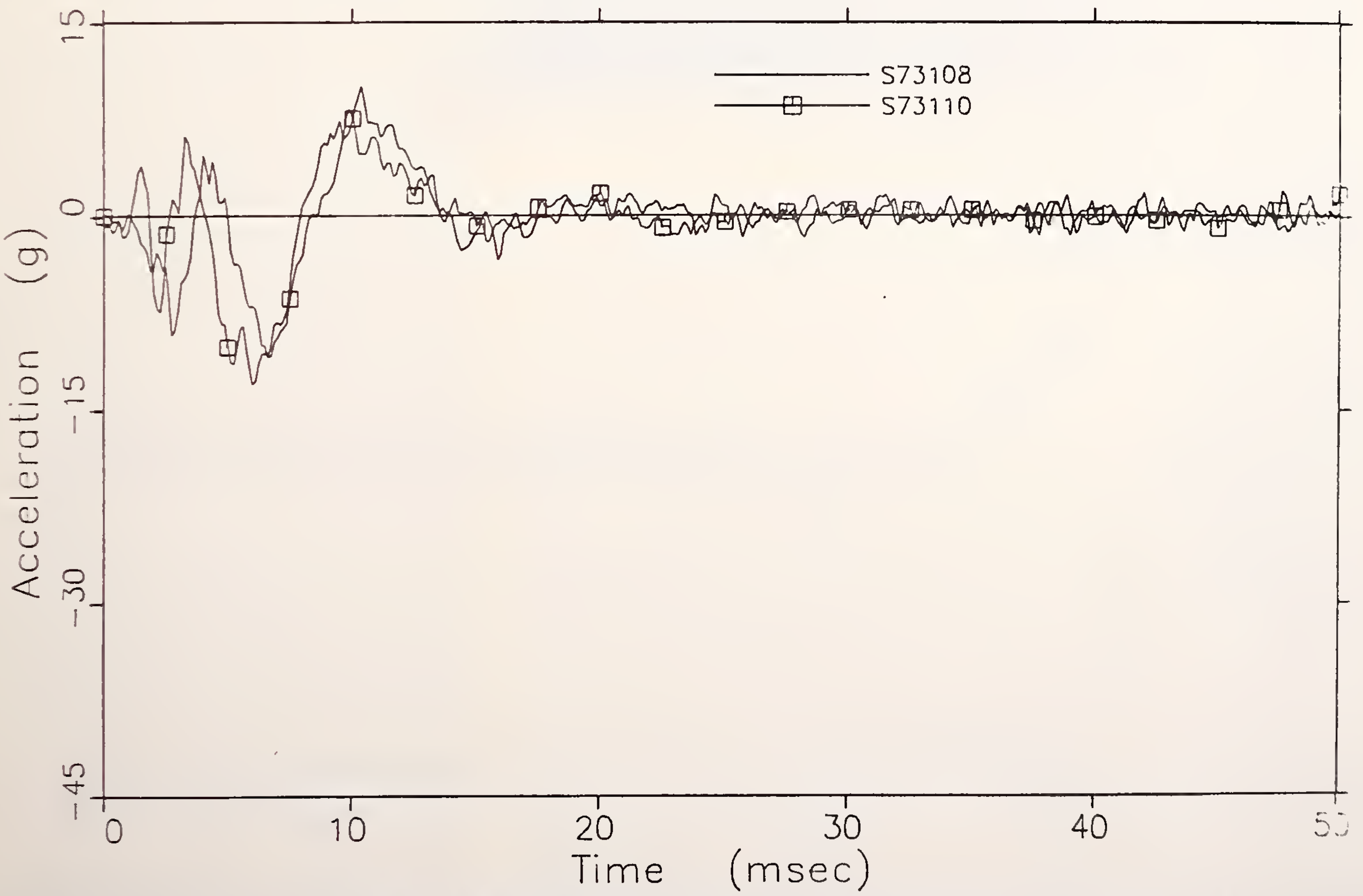

FIGURE D.10 -- Duster Reconstruction: Y-Direction Acceleration at Array Position Number 3

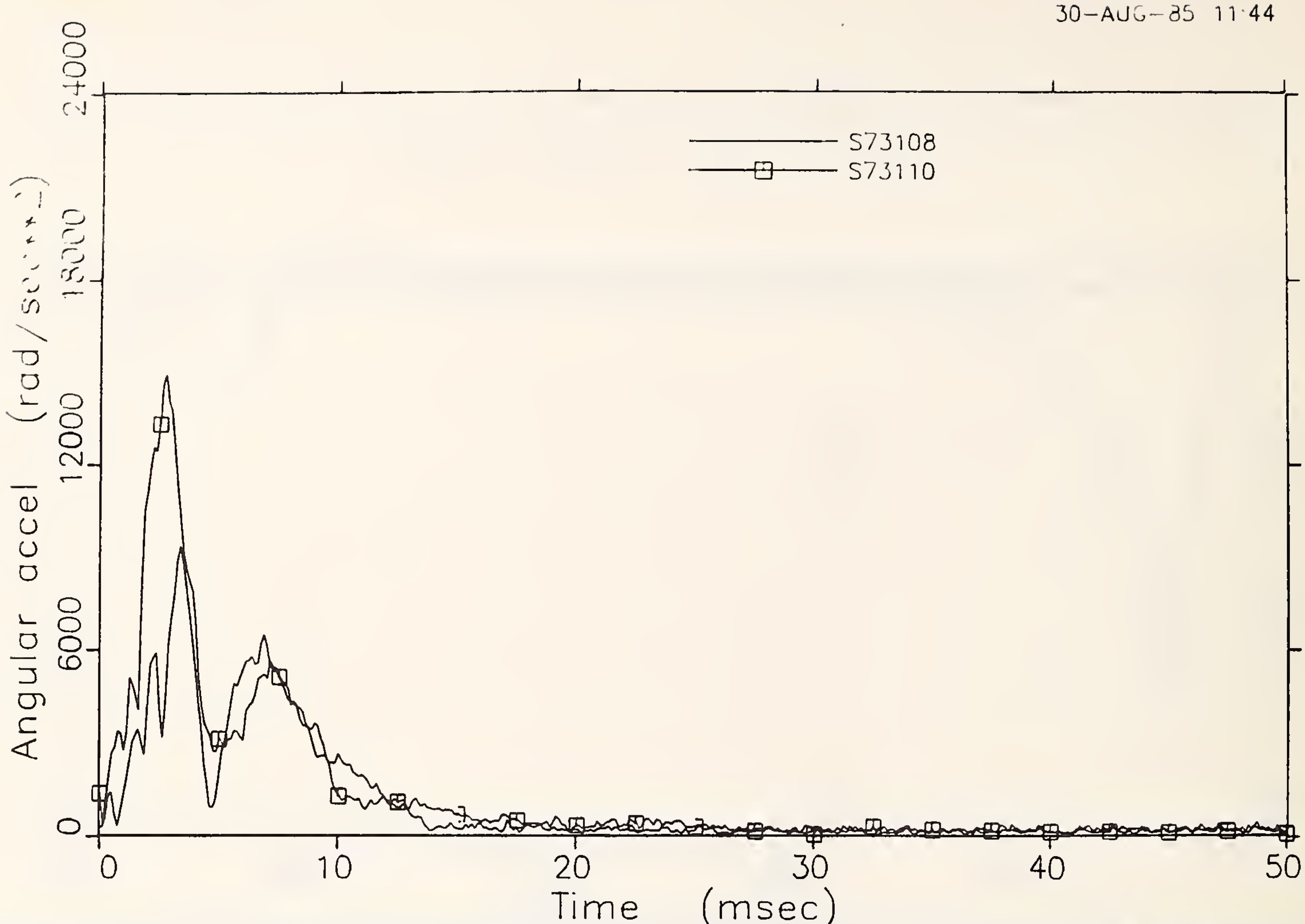

FIGURE D.11 -- Duster Reconstruction: Resultant Rotational Acceleration

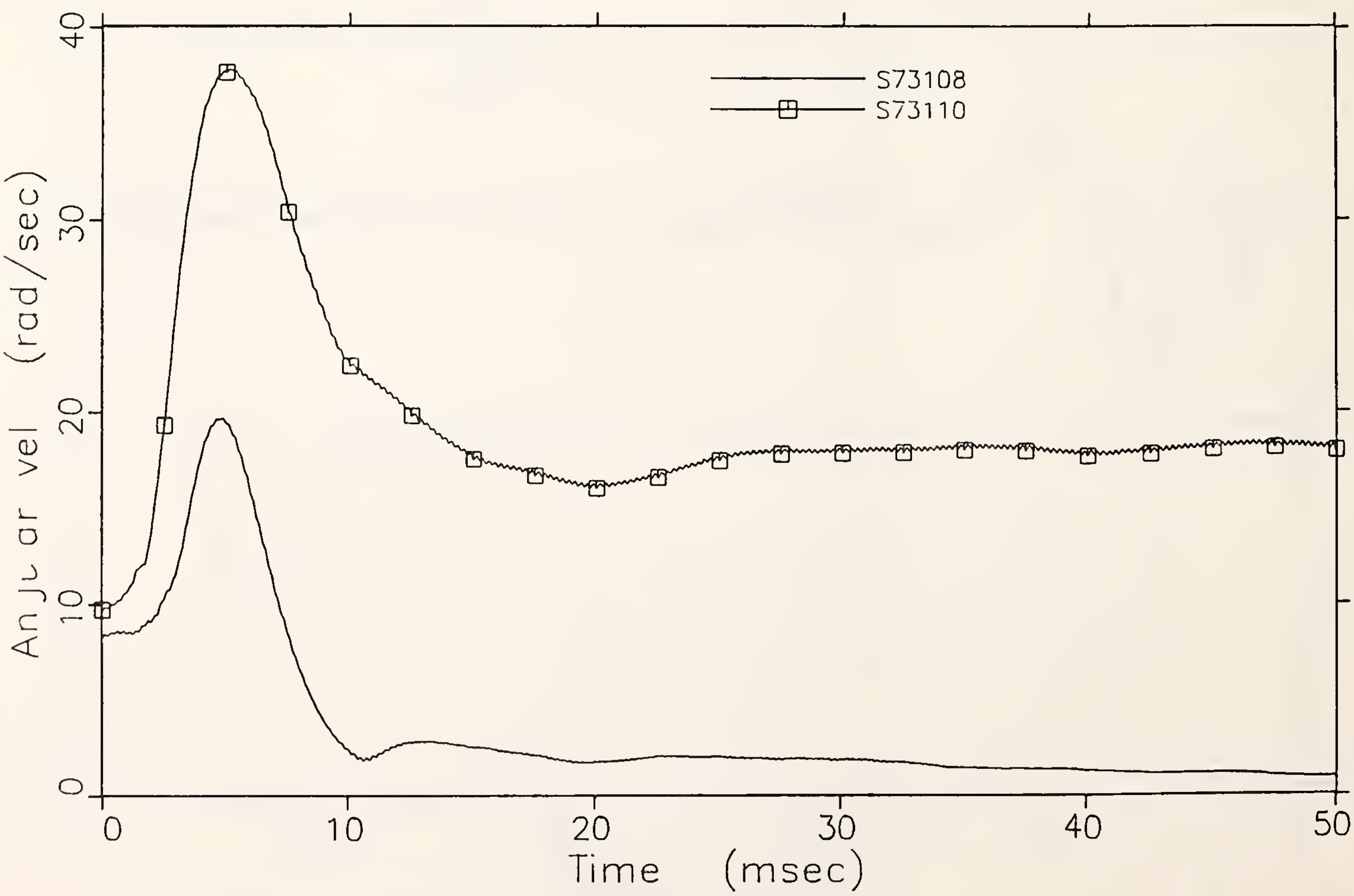

FIGURE D.12 -- Duster Reconstruction: Resultant Rotational Velocity